LOWPASS BROADBAND HARMONIC FILTER DESIGN

A THESIS SUBMITTED TO
THE GRADUATE SCHOOL OF NATURAL AND APPLIED SCIENCES
OF
MIDDLE EAST TECHNICAL UNIVERSITY

BY

HAZEM ZUBI

IN PARTIAL FULFILLMENT OF THE REQUIREMENTS
FOR
THE DEGREE OF MASTER OF SCIENCE
IN
ELECTRICAL AND ELECTRONICS ENGINEERING

SEPTEMBER 2005

Approval of the Graduate School of Natural and Applied Sciences

_____
Prof. Dr. Canan ÖZGEN
Director

I certify that this thesis satisfies all the requirements as a thesis for the degree of Master of Science.

_____
Prof. Dr. İsmet ERKMEN
Head of Department

This is to certify that we have read this thesis and that in our opinion it is fully adequate, in scope and quality, as a thesis for the degree of Master of Science.

_____
Asst. Prof. Dr. Ahmet M. HAVA
Supervisor

Examining Committee Members

Prof. Dr. Aydın ERSAK   METU, (EE)   _____

Asst. Prof. Dr. Ahmet M. HAVA   METU, (EE)   _____

Prof. Dr. Muammer ERMİŞ   METU, (EE)   _____

Prof. Dr. Nevzat ÖZAY   METU, (EE)   _____

Dr. Ahmet Erbil NALÇACI   (Energy Market
                               Regulatory Authority)   _____

I hereby declare that all information in this document has been obtained and presented in accordance with academic rules and ethical conduct. I also declare that, as required by these rules and conduct, I have fully cited and referenced all material and results that are not original to this work.

Name, Last name: Hazem ZUBI

Signature:

ABSTRACT

LOWPASS BROADBAND HARMONIC FILTER DESIGN

Zubi, Hazem

M.S., Department of Electrical and Electronics Engineering

Supervisor: Asst. Prof. Dr. Ahmet M. Hava

September 2005, 192 pages

In this thesis an analytical design method of the improved broadband passive harmonic filter (IBF) for three phase diode rectifier front-end type adjustable speed drives is presented. The method is based on frequency domain modeling of the rectifier and filter. The success of the method involves accurate representation of the load harmonics. With the harmonics well defined, the harmonic and fundamental frequency equivalent circuits are utilized to analytically calculate the voltages/currents. Thus, the size and the performance of the filter can be optimized. The analytical method is verified via computer simulations and laboratory experiments.

Also a performance comparison of various passive harmonic filters for three-phase diode rectifier front-end type adjustable speed drives is provided. The comparison involves the input current total harmonic distortion, input power factor, rectifier voltage regulation, energy efficiency, size, and cost. The parallel/series harmonic resonance problem related issues are addressed and unbalanced operation performance investigated. The comparison is based on analysis and computer simulations and the results are validated by laboratory experiments.

Keywords: ASD, broadband, design, drive, filter, harmonic, power factor, rectifier, THD.

ÖZ

GÜÇ DOĞRULTUCULARI İÇİN GENİŞBANTLI HARMONİK FİLTRELERİNİN TASARIMI

Zubi, Hazem

Yüksek Lisans, Elektrik-Elektronik Mühendisliği Bölümü

Tez Yöneticisi: Yrd. Doç. Dr. Ahmet M. Hava

Eylül 2005, 192 sayfa

Bu tezde, üç fazlı diyotlu köprü doğrultucu girişli hız ayarlı elektrik motor sürücülerin girişinde kullanılan geliştirilmiş genişbantlı harmonik filtresinin tasarımı için analitik bir yöntem sunulmuştur. Bu yöntem, filtre ve doğrultucunun frekans domeninde modellenmesi temeline dayanmaktadır. Yöntemin başarısı, yük akımının harmoniklerinin yüksek doğrulukla temsil edilmesine dayanır. Harmoniklerin doğrulukla temsil edilmesiyle, harmonik ve temel bileşen eşdeğer devreleri kullanılarak akım ve gerilimler analitik olarak hesaplanmaktadır. Böylece filtrenin boyutu ve başarımı eniyileştirilebilmektedir. Analitik yöntem, bilgisayar benzetimleri ve laboratuvar çalışmalarıyla doğrulanmıştır.

Ayrıca, üç fazlı diyotlu köprü doğrultucu girişli hız ayarlı elektrik motor sürücülerinin girişlerinde kullanılan çeşitli pasif harmonik filtrelerinin başarımları karşılaştırılmıştır. Bu karşılaştırma yapılırken, giriş akımı toplam harmonik bozulması, giriş güç katsayısı, doğrultucu geriliminin regülasyonu, enerji verimliliği, boyut ve maliyet gibi özellikler dikkate alınmıştır. Paralel/seri rezonans problemleriyle ilgili sorunlar değerlendirilmiş ve dengesizlik durumundaki başarım incelenmiştir. Karşılaştırma, analize ve bilgisayar benzetimlerine dayalı olarak yapılmış ve laboratuvar çalışmalarıyla sonuçlar doğrulanmıştır.

Anahtar Kelimeler: HAS (ASD) , genişbant , tasarım , sürücü , filtre , harmonik , güç katsayısı , doğrultucu , THB (THD)

To my parents,

who always support me in all aspects of my life

to my wife

for her patience and support in my study

to my children

Malak, Basma and Lujayn

ACKNOWLEDGEMENTS

I thank the almighty ALLAH for his mercy and grace, which enabled me to complete this work.

I would like to express my sincerest thanks to Asst. Prof. Dr. Ahmet M. Hava for his guidance, support and valuable contributions throughout the preparations for this thesis.

I am grateful to my friends in Middle East Technical University for all the support they gave me throughout my study.

I express my deepest gratitude to my parents, my father Mohamed and my mother Afaf for their encouragements throughout my education life, and to my wife Nahla for her support and effort, and my children for their patience during my study. Their love, care and encouragement has given me a great inner strength to success. This work is dedicated to them.

The Libyan secretariat of higher education is highly appreciated for its financial support during my study period.

TABLE OF CONTENTS

CHAPTER

LIST OF FIGURES

FIGURES

xiii

LIST OF TABLES

TABLES

CHAPTER 1

INTRODUCTION

1.1 Background

The application of cost effective power converter circuits which enhance the overall performance, efficiency, and reliability of industrial processes is common in all industry. The industrial applications of AC/DC and DC/AC power conversion have increased gradually since the advent of silicon controlled rectifiers (SCR) in 1957. However, the wide use of single and three phase diode/thyristor rectifiers, for DC power supplies, Adjustable Speed Drives (ASD), Uninterruptible Power Supplies (UPS), and for household and industrial appliances, took place in the last two decades. With an estimated 65% of industrial electrical energy used by electric motors, the major users in industry increasingly see energy reduction as a key to improve their profitability and competitiveness [1]. Because variable speed drives reduce energy consumption (20-30% savings) and decrease pollutant emission levels to environment while increasing productivity, their proliferation is inevitable. For variable speed applications, ASDs are widely employed in driving induction and permanent magnet motors due to the high static and dynamic performance obtained in such systems. High energy efficiency and high motion quality, low starting torque, etc. are the positive attributes of the ASDs.

ASDs, consists of AC/DC converter connected to DC/AC inverter. Of all the modern power electronics converters, the Voltage Source Inverter (VSI) is perhaps the most widely utilized DC/AC conversion device with commonly used Pulse Width Modulation (PWM) methods. The PWM-VSI consists of six power semiconductor switches with anti-parallel feedback diodes. It converts a fixed DC voltage to three phase AC voltages with controllable frequency and magnitude. In AC motor drive applications, typically a rectifier device converts the AC three phase line voltages to

1

DC voltage. Following the rectifier voltage passive filtering stage (typically capacitive filtering with/without DC link reactor), the VSI interfaces the DC source with the AC motor to control the shaft speed/position/torque. The most used front-end topology for ASDs is still the 6-pulse diode/thyristor rectifier, due to well-known advantages such as, high efficiency, low cost, robustness and reliability. The main structure of PWM-VSI drive with a 6-pulse diode rectifier front end is shown in Fig. 1.1.
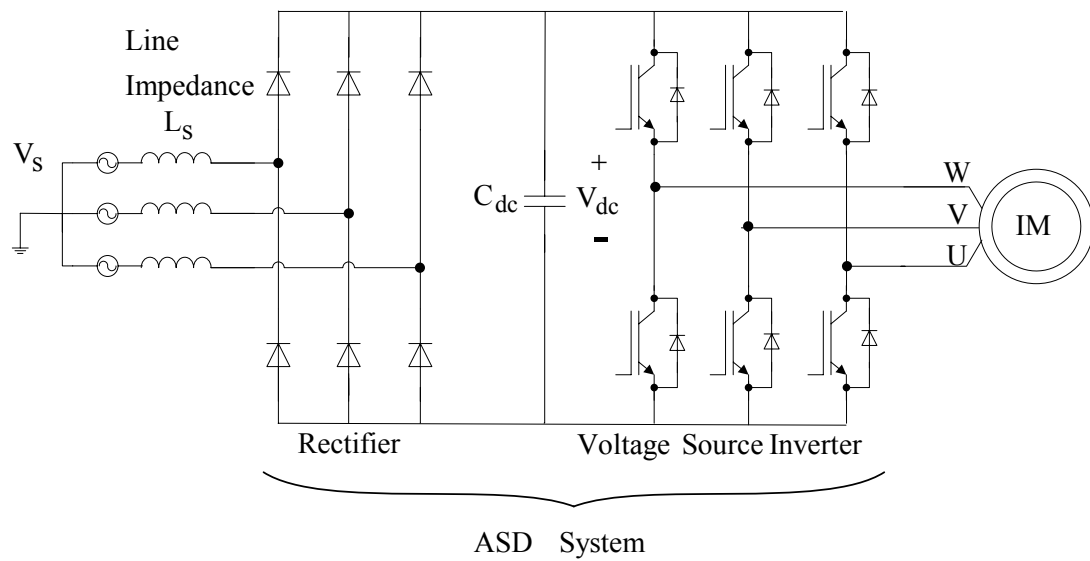
Fig.1.1 The main structure of PWM-VSI diode bridge rectifier front-end AC drive.

Line commutated diode and thyristor rectifiers exhibit nonlinear load characteristics and draw non-sinusoidal currents from the supply even when fed from sinusoidal supply voltages. These harmonic currents are injected into the supply systems and pollute the power line causing power quality problems to many power quality critical loads.

The injected current harmonics cause line voltage distortion and notches which is a major problem for both utilities and customers at distribution levels. The distorted voltage frequently results in malfunction or tripping of other linear/nonlinear loads connected to the same Point of Common Coupling (PCC), shown in Fig. 1.2. The point of common coupling is a point where the costumers are connected together and

it is generally defined as the point at which harmonic limits shall be evaluated. Specifically, from the utility side, this point will be in the supply system owned by the utility. From the customer side, it is the point where the end user is consuming energy and where other customers are (or could be in the future) provided with electric service.
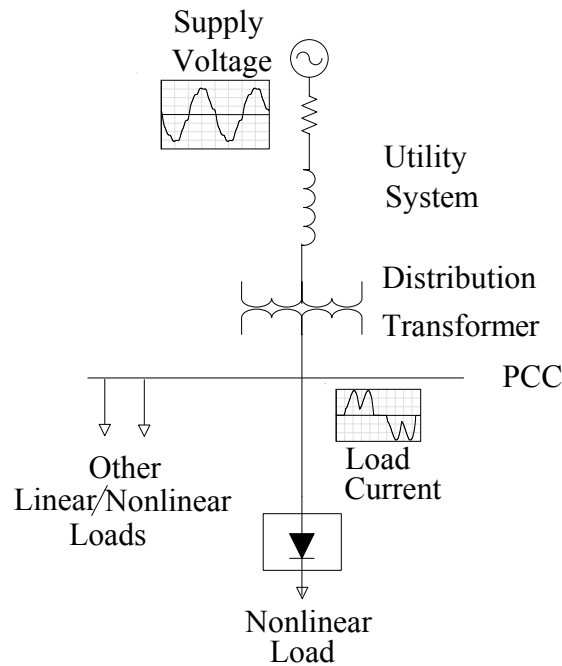
Fig.1.2 Definition of the point of common coupling (PCC).

The injected current harmonics can interact adversely with wide range of power system equipments, most notably capacitors, transformers and motors causing additional losses, overheating and overloading. They can also cause interference with telecommunication lines and errors in power metering. Furthermore, the generated supply current harmonics do not deliver real power to the load, but cause harmonic resonance or amplification in the utility distribution system. Consequently, the IEEE 519 recommended harmonic standard was introduced as a guideline in 1981, and revised in 1992 [2]. The IEEE Standard 519-1992 proposes to limit harmonic current injection from end users so that the harmonic voltage levels on the overall power system will be acceptable. The approach set recommended limitations for

both, users and utility ends. For individual end users, the standard limits the level of harmonic current injected at the PCC. This is the quantity that the end users have control over. Recommended limits are provided for both individual harmonic components and the total distortion indices. Total Harmonic Distortion (THD) is commonly used indices for measuring the harmonic content of a waveform and may be applied to either voltage or current. The current THD is given by

$$THD_I = \frac{\sqrt{\sum_{n=2}^{N} I_n}}{I_1} \qquad (1.1)$$

where the I_n is the rms value of the current harmonics and I_1 is the rms value of the fundamental current component. However, this can be often misleading. For instance, many ASD's will exhibit high input current THD values when they are operating at very light loads. This is not critical because the magnitude of harmonic current is low, even though its relative distortion is high. To account for the loading effect for characterizing the harmonic currents in a consistent fashion, the IEEE Standard 519-1992 defines an additional term, the Total Demand Distortion (TDD). This term is the same as THD except that the distortion is expressed as a percent of rated fundamental load current rather than of the fundamental current magnitude at the instant of measurement. TDD is therefore given by

$$TDD = \frac{\sqrt{\sum_{n=2}^{N} I_n}}{I_L} \qquad (1.2)$$

where the I_n is the rms value of the current harmonics and I_L is the rated demand of the fundamental current component.

Therefore, IEEE Standard 519-1992 recommended harmonic current limits, shown in Table 1.1, is expressed in terms of current TDD, rather than current THD. The I_{sc}/I_L ratio is the short circuit ratio at PCC. As I_L is previously defined, I_{sc} is the short circuit current available at the input of the nonlinear load. The short circuit ratio

defines the TDD limit that applies to a distribution transformer output, and therefore to the loads connected to it.

For the utility, since the harmonic voltage distortion on the utility system arises from the interaction between distorted load currents and the utility system impedance, the utility is mainly responsible for limiting the voltage distortion at the PCC. The IEEE Standard 519-1992 recommended harmonic voltage limits, shown in Table 1.2, are given for the maximum harmonic components and for the voltage THD. These values are expressed as the percentage of the fundamental voltage. For systems below 69 kV, the voltage THD should be less than 5% provided that the system resonances do not coincide with harmonic frequencies present in the load currents. Therefore, to comply with these limitations, utilization of efficient, reliable, and economical harmonic filters is mandatory.

Table 1.1 IEEE 519 harmonic current limits[*]

I_{SC}/I_L	<11	11≤h<17	17≤h<23	23≤h<35	35≤h	TDD
<20	4.0	2.0	1.5	0.6	0.3	5.0
20-50	7.0	3.5	2.5	1.0	0.5	8.0
50-100	10.0	4.5	4.0	1.5	0.7	12.0
100-1000	12.0	5.5	5.0	2.0	1.0	15.0
>1000	15.0	7.0	6.0	2.5	1.4	20.0

*Higher levels of harmonic current generation are allowed for higher values of SCR because a single customer has less impact on the system voltage distortion.

Table 1.2 Voltage distortion limits

Bus Voltage at PCC	Maximum Individual Harmonic Component %	Maximum THD%
69kV and Below	3.0	5.0
69.001kV Through 161kV	1.5	2.5
161.001kVand Above	1.0	1.5

Note: High-voltage systems can have up to 2.0% THD where the cause is an HVDC terminal that will attenuate by the time it is tapped for a user.

In this thesis, the THD indices will be used for both current and voltage. They will be distinguished by using THD_I and THD_V for current and voltage harmonics measurement, respectively.

1.2 Harmonic Mitigation Techniques

Various harmonic reduction techniques have been developed to meet the requirements imposed by the current harmonic standards. In general these techniques can be classified into five broad categories:

1. Passive filters (line reactors and/or DC link chokes, series, shunt, and lowpass broadband filters)
2. Phase multiplication systems (12-pulse, 18-pulse rectifier systems)
3. Active harmonic compensation systems (series, parallel)
4. Hybrid systems
5. PWM rectifiers (step-up, step-down, VSI, CSI etc.)

The intent of these techniques is to make the input current a pure sinusoidal waveform, so as to reduce the overall current THD. In passive filters, the flow of the undesired harmonic currents into the power system can be prevented by the usage of a high series impedance to block them or by diverting them to a low impedance shunt path. These two methods represent the concept of the series and the shunt passive filters, respectively.

Series passive filters can be purely inductive type or LC tuned type. AC line reactor filter and DC link inductor filter are the two purely inductive type filters. AC line reactors offer a considerable magnitude of inductance that alters the way the current is drawn by the rectifier bridge. They make the current waveform less discontinuous, resulting in lower current harmonics. To maximize the input reactance while minimizing AC voltage drop both AC line reactors and DC link inductance (choke), shown in Fig. 1.3, can be combined. The DC link inductance is electrically present

after the diode rectifier and before the DC bus capacitor and it performs very similar to the three phase AC line reactors. Both AC line or DC link inductance insertion methods provide a limited amount of THD reduction that is not sufficient to comply with the IEEE 519 standards.
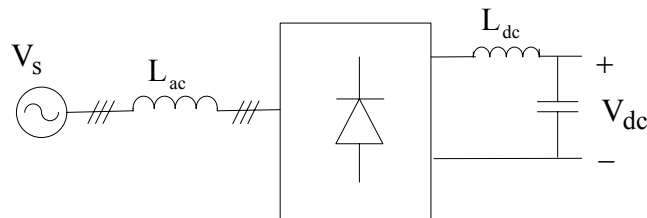
Fig.1.3 AC line reactor and DC line inductance based passive filtering.

The tuned series passive filter, shown in Fig. 1.4, is connected in series with the load. The filter consists of parallel inductance and capacitance that are tuned to provide high impedance at a selected harmonic frequency. The high impedance then blocks the flow of harmonic current at the tuned frequency only. At fundamental frequency, the filter is designed to yield low impedance, thereby allowing the fundamental current to flow. For blocking multiple harmonics, multiple series filters are needed. They must be designed to carry a full rated load current as they are connected in series to full line voltage. Therefore, they can create significant losses at the fundamental frequency. In contrast, shunt passive filters carry only a fraction of the current that a series filter must carry. Given the higher cost of a series filter, and the fact that shunt filters may supply reactive power at the fundamental frequency, the most practical approach usually is the use of shunt filters.

A shunt filter offers very low impedance path at the frequency to which it is tuned and it shunts most of the harmonic current at that frequency. Most Common shunt filter types are the single tuned and highpass filters. These two filters are the relatively simple to design and implement among the other shunt types. The layout of common shunt filter types is shown in Fig. 1.5 [3].
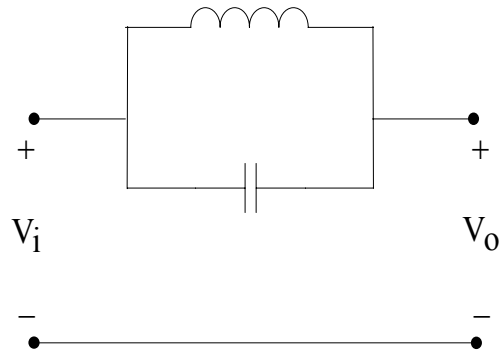
Fig.1.4 Series passive filter configuration.

Single tuned
filter

First order
filter

Second order
filter

Third order
filter
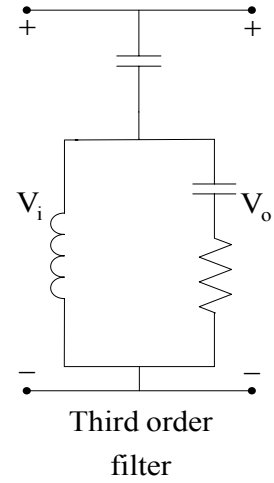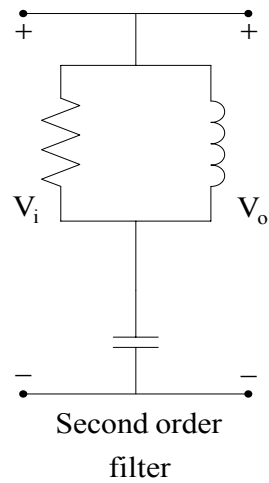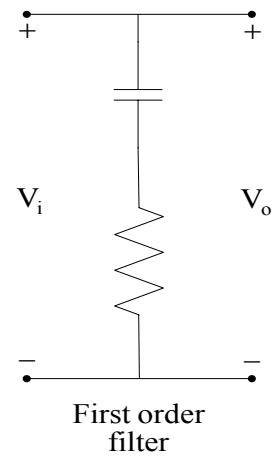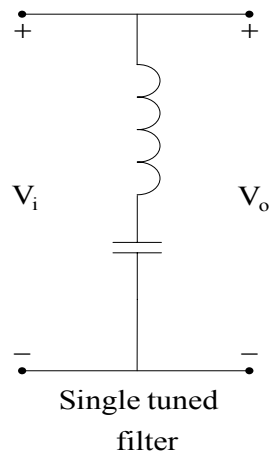
Fig.1.5 Common shunt passive filter configurations.

Unlike the shunt and series filters that have a narrow band of harmonic suppression, broadband filters have a wider range of harmonics suppression property. Broadband

filters employ a combination of the two passive techniques, with a high series impedance to block the undesired current harmonics (from flowing through the grid) and a low shunt impedance path to divert their flow through the shunt filter. They can be in different structures, shown in Fig. 1.6, LC and LLCL type [4], [5], and [6]. They are tuned to a low cut off frequency such that only fundamental component will pass from the input to the output. Therefore, they are called lowpass broadband filters. Both shown lowpass broadband filters use only one shunt filter to suppress all the harmonic broadband. On the contrary, classical shunt filters are tuned to a single harmonic frequency to be suppressed and multiple stages are used to suppress all injected current harmonics.

(a)   (b)
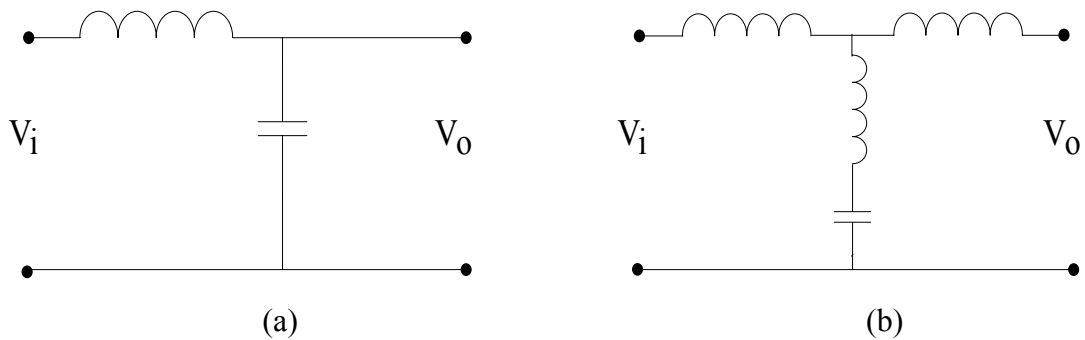
Fig.1.6 Lowpass broadband filter configurations (a): LC type, (b): LLCL type.

Phase multiplication technique is based on increasing the pulse number for the converter. This increases the lowest harmonic order for the converter and reduces the size of the passive filter needed to filter out the current harmonics. A 12-pulse converter ideally has the lowest harmonic order of 11 (5th and 7th current harmonics are theoretically nonexistent). Similarly, an 18-pulse converter has the lowest harmonic order of 17. However, a 12-pulse converter, shown in Fig. 1.7, needs two 6-pulse bridges and two sets of 30° phase shift AC inputs and an 18-pulse converter needs three 6-pulse bridges and three sets of 20° phase shift AC inputs. Many different topologies exist for the phase shift achievement. In general, the phase multiplication technique is effective to reduce low order current harmonics as long as there is a balanced load on each of the converters. However, their large size, low efficiency, and high cost are the main topology drawbacks [7].
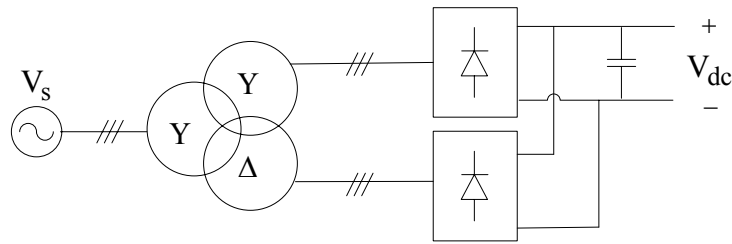
Fig.1.7 Twelve pulse rectifier system configuration.

Active harmonic compensation (filtering) method is relatively a new method for eliminating current harmonics from the line. Active filters give good system performance and current harmonics reduction. However, they are based on sophisticated power electronics components and thus they are much more expensive than passive filters. In active filters the basic idea is to inject to the line equal magnitudes of the current/voltage harmonics generated by the nonlinear load and with 180 degrees phase angle difference so they cancel each other.

Active filters can be classified based on converter type, topology, and number of phases. The converter type can be either Current Source Inverters (CSI) or VSI. CSI-based active filters employ an inductor as the energy storage device. VSI-based active filters used a capacitor as the energy storage device. The topology can be shunt, series, or a combination of both. The third classification is based on the number of phases, such as two-wire (single-phase) and three- or four-wire (three-phase) systems [8]. Three phase active filters are used for high-power nonlinear loads such as ASD and AC/DC converters. Active filters of many configurations have been introduced and improved. Shown in Fig. 1.8, are the fundamental configurations [9]. Of all various configurations, the parallel active filter using the voltage source inverter topology accompanied by high performance current regulation methods is the most frequently employed type. For harmonic compensation, the parallel active filter employs the instantaneous reactive power theory or synchronous frame transformation based compensation technique.

(a)   (b)
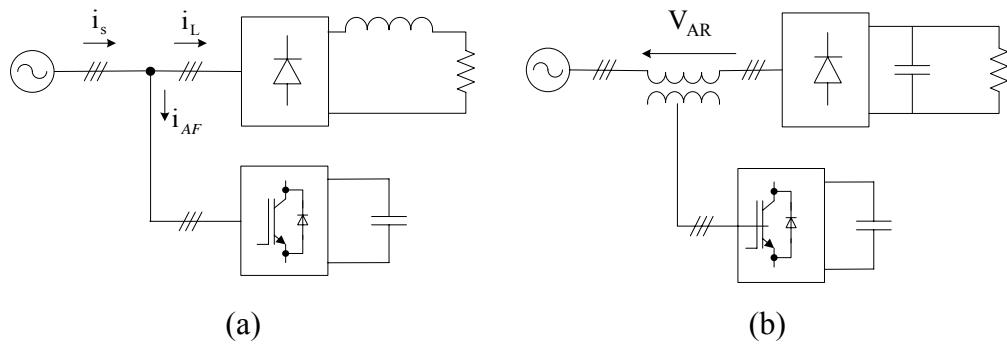
Fig.1.8 Active filter fundamental system configurations:
(a) Shunt active filter, (b) Series active filter.

Hybrid active filters, as shown in Fig. 1.9, combine active and passive filters in various configurations [9]. The main purpose of hybrid active filters is to reduce initial costs and to improve efficiency. They are also used to improve the compensation characteristics of passive filters and alleviate any series or parallel resonance due to supply or load respectively Practically, more viable and cost-effective hybrid filter topologies have been developed than stand-alone active filters. They enable the use of significantly small rating active filters that is less than 5% of the load KVA compared to stand-alone parallel (25-30%) or series active filter solutions [10]. Usually, with shunt passive filter combinations, the passive filter is tuned up to a specific frequency to suppress the corresponding harmonic and decrease the power rating of the active filter. Another typical combination is of a series active filter and a series passive filter.

(a)   (b)
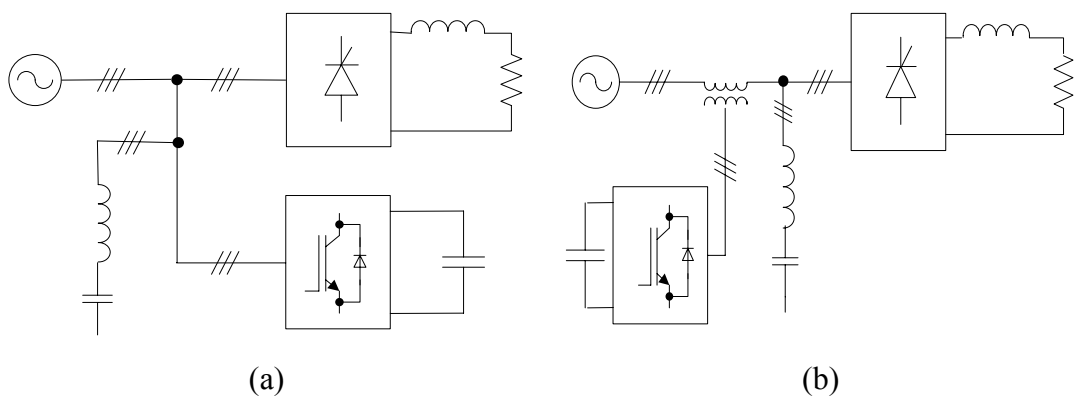
Fig.1.9 Hybrid active filters common configurations: (a) Shunt active filter and shunt passive filter, (b) Series active filter and shunt passive filter.

High fundamental component current through the series active filter and the fundamental component voltage across the shunt active filter are problematic. High initial and running cost, and complexity are major drawbacks of the active harmonic filtering technique.

For PWM- Voltage Source Rectifiers (PWM-VSR) benefits like power regeneration, low harmonic distortion, unity power factor, and controlled DC link can be obtained. They are often used in applications where substantial regenerative operating mode occurs. PWM-VSR operation principle is based on direct sinusoidal current generation, whereas the active filter is based on load harmonic compensation. However, the topology high cost is the main drawback that makes it unpractical in many applications.

To conclude, most of the mentioned filtering techniques have common drawback of higher cost compared to passive filtering techniques. Consequently, the passive harmonic filtering techniques, to a large extent, are still the most commonly used techniques for current harmonic mitigation of 6-pulse front-end diode/thyristor rectifier applications.

In this thesis, of the passive harmonic filtering techniques, lowpass broadband passive filter topologies are on the scope. The improved LLCL type broadband filter is investigated throughout the thesis.

1.3 Objective and Organization

The aim of this thesis is to establish an analytical method for the design of the Improved lowpass Broadband Passive harmonic Filter (IBF) that absorbs current harmonics caused by three phase bridge rectifiers used in motor drives. The design attempts to comply with the IEEE Standard 519-1992 recommended harmonic limits applied to the current harmonic limits of three phase rectifier systems.

The IBF topology decreases the individual current harmonics and the current total harmonic distortion of the rectifier that draws current from the utility and provides

reactive power compensation (corrects the power factor). By its high input impedance, it also blocks (isolates) the possible influences of the line harmonic voltages on the load and filter. In addition, it prevents parallel and series resonance with the utility and/or other loads, (moves the filter parallel resonance frequency away from dominant current harmonics caused by nonlinear load). Thus it is superior to other passive filtering methods.

IBF parameters obtained by the developed analytical design method will be evaluated via computer simulations, accuracy of the results will be proven via experimental work, and the performance will be compared with conventional passive filters. Design approach limitations will be identified.

The contributions of this thesis are threefold. First, a frequency domain based analytical design method of the IBF for three phase diode rectifier front-end type ASDs has been developed. The method is based on frequency domain modeling of the rectifier and filter. Second, the analytical method is implemented via computer simulations and laboratory experiments and the accuracy of the method has proven satisfactory. Third, detailed performance comparisons with other passive filters have been considered via design, simulation, and laboratory experiments.

Overall, this thesis attempts a detailed IBF analysis and design. The study yields precise filter design rules leading to high performance harmonic filtering. The IBF topology is a strong candidate for harmonic filtering of ASD systems that are IEEE 519 compliant. Through the thesis study, substantial effort has been also spent towards understanding the basic broadband filter and conventional passive filters employed in the harmonic filtering applications. This effort has led to better understanding the differences between various filter topologies and aided establishing the filter selection guideline set forth in this thesis.

This thesis is organized in six chapters. The current (first) chapter provides an introduction to the harmonic filtering concept and defines the thesis subject. The second chapter generally covers the state of the art related to passive filtering techniques for ASD systems. The third chapter classifies the lowpass broadband filters and defines in detail the design method developed for the IBF. In the fourth

chapter, for the selected design parameters, the system is implemented and tested via detailed modeling and computer simulations. Case studies for various power ratings are reported. In the case studies also detailed performance comparison with the standard in line reactors filters and shunt tuned filters is provided. The fifth chapter involves the experimental work for a 5.5kW rectifier load and filtering system prototype. Setup for three different filtering topologies is built, tested and thoroughly investigated. Performance evaluation, comparisons, and correlation with the simulation results are illustrated. The sixth and final chapter provides the concluding remarks that summarize the research results and gives future work recommendations on subjects related to the thesis.

CHAPTER 2

PASSIVE HARMONIC FILTERING METHODS

2.1 Introduction

Although the active filtering technology is well matured and its performance attributes are attractive, as briefly discussed in chapter 1, the passive filtering technique is still the most common approach for current harmonic mitigation of three phase multi-pulse diode/thyristor rectifier systems. Since all the filter components are passive and rugged, and the filter design and implementation procedure is relatively easy and most importantly the filter cost is low, the passive filtering approach is favorable in most applications.

With their simple structure, passive filters have been extensively used for ASD harmonic mitigation to meet the requirements of the IEEE Standard 519 with respect to current TDD limits at the PCC and to voltage distortion THD_V at utility supply side. On the contrary to phase multiplication, active filters, hybrid filter systems, and PWM rectifiers, in passive harmonic filtering techniques, no electronic circuits and hardware, and no complicated control algorithms are designed and implemented. Consequently, passive filters are relatively inexpensive means for eliminating current harmonic distortion and improving the system performance. Therefore, passive filters usually have the priority among other effective filtering types.

Of the passive harmonic filtering methods, the AC in line reactors, the DC link inductance, shunt tuned filter, and lowpass broadband LC filter topologies are discussed in this chapter. General design rules, performance attributes, and the most significant advantages and disadvantages are presented.

2.2 Input Current Harmonic Distortion of ASD Systems

An ASD system with a basic 6-pulse diode bridge rectifier, shown in Fig. 2.1, has typically an input line current waveform and harmonic spectrum as shown in Fig. 2.2. Harmonics generated have 2p±1 order, where p is the number of pulses in the rectifier output DC voltage. In the harmonic spectrum the first four harmonics are dominant (5th, 7th, 11th and 13th). In the illustrated particular case (low system impedance < 2%) the total harmonic current distortion (THD$_I$) is very high > 70% and the current waveform is highly distorted. The harmonic current content of the basic 6-pulse diode bridge rectifier is highly dependent on the grid where the rectifier is connected. In general a high harmonic current distortion (up to 135%) can be expected when the rectifier is connected to a strong grid and a low harmonic current distortion when connected to a weak grid (down to 30%).
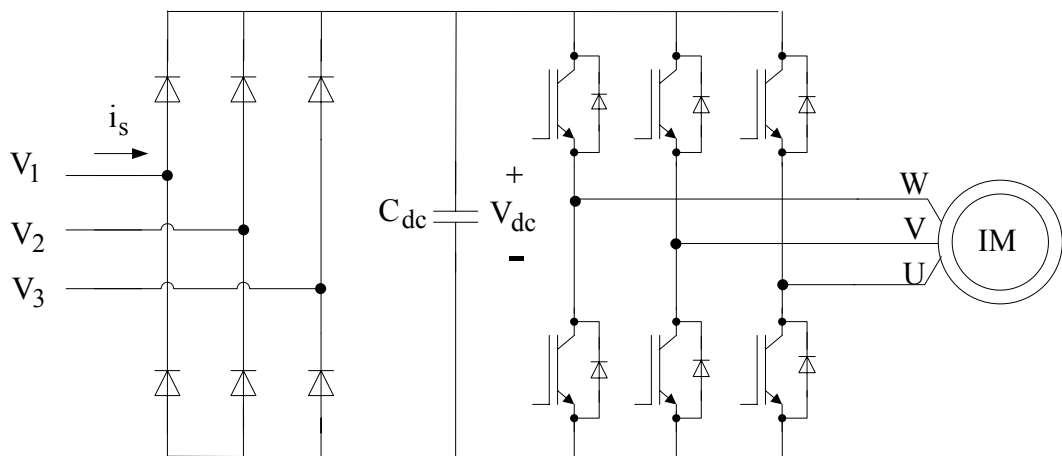
Fig.2.1 Diode bridge rectifier front-end ASD system with no harmonic filters.
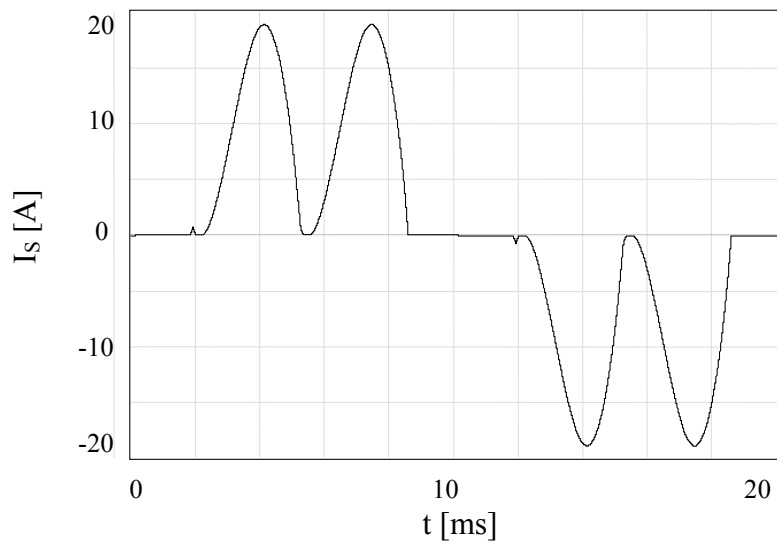
(a)
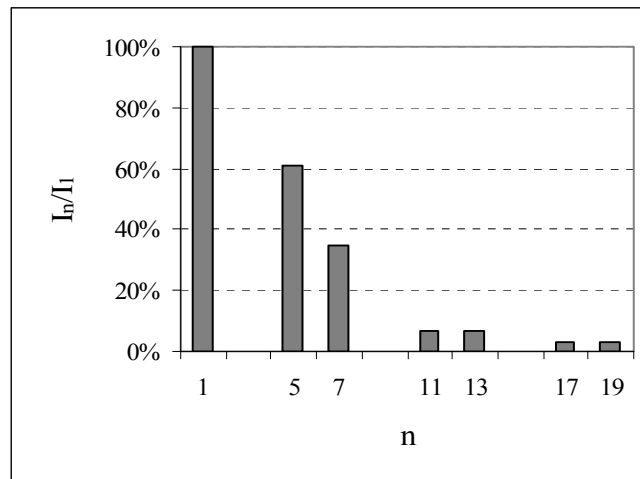
(b)

Fig.2.2 Diode bridge rectifier front-end ASD system (5.5kW) (a): Line current waveform (b): Line current harmonic spectrum.

2.3 Passive Harmonic Filtering Techniques for ASD Systems

Basically in passive filters, the flow of the injected harmonic currents into the utility lines can be prevented by utilizing a high series impedance to block them or by diverting them through a low impedance shunt path. These two methods explain the concept of the series and the shunt passive filters, respectively. Among these, the

series inductance filters provide limited amount of harmonic current suppression with the high cost of significantly reduced output voltage. The tuned filters are effective only in the narrow proximity of the frequency at which the filters are tuned. In contrast, the broadband passive filters have a broader bandwidth and attenuate almost all harmonic currents in this broadband. The broadband passive filters are employing a combination of the two principle methods, with a high series impedance to block the undesired harmonic currents (from flowing to the grid) and a low impedance shunt path to divert the undesired harmonic currents flow (to the capacitive shunt filter).

Among various passive filters, AC line reactors, DC link inductors, tuned shunt filters, and LC lowpass broadband filters are discussed in this section. The first three filters are chosen as they are quite common and will be involved in the comparison study in detail through out the work. The LC lowpass broadband filter is the basic and the first commercial lowpass broadband structure that has been in use [4]. This filter has been improved to the recently developed improved broadband filter in an attempt to overcome the topology deficiencies [6]. Therefore, the LC lowpass broadband filter is involved as the main topology background so that in the following chapter the IBF topology will be studied with sufficient background.

2.3.1 Three Phase AC Line Reactors and DC Link Inductor

The simplest and most economical passive harmonic reduction technique involves the use of AC line reactors (L_{ac}) in front of the ASD's as shown in Fig. 2.3. The series inductance filter (often termed as in-line reactance) is a well established method. Typically 1% to 5% L_{ac} inductors are used [11]. In the USA 3% and in Europe 4% values are commonly utilized. The filter reactance $\omega_e L_{ac}$ are defined as a percentage of the system base impedance (Z_{base}). Z_{base} is given by

$$Z_{base} = \frac{V_R}{I_R} \qquad (2.1)$$

where V_R is the rated phase rms voltage and I_R is the rated phase rms current.

The normalized in line reactance is given by

$$\omega_e L_{ac} \% = \frac{\omega_e L_{ac}}{Z_{base}} \times 100 \qquad (2.2)$$

where Z_{base} is the base impedance given in (2.1) and ω_e is the line electrical angular velocity.

The AC inductor's reactance increases proportional to the system frequency. Therefore, the inductance smoothens the line current drawn by the converter. Hereby, a significantly lower current harmonic distortion can be achieved down to 35 % THD_I range compared to the basic ASD THD_I. This THD_I range can be improved when a DC link inductance is combined with the AC line reactors. Unlike the AC line reactors, the DC link inductance does not cause any reactive voltage drop while contributing to shaping the current waveforms. It is known that the effective impedance of the DC link inductance, when referred to the AC side, is approximate the half of its numerical value. DC link inductor size between 3% and 5% is typically built into some of the commercial ASD systems [11].
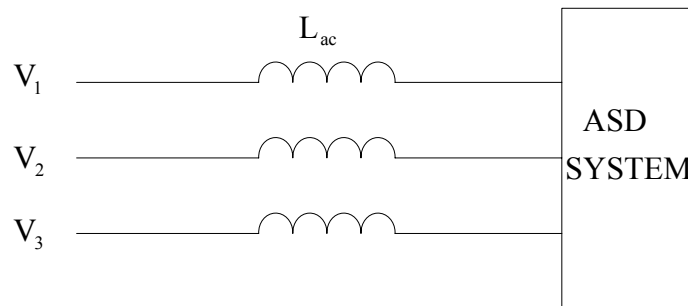
Fig.2.3 Three phase in line AC reactors passive solution for current harmonic reduction in ASD system.

Introducing a three phase AC line reactor between the AC source and the rectifier AC terminals also makes the current waveform less pulsating as the reactor impedes

sudden change in current. The DC capacitor current becomes smaller and more continuous. This increases the lifetime of the DC link capacitors at the load side. However, the drawback of the three phase AC line reactors is a reduced DC link voltage because of increased commutation time needed for current while transferring from the outgoing diode to the incoming diode in the three phase bridge rectifier. In some cases, with high AC line reactors utilized, the rectifier voltage may not be sufficient to serve the load. The reduction of the DC link voltage can be approximately calculated as follows:

At rated conditions the output DC voltage for an ideal case ($L_{ac} = 0\%$) is given by

$$V_{dco} = \frac{3}{\pi}\sqrt{2} \times V_{LL} \tag{2.3}$$

where V_{LL} is the rated rms line to line supply voltage.

The voltage reduction in the DC-link for a specific L_{ac} is given by

$$\Delta V = \frac{3}{\pi}\omega_e L_{ac} \times I_{dc} \tag{2.4}$$

where L_{ac} is the AC in line reactance utilized and I_{dc} is the rated DC load current. Therefore, the normalized DC-link voltage drop is the ratio of (2.4) to (2.3) and it is given by

$$\Delta V\% = \frac{\Delta V}{V_{dco}} \tag{2.5}$$

Assuming constant DC link current I_{dc}, the rectifier rated input current I_R is given by

$$I_R = I_{dc} \times \sqrt{\frac{2}{3}} \tag{2.6}$$

Employing (2.6), after substituting (2.3) and (2.4) in (2.5), for the normalized line reactance in (2.2) the reduction percentage in the DC-link output voltage can be related to the line reactance percentage by

$$\Delta v = 0.5(x_{ac}) \tag{2.7}$$

where x_{ac} is the AC line reactance in percentage ($\omega_e Lac\%$), Δv is the reduction of the DC link output voltage in percentage. i.e. a 3% AC line reactance reduces the DC link voltage by approximate 1.5%.

The main drawback is the high line current THD_I range (> 30%) even though a DC link inductance is combined with the AC line reactors. This THD_I range does not comply with the current harmonic distortion standards in most cases. The typical AC line reactor line current waveform and harmonic spectrum for an ASD system with 5.5 kW rating utilizing 4% three phase AC line reactor are shown in Fig. 2.4. The line current and the supply phase voltage waveforms are shown in Fig. 2.5 with 36% line current THD_I and 0.91 lagging line power factor at full-load.

Typically, this filtering approach results in lagging power factor at full-load that ranges between 0.80 – 0.90 value for three phase diode rectifier bridge front-ends.
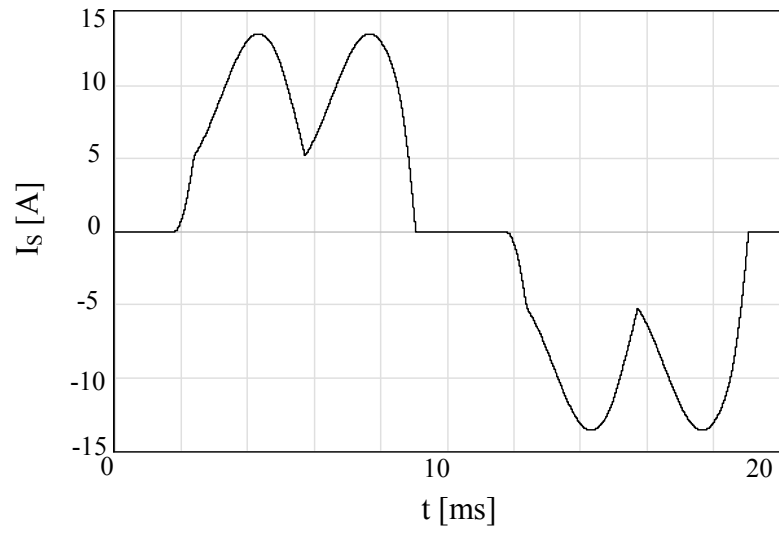
(a)
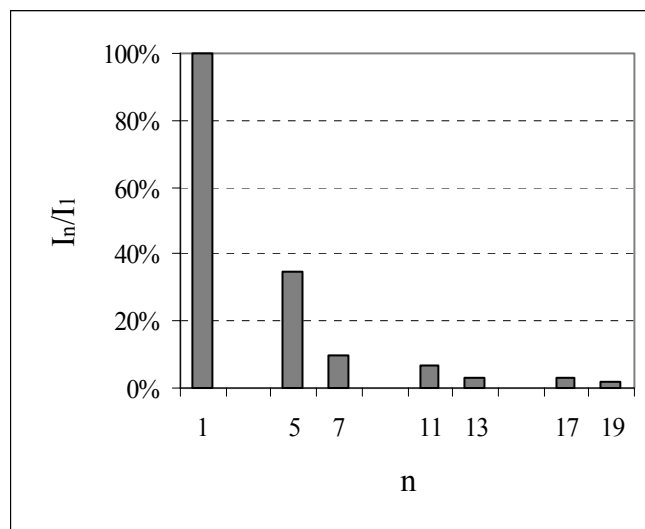
(b)

Fig.2.4 A 5.5 kW ASD system three phase 4% AC line reactor based filtering,
(a): Line current waveform (b): Line current harmonic spectrum.
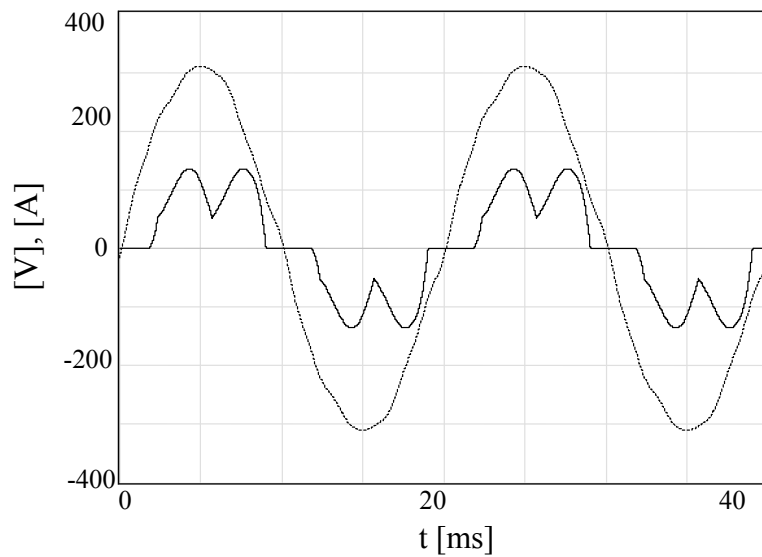
Fig.2.5 A 5.5 kW ASD system three phase 4% AC line reactor based filtering, line current and supply voltage (dotted) waveforms at full-load (current scale: 10x).

2.3.2 Passive Tuned Harmonic Filters

Passive tuned filters can be shunt or series type. In ASD systems and other rectifier applications, in particular at increasing power ratings (above several tens of kilowatts), shunt filters are frequently utilized for harmonic reduction. Shunt filters may be in various configurations, as was illustrated in Fig. 1.5. However, of the various configurations, the single tuned and high pass (2nd order) filters are more frequently implemented The single tuned filter is probably the most common shunt filter in use. It shows very low impedance at the frequency to which it is tuned with the respect to the line impedance. As a result it diverts the flow of the rectifier harmonic current through its path. Harmonic suppression is achieved provided that the line impedance magnitude is considerably higher than the shunt filter impedance at the harmonic frequency.

Single tuned shunt filters also improve the power factor at the fundamental frequency by supplying reactive power to the load. However, a single tuned shunt filter can only eliminate a single current harmonic component. This may not be adequate to

23

filter all the problematic current harmonics effectively. Therefore, for a wide range generated harmonics a single tuned filter is to be designed for each current harmonic to be suppressed, individually.

In designing a single tuned filter, generally the filter capacitor is sized for a known reactive power compensation required to improve the line power factor. Consequently, the filter reactor is defined to provide series resonance impedance (low impedance) at the harmonic frequency to be suppressed. At this resonance frequency, capacitor and inductor impedances are approximately equal in magnitude with opposite signs. Therefore they cancel each other. This impedance is given by

$$Z_o = j\left[\omega L - \frac{1}{\omega C}\right] \tag{2.8}$$

where Z_o is the resonance impedance, L is the filter reactance and C the filter capacitance. And the corresponding series resonance frequency at which the filter is tuned is given by

$$f_s = \frac{1}{2\pi\sqrt{LC}} \tag{2.9}$$

where f_s is the series resonance frequency, L is the filter reactance and C the filter capacitance. The parallel resonance frequency (f_p) that occurs between the single filter components and the total line reactor (supply and L_{ac}) is given by

$$f_p = \frac{1}{2\pi\sqrt{(L_s + L)C}} \tag{2.10}$$

where f_p is the parallel resonance frequency, L_s is the total line reactance, L is the filter reactance and C the filter capacitance.

Practically, the filter series resonance frequency (f_s) is chosen with a detuning factor. The detuning factor (df), given in (2.11) defines the percentage amount of the frequency shift required for the filter series resonance value. The shifted series

resonance frequency usually is chosen 3-8 % below the dominant harmonic frequency considered to be compensated for [12].

$$\text{df} \% = \frac{f_h - f_s}{f_h} \times 100 \tag{2.11}$$

where f_h is the harmonic frequency to compensate for, and f_s is the filter series resonance frequency.

This is done for several practical reasons. One is that a perfect tuning would attract the dominant harmonics of the neighboring nonlinear loads and result in overcurrent condition in the filter and fail. Another reason is that the filter components, in particular the capacitor C parameter decreases due to aging and the tuning frequency moves upwards and design at or above the tuning frequency would result in degraded filter performance as the capacitors age. With lower frequency detuning, the series resonance frequency increases and shift the minimum impedance point closer to the harmonic frequency. This increases the effectiveness of the filters by suppressing more current harmonics. Third, lower frequency detuning may be necessary to move the parallel resonance frequency away from the dominant harmonic frequency to be compensated for. Depending on the line impedance parameters, this may be necessary to avoid large overvoltage stresses on the rectifier terminals due to parallel resonance at the discussed harmonic frequency.

Therefore, the minimum impedance provided by a 5th and 7th single tuned designed filters, shown in Fig. 2.6, will be at a frequency just below the corresponding harmonics frequencies. For instant, applying 4% detuning factor will result in minimum impedance for the 5th and 7th single shunt filters at 240Hz and 336Hz, respectively.

Another design parameter is the sharpness of the filter. The sharpness of the filter depends on the quality factor (Q) which is given by

$$Q = \frac{X_o}{R} = \frac{\sqrt{L/C}}{R} \qquad\qquad\qquad (2.12)$$

where X_o is the reactance of the capacitor or the reactor of the filter at its tuned frequency and R is the damping resistance (a combination of the equivalent filter resistor and the resistance added to the filter). The higher the Q factor, the higher the sharpness of the tuned filter. This factor is seldom considered in regards to filtering action. This is due the fact that the values of R usually result in a significant increase in losses within the filter. Therefore, practically the value of R consists only of the internal resistance of the inductor. In this case the equivalent resistance of the filter usually results in a large value of the Q factor and a sharp filtering action.

In practice the tuned filters are employed for at most a few dominant harmonics. Filtering must begin with the highest harmonic frequency to be filtered and the utilization of the filters for the lower frequency harmonics is necessary to avoid parallel resonance related overvoltages at the lower harmonic frequency. Therefore, filtering the dominant 7th harmonic would require a 7th harmonic filter along with the 5th harmonic filter. In ASD systems below megawatt levels 5th and 7th harmonic filtering is sufficient (higher order harmonic filtering is cost prohibitive also), while at higher power the 11th and 13th harmonics may be considered. A practical filtering system with the 5th and 7th harmonic shunt filters (most dominant) with added input reactors (L_i) and output reactors (L_o) that forms a T-shape topology is configured as shown in Fig. 2.7.
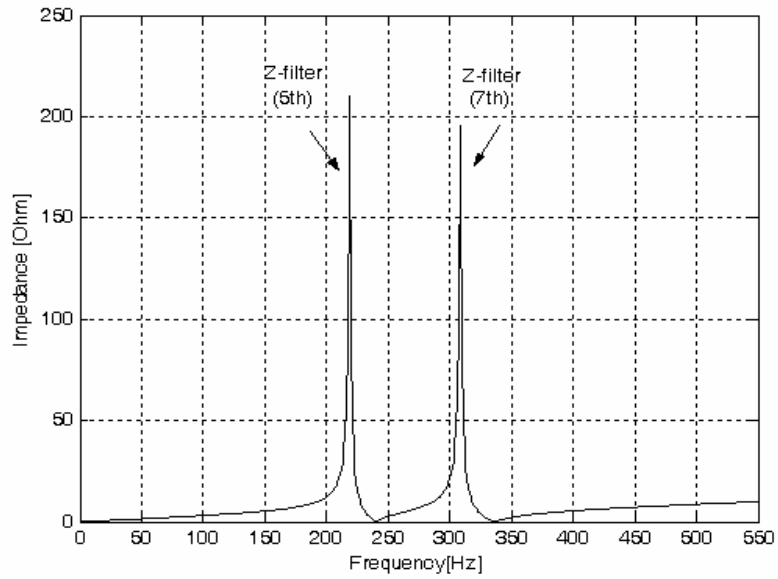
Fig.2.6 The output impedance characteristics of an ASD system
with single tuned 5th and 7th filters.
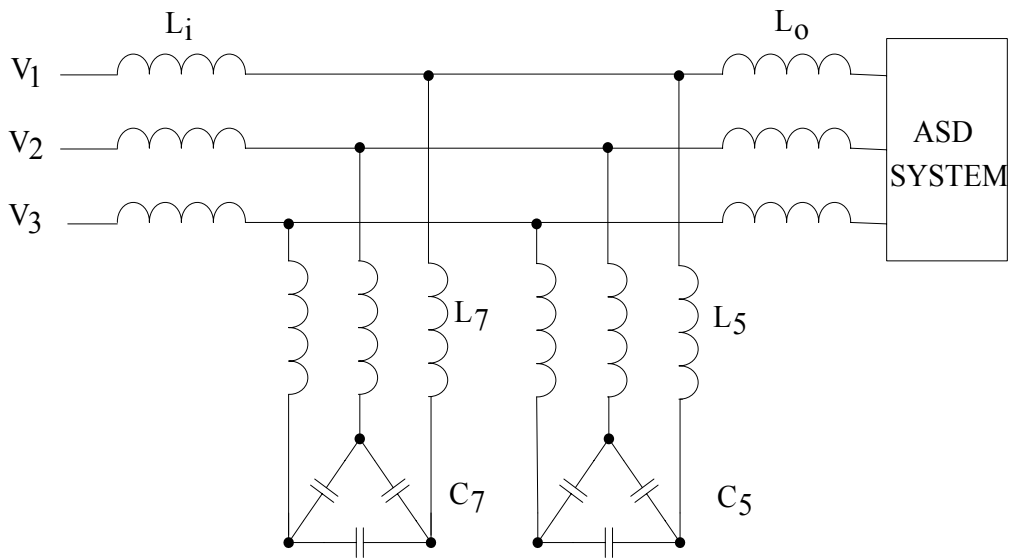
Fig.2.7 An ASD system filter configuration with single tuned 5th and 7th passive
shunt filters and the additional input and output AC reactors.

The rectifier side inductance L_o provides additional smoothing of the rectifier current
and decreases the stress on the shunt filter components while L_i specifies the
impedance ratio that defines the harmonics current fraction that will pass through the

27

shunt filters. The THD$_I$ % reduction is directly proportional to the added line reactor percentages. AC line current waveform and its harmonic spectrum for a typical ASD system are shown in Fig. 2.8. The input power factor is nearly unity (> 0.97) with lagging current at full-load due to the reactive power provided by the capacitors at fundamental frequency.
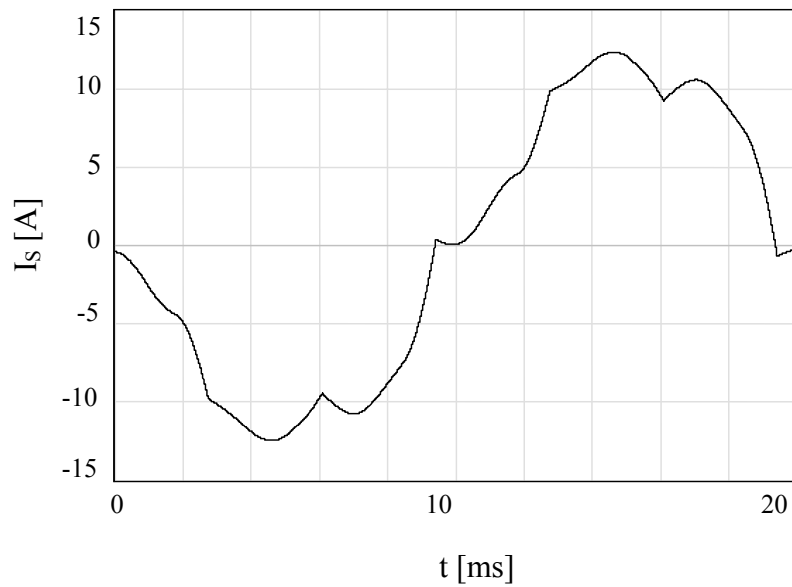
(a)
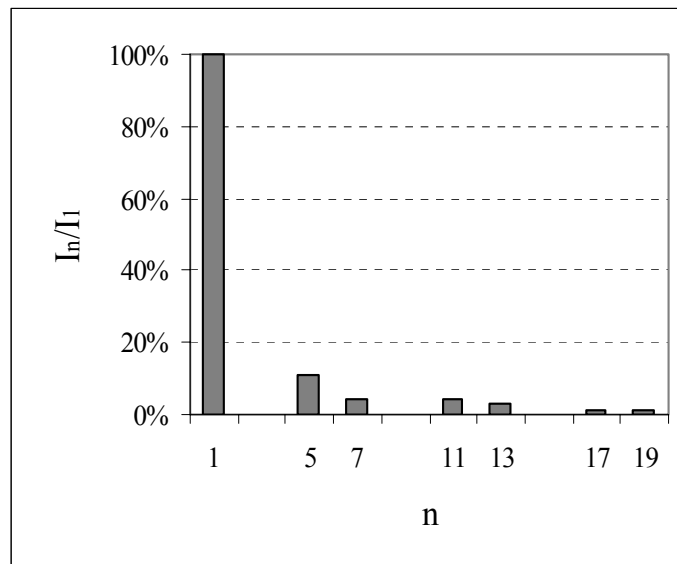
(b)

Fig.2.8 AC line current of the ASD system with the single tuned 5th and 7th passive shunt filters (a): Line current waveform (b): Line current harmonic spectrum.

For a 5.5 kW ASD system with a 6% L_i and 3% L_o and 4% detuning factor, the line current and the supply phase voltage waveforms are shown in Fig. 2.9. The line current has a 13.5% THD_I value and the line power factor is 0.98 lagging at full-load conditions. This is an improvement over the only AC line reactor based filtering approach.
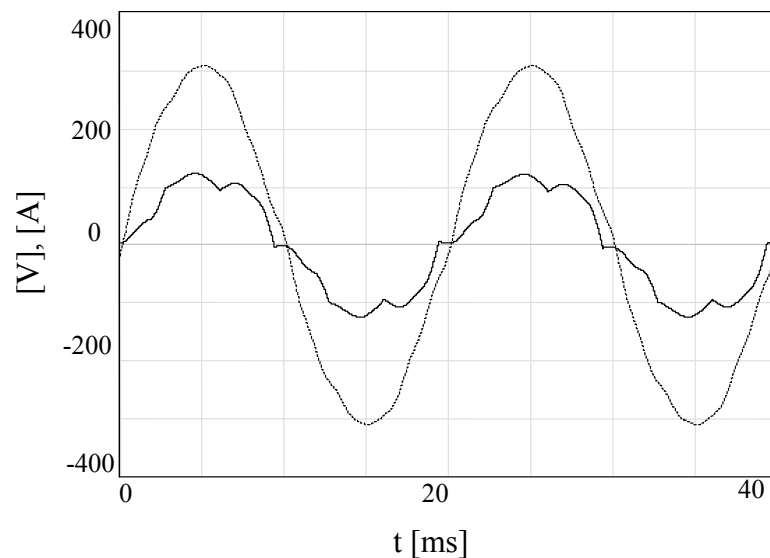
Fig.2.9 Line current and supply voltage (dotted) waveforms at full-load (current scale: 10x).

The filter performance depends on the source impedance value which is usually not accurately known and can vary with system changes. Instability may occur due to parallel resonance with the source impedance. The filter effectiveness is highly affected by the source stiffness. The more the source impedance the more current harmonic suppression is gained. For stiff systems (low source impedance) the design also may require the addition of large AC line reactors (L_i) to achieve the required THD_I performance criteria. Therefore, single tuned filters are not suitable for changing system conditions. Once installed, they are rigidly in place. Neither the tuning frequency nor the size of the filter can be changed easily. Outage of a parallel branch can totally alter the resonant frequency, resulting in overvoltage/overcurrent

29

stressing of filter components [13]. Most of all, the THD$_I$ value is usually difficult to decrease to less than 10% with an economical filtering system size, and that makes the tuned filter approach not IEEE 519 compliant. These main disadvantages have been the driving force behind the development of the lowpass broadband filters.

2.3.3 Passive Lowpass Broadband Harmonic Filters

As detailed in the previous section, often multiple stages of single tuned shunt filters are required in practical ASD applications for effective filtering of the rectifier currents. In a six-pulse rectifier (ASD front-end), the generated characteristic harmonics are the 5th, 7th, 11th, 13th, etc. harmonics. Designing a single tuned shunt filter for each dominant current harmonic so that the widespread harmonics are all filtered would be impractical due to high cost and complexity. Therefore, an alternative harmonic filtering method must be devised.

The lowpass broadband filtering method, briefly discussed in chapter one, is an ideal approach to block the harmonic currents at multiple (widespread) frequencies. The rectifier current components with frequencies below the filter cutoff frequency can pass to (from) the AC line. However, current components with frequencies above the cutoff frequency are filtered out. Practically, broadband filters are designed to achieve a cutoff frequency that is less than the first dominant harmonic frequency.

Lowpass broadband filters utilize a large series AC line reactor to prevent the unwanted harmonics from flowing to the line. A capacitor bank is installed in parallel with the rectifier (with or without an additional filter reactor) in order to divert the undesired harmonic current's from flowing through the AC line and direct the harmonics towards its lower impedance at the harmonics frequencies (compared to the line impedance at the same harmonic frequencies). This single shunt filter is sufficient to suppress all the harmonics (the broadband) and avoids the harmonic magnification problem by decreasing the parallel resonance frequency away from the dominant injected harmonics frequencies. This is one major advantage of utilizing lowpass broadband filters.

A simple LC type lowpass broadband filter, shown in Fig. 2.10, consists of a large input AC line reactor (L_i) along with the shunt filter capacitor (C_f) which is usually Δ connected ($C_f = C_{fY} = 3C_{f\Delta}$).The capacitor terminals are connected to the rectifier load. This simple filter can be designed to achieve satisfactory line current THD level and to a lesser extent input power factor. However, due to the overvoltage at the capacitor and therefore rectifier terminals (over a wide range of load from no-load to full load), the components and the drive get overstressed and may fail. Typical waveforms relating to the simple LC filter and its overvoltage problem are shown in Fig. 2.11 and Fig. 2.12 at full-load and no-load respectively. The rectifier terminal voltage is much larger than the AC line voltage, and therefore the DC bus voltage can be significantly higher than the nominal value leading to drive failure. To avoid the overvoltage problem related issue, the input AC line reactor is designed in combination with a step-down transformer (buck transformer). The structure of such a filtering system is shown in Fig. 2.13, [4]. The buck transformer can be realized in of the following methods; three single-phase transformers or one three-phase transformer wound on a three-phase E-core. Considering space and cost, the three-phase transformer is preferred. An alternative to using the buck transformer configuration would be the use of an autotransformer with taps appropriate to the reduced output voltage desired, or other passive means of reducing the line voltage [4]. With the inclusion of the buck transformer, the filter overvoltage problem is eliminated at the expense of higher cost, reduced efficiency, and increased complexity. However, the input power factor and current THD performance is about the same as the simple LC structure.

31
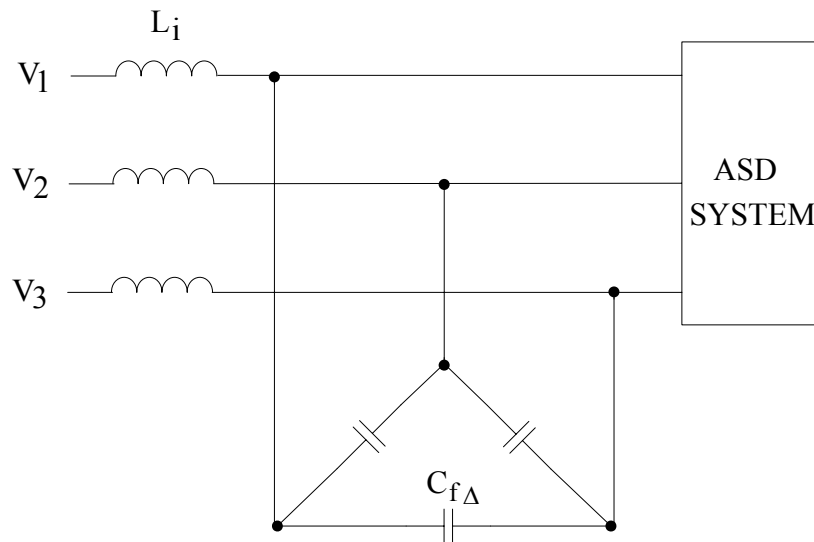
Fig.2.10 A simple lowpass LC broadband filter.

t [ms]
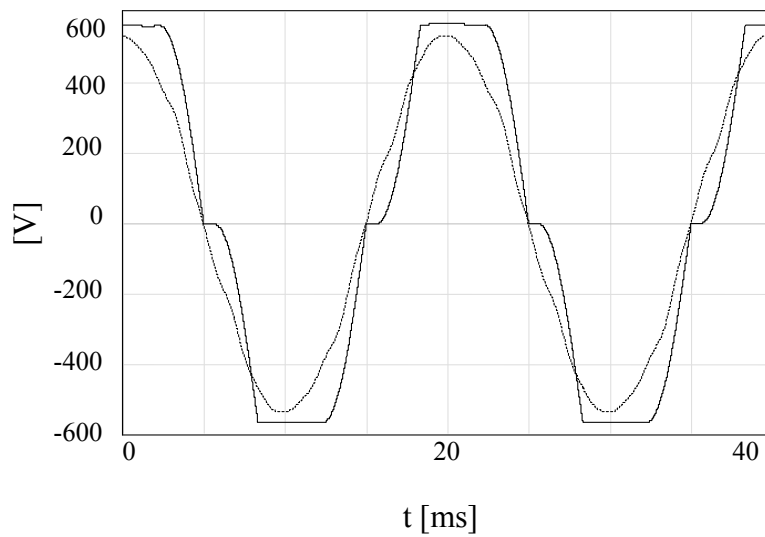
Fig.2.11 LC Lowpass broadband filtering based system line-to-line supply (dotted)
and rectifier voltage waveforms at full-load (5.5 kW ASD system)
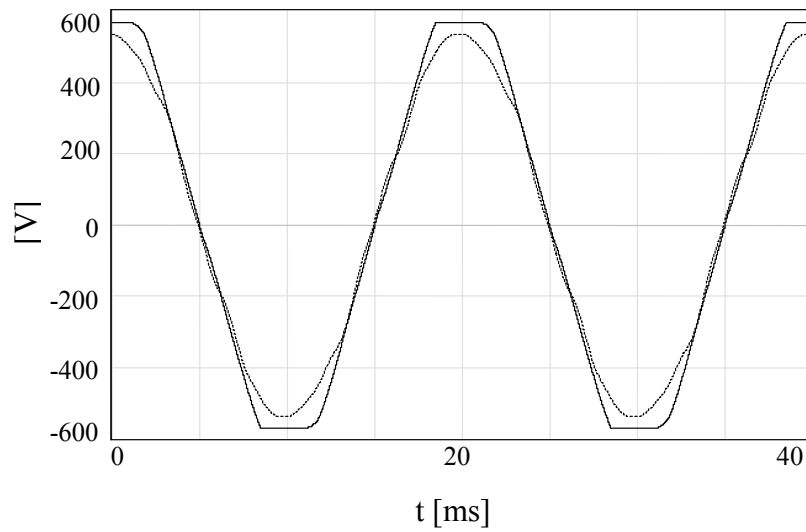
Fig.2.12 LC Lowpass broadband filtering based system line-to-line supply and rectifier (dotted) voltage waveforms at no-load (5.5 kW ASD system).
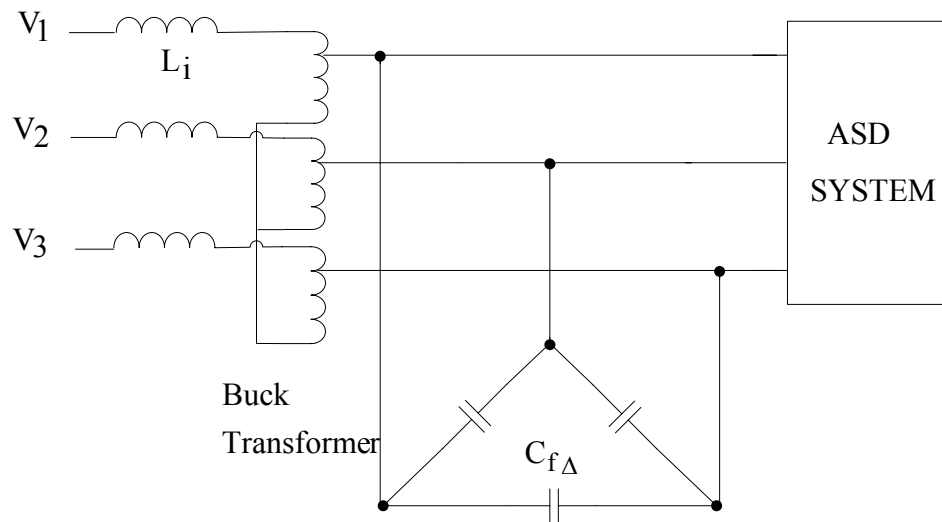
Fig.2.13 A lowpass LC broadband filter with step-down (buck) transformer.

The design rule for the LC broadband filter as a first step involves installing 25% three phase AC line reactors in series with the main AC lines. These large AC

33

reactors provide sufficient impedance to minimize importing any current harmonics already existing in the AC lines. Consequently, filter capacitors do not get overloaded. Furthermore, the rectifier harmonics are also blocked and can not flow to the AC grid. The AC line reactors also act as buffer between the power system and the drive. They prevent parallel resonance at the harmonic frequencies and therefore no harmonic amplification.

The filter capacitors are sized to result in a low parallel resonance frequency value between 80 to 170Hz with the AC line reactors as practically there is no current harmonic to be injected in a three-phase ASD system in this frequency band. With this low parallel resonant frequency, the filter is unlikely to excite any undesired resonance with the rest of the system. With this choice, the filter capacitors will show low impedance at the injected harmonic frequencies with respect to the large AC input line reactors impedance (shown in Fig. 2.14), and the rectifier harmonic currents will mainly flow to the filter capacitors. In Fig. 2.14, Z_{line} is defined in the following.

$$Z_{line} = \left|(R_i + R_s) + jn\omega_e(L_i + L_s)\right| \tag{2.13}$$

where R_i and R_s are the filter inductor equivalent series resistor and the line equivalent series resistor, L_i and L_s are the input series filter inductor and the source equivalent inductor, respectively and

$$Z_{capacitor} = \left|\frac{1}{n\omega_e C_f}\right| \tag{2.14}$$

where C_f is the shunt filter capacitor.

A high impedance ratio between the line impedance and the capacitor impedance at all generated dominant harmonic frequencies in 6-pulse full bridge rectifiers is sufficient to divert the harmonics through the shunt path. Meanwhile, it is apparent that the fundamental component current will flow from the AC line to the rectifier as the impedance ratio is quite low at 50Hz.
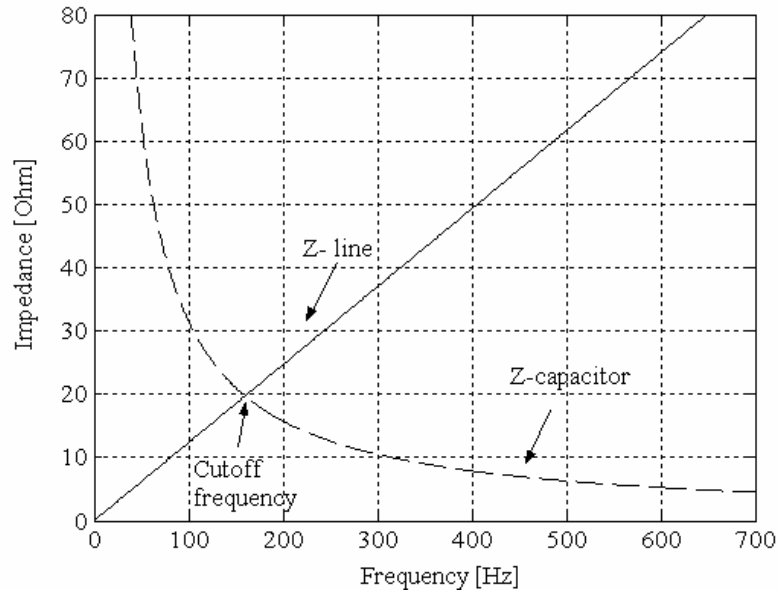
Fig.2.14 LC Lowpass broadband filter parallel branch (capacitor) impedance and series branch (inductor) impedance characteristics of a 5.5kW ASD system.

The LC broadband filter line current THD performance is certainly significantly better than a simple AC line reactor. The AC line current waveform and its harmonic spectrum for a typical ASD system with LC filter are shown in Fig. 2.15. The filter can generally reduce the overall line current harmonic distortion from 50% to approximately 9 -12% range under rated load conditions [3]. The line power factor is high ($\geq$ 0.9) and leading at all loading conditions.
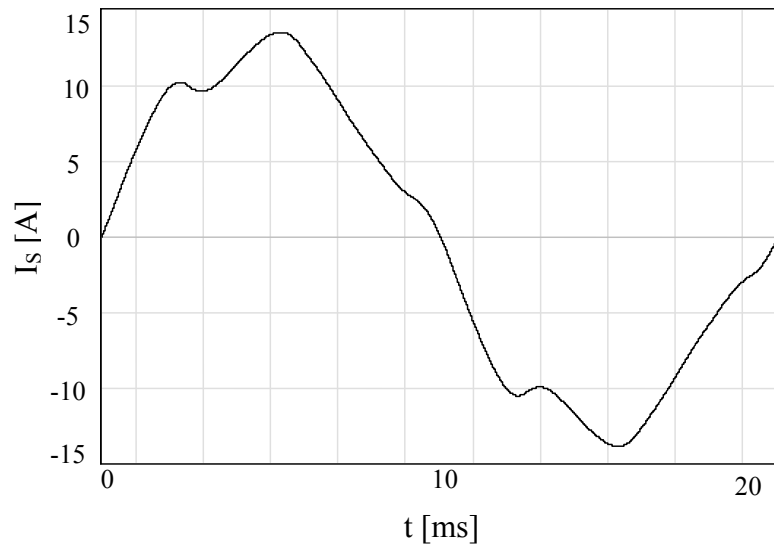
(a)
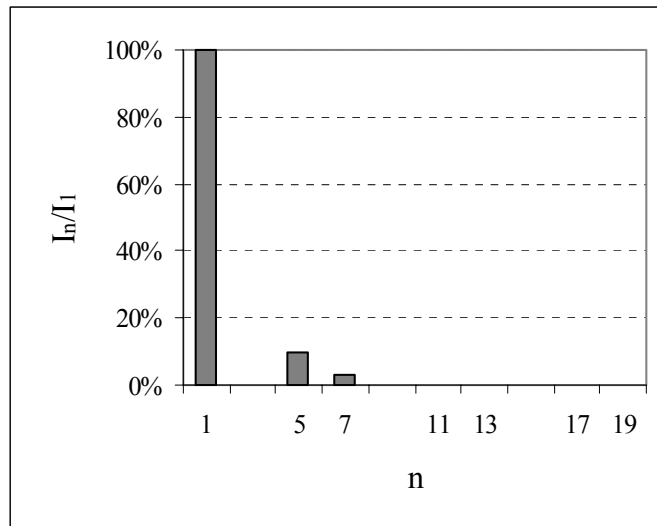
(b)

Fig.2.15 Lowpass LC broadband filter at full load (5.5 kW ASD system) (a): Line current waveform (b): Line current harmonic spectrum.

For a 5.5kW ASD system, a 25% AC in line reactor is utilized and the capacitor is sized for 170Hz parallel resonant frequency. The line and rectifier current waveforms are shown in Fig. 2.16. The line current has a 10.3% THD_I value. The supply phase voltage and line current waveforms are illustrated in Fig. 2.17, with 0.91 leading line power factor at full-load.

Filtering is free of harmonic resonance problem with the other harmonic sources, which is risky with the conventional single tuned filters. However, the light-load and full-load overvoltages are problematic in this simple lowpass LC broadband filter structure. The leading power factor requires improvement and the use of the buck transformer increases the cost and the installation space required.
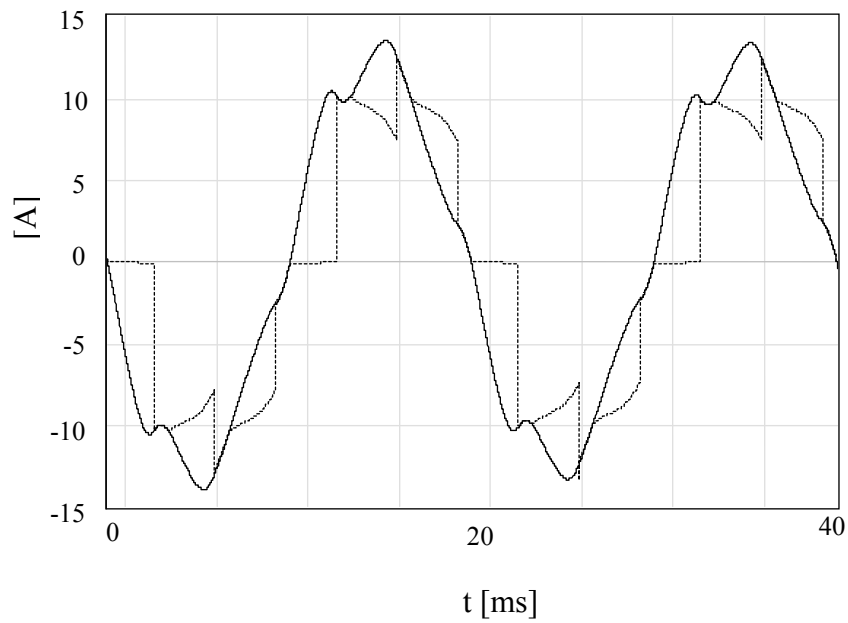
Fig.2.16 Line and rectifier (dotted) current waveform of a 5.5kW ASD system.
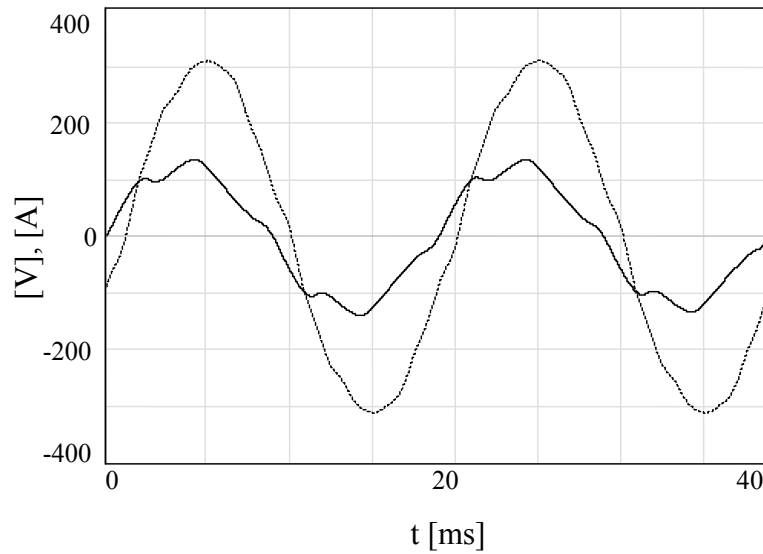
Fig.2.17 Line current and supply voltage (dotted) waveforms at full-load (5.5 kW ASD system).

In the LC broadband filter, improvement of the line power factor value requires utilizing smaller filter capacitors. As a result, this will reduce the overvoltage problems. However; the line current THD increases and will not meet the requirements of the harmonic standard limitations. This trade-off relation between the power factor and current THD_I is another major weakness, shown in Table 2.1, of the LC broadband filter. The trade-off relations are illustrated numerically for a 5.5 kW rating filter in Table 2.1. Considering L and C as base values, incrementing and decrementing one variable at a time by 5%, the performance is evaluated and posted in the table. As the table indicates, the power factor and current THD trade-off relations are strong. Therefore, reduced THD comes at the cost of bad power factor while improved power factor comes at the cost of high THD. To overcome this deficiency, the improved broadband filter has been developed.

Table 2.1LC broadband filter performance for various LC values for 5.5kW ASD system

Li (mH)	CfΔ (µF)	Line THD$_I$ (%)	Line PF (Leading)	V$_{dc}$ Mean Full-Load	V$_{cf}$ Peak Full-Load	V$_{dc}$ Mean No-Load	V$_{cf}$ Peak No-Load
19.6	14.9	10.2	0.914	556	560	689	693
18.6	14.9	10.8	0.911	553	556	691	680
20.58	14.9	9.5	0.918	560	563	687	690
19.6	14.1	10.7	0.920	552	556	683	683
19.6	15.6	9.75	0.909	559	563	694	698

2.4 Summary

This chapter provided general knowledge of the common passive harmonic filtering methods and their associated circuit topologies that are utilized for ASD harmonic mitigation. The study involved the three phase AC line reactors, the DC link inductance, shunt tuned filters and the simple lowpass LC broadband filter. Weakness, strength, basic design rules and performance characteristics of the various passive harmonic filtering alternatives have been presented.

As illustrated in the previous chapter and this chapter with examples, diode rectifier front-end based ASDs without appropriate filtering inject significant amount of harmonic currents to the AC line and pollute the AC grid resulting in power quality problems. Therefore it becomes apparent that harmonic mitigation is mandatory for ASD systems.

Of the various passive harmonic filtering methods presented, the lowpass broadband filtering method is more attractive due to its superior performance. However, the simple lowpass LC broadband filter has a main deficiency and further progress in the

topology is inevitable. Therefore the improved broadband filter topology (presented in next section) has been developed to achieve better performance at all operating conditions. With significant performance improvement, the improved broadband filter has been gaining wide acceptance and becoming a viable method for harmonic mitigation in ASD applications. The next chapter involves a thorough study of the improved broadband filter.

CHAPTER 3

THEORY AND DESIGN OF THE
IMPROVED LOWPASS BROADBAND FILTER

3.1 Introduction

In the previous chapter, the common passive filtering methods used for ASD harmonic mitigation were studied. Their general design rules and performance attributes were discussed. Among the passive harmonic filters discussed, the LC lowpass broadband filter has been found as a more practical approach for harmonic filtering. The filter has superior performance to the other filtering methods discussed. It is effective in suppressing the rectifier current harmonics, it is simple and free of harmonic resonance problems. However, the simple structure of the filter comes with a serious drawback which is the rectifier terminal overvoltages. As a result, the Improved Broadband Filter (IBF) has been developed in order to overcome the deficiency of the LC filter and obtain superior overall performance characteristics.

In this chapter the IBF topology is under investigation. The filter construction, operating principle, behavior analysis and finally detailed design method are described.

3.2 The Improved Lowpass Broadband Filter Topology and Its Operating Principle

The IBF circuit topology is configured as shown in Fig. 3.1. The three phase AC power line is connected to a three phase AC input reactor (L_i) and to a damping

resistor (R_d). The center leg consists of an AC series filter reactor (L_f) and capacitor bank (C_f) which forms a shunt filter. The capacitor bank is usually Δ connected ($C_f = C_{fY} = 3C_{f\Delta}$). Finally, a three phase AC output reactor (L_o) is inserted between the rectifier terminals and the L_i-L_f connection terminals of the filter.

With an appropriate design, at the dominant rectifier current harmonic frequencies (over a wide frequency range), the large input reactor (L_i) provides high impedance (rectifier to line impedance Z_{RL}) with respect to the shunt filter impedance, as shown in Fig. 3.2, so that all rectifier current harmonics will be impeded by the line and diverted to pass through the shunt filter. The line impedance Z_{line} is found by Equation (2.13) and the shunt filter impedance is given by

$$Z_{shunt} = \left| R_{Lf} + j(n\omega_e L_f - \frac{1}{n\omega_e C_f}) \right| \qquad (3.1)$$

where R_{Lf} is the filter inductor equivalent series resistor, L_f and C_f are the shunt filter reactor and capacitor, respectively.

Not only L_i provides sufficient impedance that minimizes current harmonics flow from the rectifier to the AC line, but it also minimizes the effect of the line voltage harmonics on the rectifier as a result of the line to rectifier high impedance Z_{LR} provided at the line dominant harmonics (i.e. provides harmonic isolation between the source and the rectifier). Due to large L_i the line voltage harmonics can not force significant harmonic current on the shunt filter either. Therefore, the duty of L_i reactor is to block current harmonic flow either way.

As the parallel resonance frequency is lower than the dominant rectifier current harmonic frequencies, the risk of harmonic resonance is avoided. The filter capacitor C_f improves the input power factor by providing full fundamental frequency reactive power compensation. The real power P is flowing from the supply to the load. L_f is partitioned with L_i such that there is no overvoltage at the rectifier terminals (unlike the LC filter) and no-load to full-load filter output voltage change is confined within the specified range. The filter components L_f and C_f are connected in series to

42

provide very low series impedance to the rectifier current harmonics and short circuit them through its path. The output reactor (L_o) is a current smoothing reactor that makes the rectifier current waveform less discontinuous, resulting in lower current harmonics. Utilizing L_o reduces the rectifier THD_I significantly (by approximately 50%). The reduction in the rectifier current harmonics implies less harmonic current and voltage stress on the shunt branch components L_f and C_f. Hence, smaller, lower cost, and more efficient filter structure. The resistance R_d is employed to damp the voltage/current peaks during switching transients.
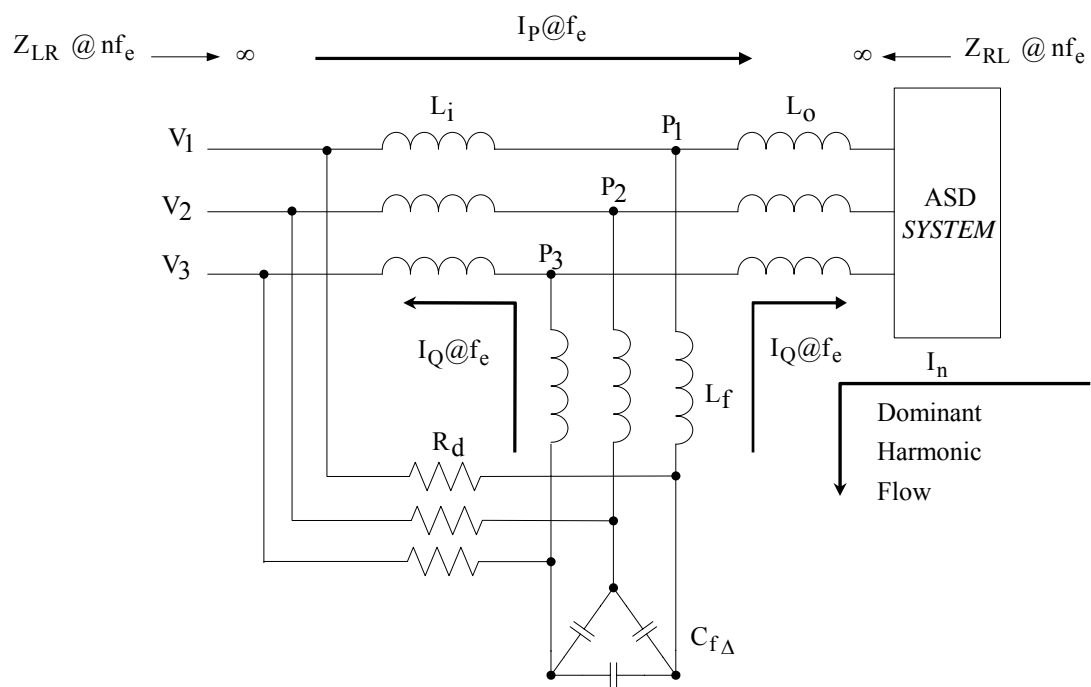
Fig. 3.1 Improved broadband filter circuit diagram.
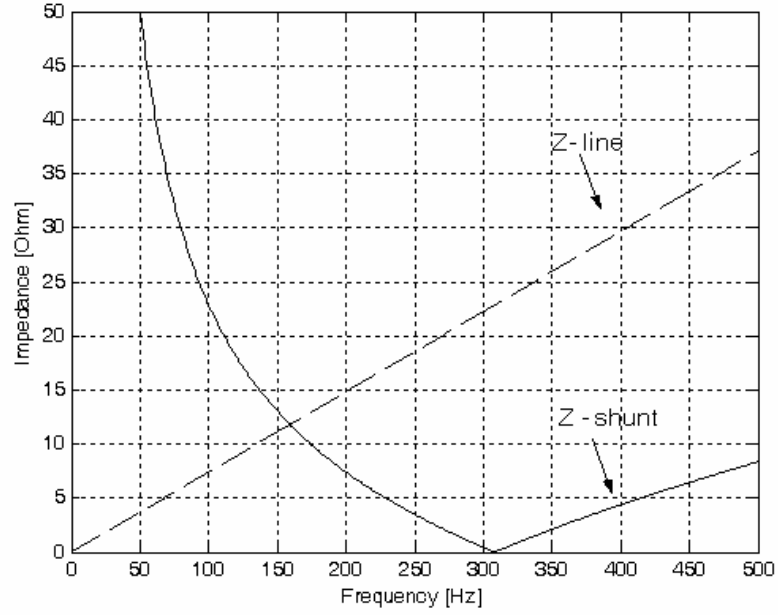
Fig. 3.2 Line and shunt branch impedance for the IBF (5.5 kW system).

3.3 Improved Broadband Filter Design

In the filter design process, several practical constraints are considered for full-load and no-load operating conditions. These are the AC line (input) current THD_I, line (input) power factor (PF), filter output voltage (rectifier input voltage) regulation (ΔV_o %), filter parallel resonance frequency (f_p), and no-load input current (I_{NL}). Cost, size, and efficiency are either implicitly dependent on these variables, or they could be considered as additional constraints in the design.

The line (input) current total harmonic distortion, THD_I is given by

$$THD_I = \frac{\sqrt{\sum_{n=2}^{N} I_n}}{I_1} \qquad (3.2)$$

where I_n and I_1 are the rms values of the individual line current harmonics and line current fundamental component, respectively.

The line (input) power factor is basically given by

$$PF = \frac{P}{S} \tag{3.3}$$

where P is the real average power and S is the apparent power. Assuming the line voltage is free of harmonics, for non-sinusoidal line current waveforms, utilizing the P and S formulas, the power factor is given by

$$PF = HF \times DPF \tag{3.4}$$

where HF is the harmonic factor given by

$$HF = \frac{I_1}{I} \tag{3.5}$$

where I is the line (input) current rms value.
The displacement power factor DPF is given by

$$DPF = \cos\phi \tag{3.6}$$

where ϕ is the phase angle (displacement angle between the line voltage and phase fundamental current).

The filter output voltage regulation in percentage (ΔV_o %) at the filter node (P), shown in Fig. 3.1, from full-load to no-load is given by

$$\Delta V_o\% = \frac{V_P(NL) - V_P(FL)}{V_P(NL)} \times 100 \tag{3.7}$$

where $V_p(NL)$ and $V_p(FL)$ are the no-load and full-load filter node (P) rectifier voltage. Equation (3.7) could also be defined in terms of line-to-line voltages.

As there is no current harmonics injected to the line at no-load, the I_{NL} total rms and fundamental rms values are assumed to be equal. At the fundamental frequency, the reactance formed by L_i and L_f is significantly lower than the damping resistor R_d. Therefore, R_d can be considered open circuited for the purpose of no-load current calculation. Then, the rms fundamental no-load line current is given by

$$I_{NL} = \frac{V_1}{Z_f + Z_i} \tag{3.8}$$

where V_1 is the rated utility phase voltage fundamental component rms value, Z_f is the shunt filter impedance (L_f, C_f) and Z_i is the input impedance, both at the fundamental frequency.

The parallel resonance frequency (f_p) is given by

$$f_p = \frac{1}{2\pi\sqrt{(L_i + L_f)C_f}} \tag{3.9}$$

where L_f is the filter reactor, L_i is the input reactor and C_f is the filter capacitor.

For a given set of design constraints, the design problem is progressed in two steps. First, employing analytical formulas approximate filter parameter values are obtained. Second, these values are utilized (as initial values) in the detailed frequency domain model of the rectifier and the filter system such that accurate filter parameters are calculated in a computer program. For the frequency domain model, the system equations are evaluated in a MATLAB [14] code that increments (decrements) the parameters until optimal results are obtained. It is observed that the first step that provides the approximate filter parameter values is essential in reducing the total calculation time to obtain accurate results. In the following, the approximate design method will be discussed and the accurate design method will

follow. However, before further delay, the assumption regarding the choice of the AC reactor L_o will be stated first.

3.3.1 Output Reactor L_o Selection Method

In all cases, for the purpose of THD_I reduction and L_i, L_f, C_f stress reduction, 4 % L_o is selected and utilized. If not, THD_I can increase and the filter components may become larger as the current rating increases. Contrarily, if L_o is selected larger, THD_I can be further decreased, but the filter cost will increase. A practical value lies between 3% and 4%. Therefore, 4 % L_o will be assumed throughout this work.

3.3.2 Approximate Design Method of IBF

In the approximate method, the filter parameters L_i, L_f, and C_f are calculated by selecting approximate range for the parallel resonance frequency, series resonance frequency, and the no-load to full-load line current ratio. In the approximate method, the effect of the damping resistor R_d is considered negligible and R_d is not included in the circuit model. While the parallel resonance frequency is defined in (3.9), the shunt branch series resonance frequency is given by

$$f_s = \frac{1}{2\pi\sqrt{L_f C_f}} \tag{3.10}$$

where L_f and C_f are the filter reactor and capacitor respectively.

The input current no-load value to full-load value ratio, α is given by

$$\alpha = \frac{I_{NL}}{I_{FL}} \tag{3.11}$$

where I_{NL} is the no-load input current fundamental component rms value given by (3.8), and I_{FL} is the full-load input current fundamental component rms value.

The rated rectifier input current rms value and its fundamental component value can be found from the ASD input ratings and the rectifier filter parameters (excluding the broadband filter parameters). Based on the values of the DC link inductor and AC line reactors utilized in the drive, there may be two different practical rectifier current waveforms. If the DC link inductance is very large and no large AC line reactors are utilized, then the rectifier input current becomes nearly rectangular waveform (Fig. 3.3) which is named stiff current source. Based on the rms value formula and the Fourier series analysis, the rated rectifier input current rms value and its fundamental component rms value can be calculated.

The rectifier current rms value for the rectangular waveform is given by

$$I_R = A \times \sqrt{1 - \frac{u}{\pi}} \tag{3.12}$$

where A is the waveform amplitude and u is the phase shift between the positive and the negative halves of the current waveform.

Assuming that the DC link current magnitude I_{dc} (A in Fig. 3.3) is constant and u equals to 60°, the rated rectifier current rms value I_R is given by

$$I_R = 0.816 \times I_{dc} \tag{3.13}$$
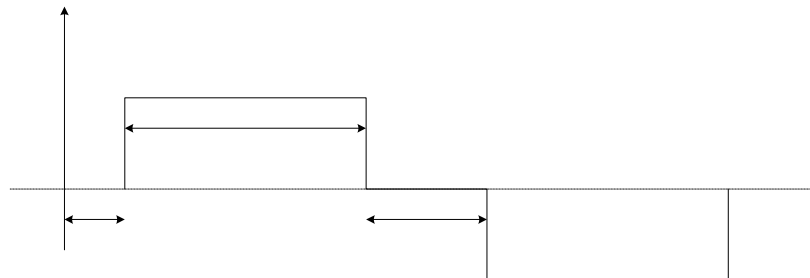
Fig. 3.3 Rectangular wave rectifier phase current waveform ($L_{load} = \infty$).

48

From Fourier analysis, the rectifier current fundamental component peak value is given by

$$I_{1peak} = \frac{2\sqrt{3}}{\pi} \times I_{dc} = 1.103 \times I_{dc} \tag{3.14}$$

and the corresponding rectifier current fundamental component rms value is given by the following.

$$I_{1rms} = \frac{I_{1peak}}{\sqrt{2}} \cong 0.78 \times I_{dc} \tag{3.15}$$

In a typical ASD, on the other hand, there is a small DC link inductance or no inductance is used at all. On the AC side of the rectifier, usually AC line reactors are employed. In this case, the rectifier input current waveform is smoother (Fig. 3.4(a) soft current source) with harmonic spectrum shown in Fig.3.4 (b). Typically, the rectifier input current waveform in this case involves a relatively larger 5th harmonic compared to the stiff current source case (Fig. 3.5).
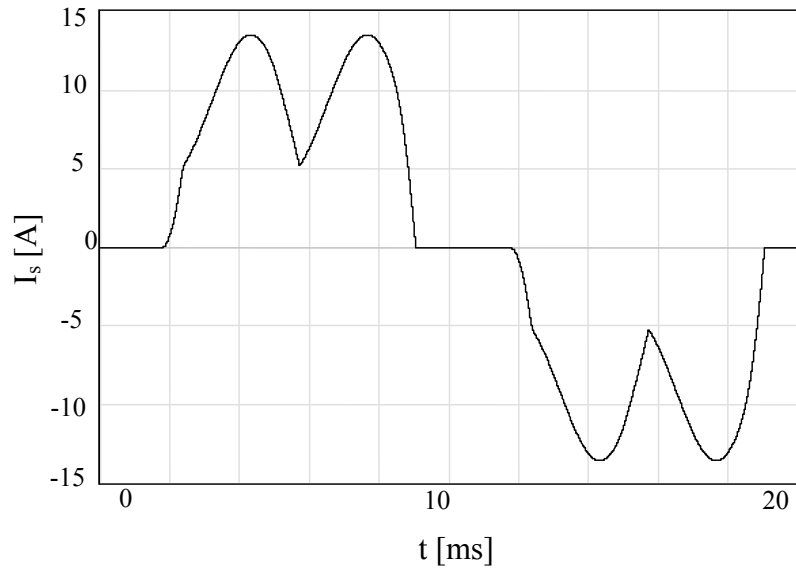
(a)
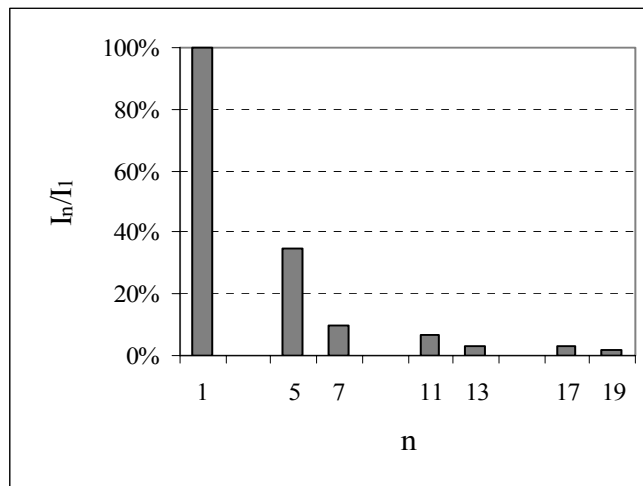
(b)

Fig. 3.4 Soft DC current source (a): Rectifier current waveform (b): harmonic spectrum.
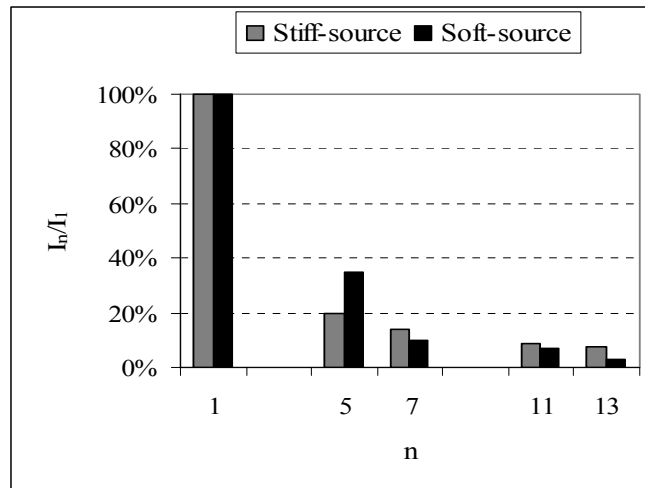
Fig. 3.5 Rectifier current harmonic spectrum comparison of stiff and soft DC current sources.

The commonly used (in Europe) 4% AC line reactance in ASD systems (with no large DC link inductance) results in a rectifier current such that the rectifier can be considered as the soft (non-stiff) current source. The rectifier current harmonic numerical values for the soft current source case are shown in Table 3.1 and compared to the stiff current source case. These ratios will be utilized in all the power ratings as the power rating dependency of ratios is minimal and negligible.

Table 3.1 Rectifier current harmonic ratios for soft and stiff current source cases

	Soft Current Source	Stiff Current Source
I_1/I_1 (%)	100	100
I_5/I_1 (%)	34	20
I_7/I_1 (%)	9.5	14
I_{11}/I_1 (%)	7	9
I_{13}/I_1 (%)	3.5	7.7
Higher Order Terms	Neglected	Neglected

The full load rectifier AC side current fundamental component I_{FLR} is related to the full load DC link current mean value I_{dc} with the fundamental stiffness factor β_1 as defined in the following.
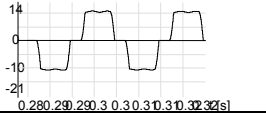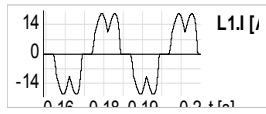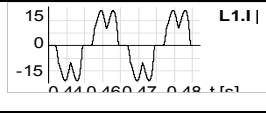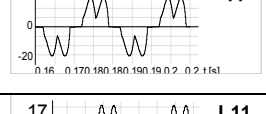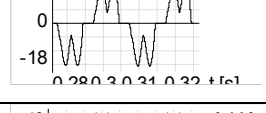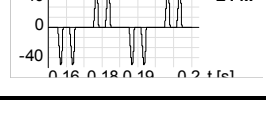
$$\beta_1 = I_{FLR}/I_{dc} \qquad\qquad (3.16)$$

The full load rectifier AC side current rms value I_R is related to the full load DC link current mean value I_{dc} with the rms stiffness factor β_{rms} as defined in the following.

$$\beta_{rms} = {I_R}\Big/{I_{dc}} \qquad\qquad (3.17)$$

Both stiffness factors β_1 and β_{rms} were investigated for various filter types and various rectifier current waveform types by means of computer simulations and compared to its value for the rectangular rectifier current waveform. As shown in Table 3.2, the fundamental stiffness factor has a value that varies in a narrow range (0.78-0.79) for various rectifier current waveforms while the THD_I values vary over a wide range (24 – 44 %) depending on the filters utilized. Even at the extreme value of 135 % THD_I (with no filter utilized), the β_1 value is 0.81. Therefore, the fundamental stiffness factor for 4 % AC line reactor (L_{ac}) based filtering method is considered 0.79 which is approximately the same value for as in the rectangular rectifier current waveform. However, the rms stiffness factor β_{rms} has a value that varies in a wider range (0.8-0.9) for the same rectifier current waveforms with an extreme value of 1.37. An rms stiffness factor value of 0.84 is considered for the 4 % L_o value chosen. This conclusion is also valid for various power ratings considered (proven but not shown).

Table 3.2 Stiffness factor values for various filtering topologies for 5.5 kW system

Filter Type	Rectifier Current Waveform	THD$_I$ (%)	I$_{dc}$ Mean (A)	I$_1$ rms (A)	β_1	β_{rms}
L$_{dc}$ (∞)		24	10.57	8.23	0.779	0.801
6% L$_{ac}$		31	11.30	8.86	0.784	0.820
TF 5th,7th		33	11.05	8.67	0.785	0.825
4% L$_{ac}$		36	11.16	8.79	0.787	0.837
3% L$_{ac}$		41	11.14	8.79	0.789	0.854
IBF		44	10.65	8.43	0.791	0.893
0% L$_{ac}$		135	10.38	8.44	0.813	1.369

Assuming that an L$_{ac}$ of approximately 4 % is being utilized in the IBF based system, the fundamental stiffness factor can be taken as 0.79. Therefore Equation (3.16) can be utilized as a defining relation between the AC side fundamental component and DC side currents of the rectifier.

In IBF, if the filter is assumed to be lossless, the utility side power factor near unity, the rectifier output voltage rms value equal to the rated line voltage, and the diode rectifier displacement power factor being unity, then a power balance equation involving the fundamental components can be written. With the design completed and the results obtained, it will be shown that all these assumptions are acceptable for the purpose of initial parameter calculation. The first result of such assumptions is

that the rectifier full load current fundamental component is equal to the line current fundamental component.

$$I_{FL} = I_{FLR} \tag{3.18}$$

Utilizing (3.16) and (3.18) the full-load line current fundamental component is given by the following.

$$I_{FL} = \beta_1 \times I_{dc} \tag{3.19}$$

The output DC voltage (V_{dc}) for 6-pulse diode bridge rectifier with no AC in line reactors utilized is given by

$$V_{dc} = \frac{3\sqrt{2} \times V_{LL}}{\pi} = 1.35 \times V_{LL} \tag{3.20}$$

where V_{LL} is the line-to-line rms supply voltage.

The full load DC link current mean value is given by

$$I_{dc} = \frac{P_{dc}}{V_{dc}} = \frac{P_{dc}}{1.35 \times V_{LL}} \tag{3.21}$$

where P_{dc} is the rated DC output power (with the assumption of lossless power conversion, the rated ASD power P_R) and consequently Equation (3.19) is rewritten in the following form

$$I_{FL} = \beta_1 \times \frac{P_R}{1.35 \times V_{LL}} \tag{3.22}$$

Utilizing the input current no-load value to full-load value ratio (α) constraint, Equation (3.11) is rewritten, using the I_{NL} and I_{FL} equations in (3.8) and (3.22) respectively, yields in

54

$$\alpha = \frac{\left(\dfrac{V_1}{Z_f + Z_i}\right)}{\left(\beta_1 \times \dfrac{P_R}{1.35 \times V_{LL}}\right)} \tag{3.23}$$

and defining the magnitude of Z_f and Z_i in terms of L_i, L_f and C_f components in Equation (3.23), result in

$$\alpha = \frac{V_1 \Big/ \left|\omega_e\left(L_i + L_f\right) - \dfrac{1}{\omega_e C_f}\right|}{\left(\beta_1 \times \dfrac{P_R}{1.35 \times V_{LL}}\right)} \tag{3.24}$$

where ω_e is the fundamental electrical angular velocity (rad/sec).

The L_i, L_f, and C_f filter parameters are separated and defined depending on the operating conditions and design constraints in (3.25).

$$\left|\omega_e\left(L_i + L_f\right) - \frac{1}{\omega_e C_f}\right| = \frac{V_1 \times 1.35 \times V_{LL}}{P_R \times \beta_1 \times \alpha} = \frac{0.78 \times (V_{LL})^2}{P_R \times \beta_1 \times \alpha} \tag{3.25}$$

Utilizing (3.25) the L_i, L_f, and C_f filter initial parameters can be calculated for a given operating conditions and design constraints.

Based on (3.9) and (3.10), Equations (3.26) and (3.27) define the series and parallel resonance values in rad/sec.

$$\omega_p^2 = \frac{1}{(L_i + L_f)C_f} \tag{3.26}$$

$$\omega_s^2 = \frac{1}{L_f C_f} \tag{3.27}$$

Utilizing (3.27), Equation (3.26) is rewritten in (3.28) and consequently in (3.29)

$$\omega_p^2 = \frac{1}{\left(L_i C_f\right) + \left(\dfrac{1}{\omega_s^2}\right)} \tag{3.28}$$

$$L_i \times C_f = \left(\frac{1}{\omega_p^2} - \frac{1}{\omega_s^2}\right) \tag{3.29}$$

According to (3.27) and (3.29) the L_f and L_i are defined in terms of C_f for a selected ω_s and ω_p values, in (3.30) and (3.31), respectively.

$$L_f = \frac{1}{\omega_s^2 \times C_f} \tag{3.30}$$

$$L_i = \frac{1}{C_f}\left(\frac{1}{\omega_p^2} - \frac{1}{\omega_s^2}\right) \tag{3.31}$$

Substituting L_i and L_f with their equivalents from (3.30) and (3.31) in Equation (3.25), the C_f is finally given by

$$C_f = \frac{P_R \times \beta_1 \times \alpha}{0.78 \times (V_{LL})^2}\left[\frac{1}{\omega_e} - \frac{\omega_e}{\omega_p^2}\right] \tag{3.32}$$

At this stage the approximate filter design method formulas are complete. The equations must be executed in the order of (3.32), (3.30) and (3.31). The parameters involved in the equations must be carefully selected in order to make the initial parameter calculations accurate enough for the purpose of reducing the number of calculations required in the accurate design method.

Selection of the series resonant frequency value f_s (ω_s) depends on the rectifier current harmonic content, and therefore depends on the rectifier current waveform

56

stiffness. The filter impedance diagram of Fig. 3.6 shows the harmonic content dependency on the rectifier current stiffness for both the non-stiff and the stiff current source cases.
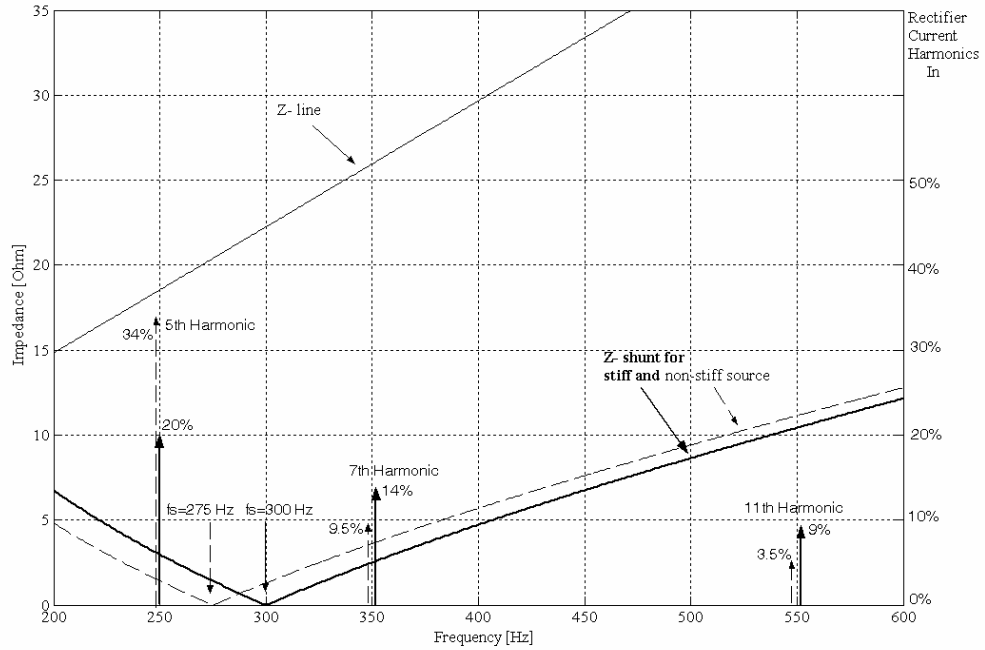
Fig. 3.6 Line and shunt branch impedance with current harmonics for stiff and non-stiff rectifier currents (5.5kW system).

The series resonant frequency f_s is selected in the vicinity of the two most dominant current harmonic (5th and 7th) frequencies. If the rectifier load is a stiff DC current source, f_s is selected such that it is nearly at the center between the 5th and 7th harmonic. Since in stiff DC link case the 5th harmonic is one-fifth and the 7th harmonic is one-seventh of the fundamental component, the 7th harmonic is not negligible compared to the 5th harmonic in terms of compensation requirements. For example, in such a case, 300 Hz can be selected (for 50 Hz utility applications). For the soft current waveform case, which is the most frequently encountered case in practice, the tuning frequency should be selected much closer to the 5th harmonic that is the most dominant harmonic. In this case, for example, a series resonant frequency of 275 Hz can be selected.

57

The parallel resonance frequency (f_p) can be selected in a wide range of 150 – 200 Hz. For higher frequency values (>200 Hz) there is a harmonic resonance amplification risk as f_p comes closer the fifth (dominant) harmonic and lower frequency range (<150 Hz) results in very large filter parameters rendering the design cost prohibitive.

To confine the f_p value, based on the approximate method, filter parameter calculation and following this procedure a simple performance estimation study is conducted. The performance estimation involves harmonic equivalent circuits. The rectifier along with L_o are modeled as a current source. Therefore, the input performance of the calculated filter parameters could be predicted (approximately). The equivalent circuit approach based performance prediction will be discussed in this section. However, the method will be utilized here for the purpose of aiding the parallel resonant frequency selection. Shown in Table 3.3, the results illustrate the relation between the parallel resonant frequency, filter parameters, and input power quality. A 4% L_o is assumed and the rectifier current harmonics ratios are assumed to be the same as shown in Table. 3.1. For the upper half of f_p range (175-200 Hz), for all α values, the line THD_I is high (11%) and/or the line power factor is low (<0.95). Therefore, the lower range (150-170 Hz) results in more reasonable line side performance ($THD_I \leq 5\%$ and/or PF>0.95). Consequently, vicinity of 150 Hz is selected as initial value range of parallel resonant frequency as there is no rectifier current harmonic in this range and the possibility of exciting resonance is practically non-existent.

The no-load line current should be significantly less than the rated line current (typically about α<50%). However α <50% implies small filter capacitor (C_f< 15 μF) and result in very large L_i (>23%) for the selected f_s and f_p values. Therefore, α is selected as 50 %.

Table 3.3 Filter initial parameters for 5.5 kW ASD system with soft source f_s=275Hz

f_p (Hz)	α	$C_{f\Delta}$ (μF)	L_f (mH)	L_f %	L_i (mH)	L_i (%)	Line THD$_I$ (%)	Line DPF
150	0.6	22.2	5.0	6.6	11.9	15.6	4.0	0.94
	0.5	18.5	6.0	7.9	14.2	18.7	4.0	0.97
	0.4	14.8	7.5	9.9	17.8	23.3	4.0	0.99
162	0.6	22.6	4.9	6.5	9.3	12.2	5.1	0.92
	0.5	18.8	5.9	7.8	11.2	14.6	5.1	0.95
	0.4	15.1	7.4	9.7	14.0	18.3	5.1	0.98
175	0.6	23.0	4.9	6.4	7.2	9.4	6.6	0.91
	0.5	19.1	5.8	7.6	8.6	11.2	6.6	0.94
	0.4	15.3	7.3	9.6	10.7	14.1	6.6	0.97
200	0.6	23.4	4.8	6.3	4.2	5.6	11.4	0.89
	0.5	19.5	5.7	7.5	5.1	6.7	11.4	0.92
	0.4	15.6	7.2	9.4	6.4	8.3	11.4	0.96

Given the power ratings of an ASD and its current stiffness information (if not given, it can be assumed as soft current source), with the series and parallel resonant frequencies as selected above, and α as 0.5, the initial filter parameters can be calculated from (3.33), (3.31), and (3.32). For example, for 50 Hz ASD applications with 5.5 kW, 55 kW, and 500 kW power ratings, 275 Hz series resonant frequency and 150 Hz parallel resonant frequency, the calculated approximate filter parameters are illustrated in Table 3.4.

The flow chart of the MATLAB code constructed for the approximate method is shown in Fig. 3.7 [14].
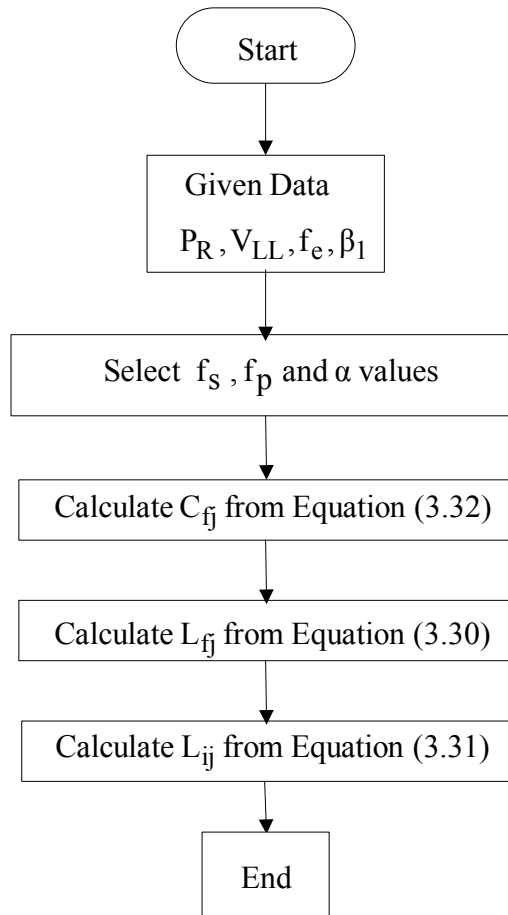
Fig. 3.7 Approximate IBF parameter determination method flowchart.

Table 3.4 Initial IBF filter parameters for various power rating ASDs
(f_s=275 Hz, f_p=150 Hz and α=0.5)

P_R (kW)	5.5	55	500
L_{ij} (mH)	14.2	1.40	0.159
L_{fj} (mH)	6.0	0.60	0.0675
$C_{fj\Delta}$ (μF)	18.5	185	1700

3.3.3 Accurate Design Method of IBF

The accurate design method utilizes the initial filter parameters of Table 3.4 to obtain accurate filter parameters for a given set of constraints and also obtain performance results regarding the filter behavior. In the accurate design method, the filter parameters are calculated from the frequency domain model of the total system involving the AC line, the broadband filter, and the rectifier. Fig. 3.8 and Fig. 3.9 show the fundamental component model and the harmonic component model of the system at full-load (rated power), while Fig. 3.10 shows the no-load fundamental component model. Note that the rectifier and DC side load are reflected to the AC side as an R-L impedance circuit. Therefore, the equivalent circuit becomes a linear circuit where closed form calculations can be made in order to analyze the circuit behavior.
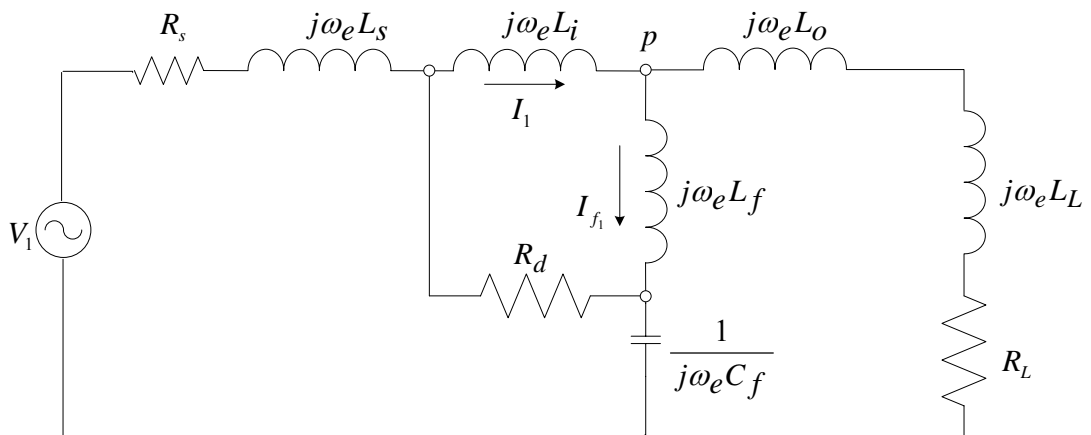
Fig. 3.8 Full-load fundamental frequency model of the ASD system.

In the AC side full-load fundamental frequency equivalent circuit, shown in Fig. 3.8, R_L represents the power consumed by the motor drive. Since the generally large DC bus capacitor decouples the high PWM frequency switching ripples and drive dynamics from the rectifier side, the motor drive and inverter can be represented with an equivalent DC side resistor when investigating the low frequency behavior (significantly lower than the PWM frequency that is typically in the range of several

kHz and above). Therefore, it is possible to study the ASD system behavior by representing the whole inverter drive system by an equivalent DC resistance R_{dc} and calculate R_{dc} from the power balance equation. Assuming a lossless system, the rated ASD power P_R is equal to the DC link power P_{dc}.

$$P_{dc} = \frac{V_{dc}^2}{R_{dc}} = P_R \tag{3.33}$$

Since V_{dc} is given by (3.20), the R_{dc} value can be obtained as

$$R_{dc} = \frac{V_{dc}^2}{P_R} = \frac{\left(\dfrac{3\sqrt{2} \times V_{LL}}{\pi}\right)^2}{P_R} \tag{3.34}$$

Given the R_{dc} value, the next issue involves the representation of the rectifier DC side quantities on the AC side, that is reflection of the DC side circuit to the AC side circuit. This approach is necessary for the purpose of obtaining closed form analytical formulas for the filter size optimization study. Assuming that the diode rectifier has unity displacement power factor and the rectifier is lossless, the fundamental component power AC and DC sides can be equated.

$$P_{ac} = \frac{3 \times V_{LN}^2}{R_{ac}} = \frac{V_{LL}^2}{R_{ac}} = P_{dc} = \frac{V_{dc}^2}{R_{dc}} = \frac{(\dfrac{3\sqrt{2} \times V_{LL}}{\pi})^2}{R_{dc}} \tag{3.35}$$

where V_{LN} is the line-to-neutral voltage at the input to the three phase rectifier. From the above equation, R_{ac} can be obtained in terms of R_{dc}, in the following

$$R_L = R_{ac} = \frac{R_{dc}}{1.823} \tag{3.36}$$

In the fundamental component full load model, for highly accurate representation of the rectifier; a load inductor (L_L) should be added and connected to L_o in attempt to

represent the rectifier commutation effect and the output voltage drop. The L_L empirical value is assumed to be the sum of L_i and L_o.

$$L_L = (L_i + L_o)$$ (3.37)

It has been found that including the load inductor (L_L) in the equivalent circuit improves the accuracy of the method.

To test the accuracy of the full load fundamental component equivalent circuit model of the system, the model was compared to the computer simulation based full system simulation for 5.5 kW, 380V, 50 Hz rating system. The initial filter parameters of Table 3.4 were used in the study. The circuit simulation software will be detailed in the next chapter, therefore details regarding the simulation method will be omitted at this stage. In the computer simulation, the rectifier line-to-line voltage V_{ab} and line current I_a are measured at full load in an attempt to find the accurate equivalent AC impedance that represents the rectifier. V_{ab} and I_a have a phasor form peak values of $547 \angle 138°$ V and $12 \angle 158°$ A, respectively. To find the AC equivalent impedance Z_{ac} in the star connection configuration, V_{ab} is shifted by $+30°$ and converted to the phase voltage value. Utilizing the I_a value, the equivalent AC rectifier side impedance is given by

$$Z_{ac} = R_{ac} + jX_{ac} = 25.9 + j4.57\Omega$$ (3.38)

where Z_{ac} is the equivalent rectifier impedance at the AC rectifier side, R_{ac} and X_{ac} are the corresponding AC side resistance R_L and reactance ($\omega_e L_L$) values that are implemented in the full-load fundamental equivalent circuit (Fig. 3.8). The R_{dc} estimated utilizing Equation (3.34) for the 5.5 kW system result in a resistance value of 47 Ω which is very close to the simulation value (48 Ω). Employing (3.36) the equivalent resistance can be found as 26.3 Ω, which is close to 25.9 Ω in (3.38). The load inductor L_L value is 14.5 mH, which is a close value to the summation of L_i initial filter parameter and the utilized 4 % L_o (17.3 mH). The 50 Hz load reactance is therefore 5.4 Ω which is quite close to 4.57 Ω of (3.38). The accuracy of the full

load fundamental component equivalent circuit load model was also tested for the 55 kW and 500 kW ratings and results favored the accuracy of the method.

In the harmonic model equivalent circuit, shown in Fig. 3.9, the rectifier is modeled as harmonic current source for the dominant harmonic frequencies. The harmonic currents are found from the harmonic ratio Table of 3.1. The line voltage harmonics are also considered in the harmonic equivalent circuit. As the worst case condition, it is assumed that the line voltage harmonics and rectifier current harmonics result in an in-phase harmonic currents in the circuit, leading to maximum distortion, stress and losses. This assumption is pessimistic, however simplifies the calculation procedure. With this approach, the individual effect of each harmonic source is calculated and the resulting quantities are scalarly added in magnitude. Therefore, the representation is simpler than the fundamental component and the analysis is easier. If its numerical value is available, the damping resistor (R_d) should be included in the harmonic model as its magnitude is comparable to the filter impedances at the relatively high dominant harmonic frequencies. The damping resistor is not included in the fundamental component model because at the fundamental frequency, the filter impedances in parallel with the damping resistor are significantly smaller and the damping resistor can be considered open circuit. At this stage, since the design of R_d is not discussed, it will be assumed open circuit. Excluding the resistor from the calculation results in a small and negligible steady-state performance prediction error. In the later stages, when the resistor value is available it will be included in the calculation to increase the accuracy. Discussion regarding R_d and its main functionality which is to suppress the switching transient related overvoltages will be provided later in this chapter.
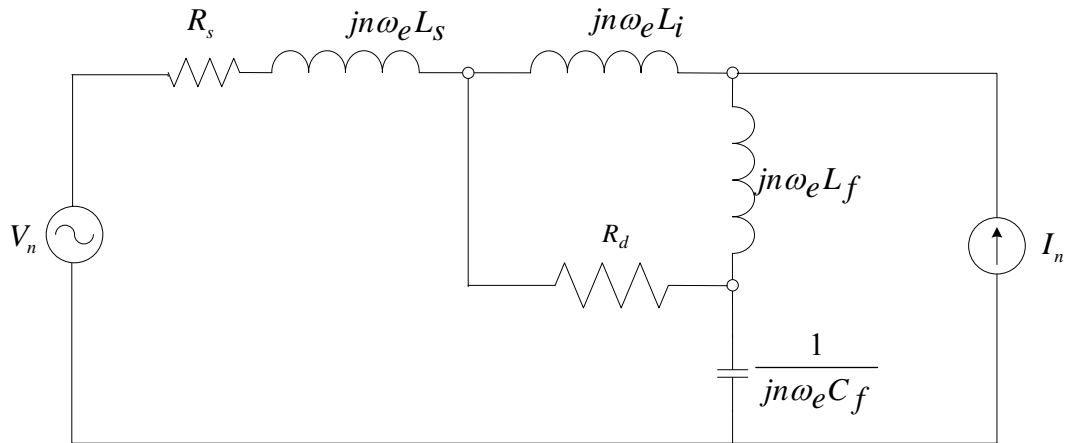
Fig. 3.9 Full-load harmonic frequency model of the ASD system.
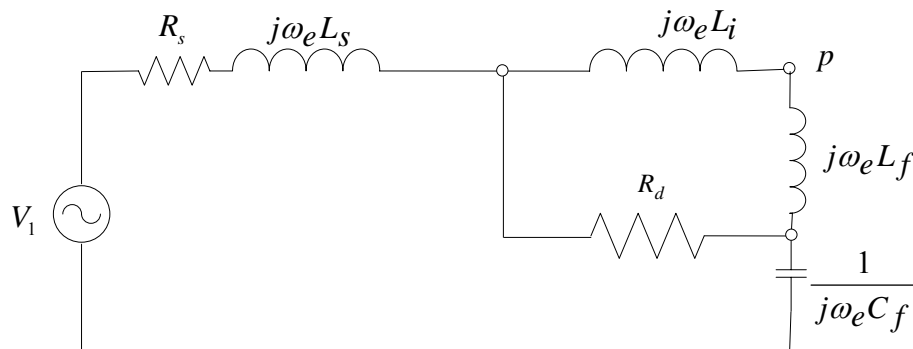
Fig. 3.10 No-load fundamental frequency model of the ASD system.

The no-load fundamental component model of the system, as shown in Fig. 3.10, is simple and easy to analyze. This equivalent circuit will be later utilized in calculating the no-load voltage at the output terminals of and no-load current through the filter.

Utilizing the ASD system equivalent circuits, the mathematical equations needed to calculate the performance of the system for a given set of parameters becomes possible. Thus, the filter parameter values can be incremented/decremented in the appropriate direction for meeting the given performance criteria in order to find more accurate (optimal) filter parameters than the approximate parameters found in the previous section. The line current THD_I value, given in (3.2), is found by calculating the values of the current harmonics injected to the line I_n for a known I_{FL}

65

fundamental component rms value (I_1) and the current harmonics ratios (rectifier stiffness). Calculating the total line and the shunt filter equivalent impedance ratio at each dominant harmonic frequency, the I_n values and then the corresponding line current THD_I is calculated at full-load.

Calculating the line power factor value at full-load requires the line displacement power factor information $\cos(\phi)$. This is achieved by utilizing the fundamental frequency model, shown in Fig. 3.7. The line PF is calculated by (3.6) assuming that the I_1/I ratio is near unity for a low line THD_I value design criteria ≤10 %. Thus, the input power factor angle ϕ becomes equal to the angle of the input impedance Z_T (impedance seen from the AC line side) at the fundamental frequency. As a result $\cos(\phi)$ is calculated. The line current full-load fundamental component rms value I_1 is calculated by (3.39).

$$I_1 = \frac{V_1}{Z_T} \tag{3.39}$$

To calculate the output voltage regulation (ΔV_o %) at the filter node (P), the $V_P(NL)$ and $V_P(FL)$ are calculated using the drive system fundamental frequency equivalent circuits for both loading conditions. At full-load, based on Fig. 3.8 equivalent circuit, the shunt filter current I_{f1} is found as

$$I_{f_1} = \frac{Z_L}{Z_L + Z_f} \times I_1 \tag{3.40}$$

where Z_L is the total load side impedance (involving L_o, L_L, and R_L) and Z_f is the filter impedance (L_f, C_f) both at the fundamental frequency. Consequently, the full-load node voltage fundamental component rms value is given by

$$V_P(FL) = I_{f_1} \times Z_f \tag{3.41}$$

At no-load, based on the equivalent circuit in Fig. 3.10, the node voltage fundamental component rms value is given by

66

$$V_P(NL) = \frac{V_1}{Z_f + Z_i} \times Z_f = I_{NL} \times Z_f \qquad (3.42)$$

where Z_i is the total input impedance (involving Li and the utility line impedance). Finally the output voltage regulation at node P (ΔV_o %) is calculated by (3.7).

Based on the obtained drive system equivalent circuit formulas (3.39-3.42), and for a given set of performance constraints defined previously, the filter parameters L_i, L_f, and C_f are precisely calculated in MATLAB M-file based computer program that implement the obtained formulas for a given ASD and power system parameters. The algorithm involves an incremental parameter variation procedure. The optimal parameters are sought in a fairly narrow three dimensional space involving the three filter parameters. Since the approximate method gives the first estimate of the parameters, the optimal filter parameters are within the proximity of these initial values. Therefore, by linearly incrementing the parameters and scanning the three dimensional parameter space, the performance is sequentially calculated and the parameters yielding poor performance are discarded until a sufficient performance is obtained. Therefore, the code returns practically optimal parameters within a relatively small number of iterations, typically less than several hundred. The modern computers, this computational requirement is completed in a few seconds. It should be noted that the system equations that are based on the equivalent circuits are fairly complex and any closed form optimization procedure is prohibitive in terms of formulation efforts. Although it is possible to employ more efficient algorithms than linear parameter increment approach (such as bisection method), the practically low number of iterations needed to obtain the optimal parameters favors the preferred direct approach. The success of this method is due to the simple approximate parameter calculation method involved in the initial filter parameter determination stage. Without such pre-processing, the direct linear parameter increment approach would have to span a large 3-D parameter space consuming significant amount of computation effort. In addition, it might converge to local optimum points that are inferior to the global optimum obtained in the accurate method.

The flow chart of the MATLAB code constructed for the accurate proposed method is shown in Fig. 3.11. The MATLAB file is included in Appendix A. In the flow

chart, the given data involves the initial filter parameters (obtained from the approximate method) and both utility side and rectifier side information.

From the utility side, the line-to-line voltage (V_{LL}), supply frequency, the source impedance (Z_s), and supply voltage harmonic ratios ($V_n\%$) are required. From the rectifier side, the ASD rated power (P_R), full-load rectifier current harmonics ratios ($I_n \%$), $L_o\%$ utilized, and the corresponding stiffness factors β_{rms}, β_1 values are given in the first step. The line $THD_I\%$ and output voltage $\Delta V_o\%$ design criteria are also defined.

In the second step the other necessary variables are calculated. The DC rated output voltage (V_{dc}) is calculated by Equation (3.20). Consequently, rated DC load current (I_{dc}) and resistance (R_{dc}) are calculated by Equations (3.21) and (3.34), respectively for the given rated ASD power P_R value. Full-load line current fundamental component rms value (I_{FL}) is calculated by Equation (3.19) and the rated rectifier current rms value (I_R) is calculated utilizing Equation (3.17) for the given β_{rms} value. The base impedance Z_b is found by Equation (2.1) and is utilized to define the initial L_{ij} and L_{fj} filter parameters in percentage values ($L_{ij}\%$ and $L_{fj}\ \%$). This is required in the next step where the L_i and L_f step sizes are also defined in percentage values. It is also utilized for defining the L_o actual value (in H units) and estimating the equivalent series resistance values of the filter reactors.

Assuming that the AC reactors utilized have approximately 99% efficiency (their VA rating defines their nominal power that passes through them), their equivalent series resistance can be calculated as follows.

$$R_{intL} = \frac{1\% (V_{LR})}{I_{LR}} \tag{3.43}$$

where V_{LR} and I_{LR} are the reactor rated voltage and current rms values.

In the third step, the three initial filter parameters $L_{ij} \%$, $L_{fj} \%$ and C_{fj} (μF) are implemented in three nested loops to increment/decrement their values with a defined negative or positive step sizes. From the initial filter parameters, shown in

68

Table 3.3, it is seen that the L_{ij} and L_{fj} normalized values are high (19% and 8%, respectively) resulting in very low line THD_I (4%) for the selected f_p, f_s and α values. This implies decreasing their values by assigning a negative step size for both quantities. The opposite involves the C_{fj} step size (positive value) in order to keep the f_s value in the vicinity of the selected range value (275 Hz). The L_{ij} and L_{fj} negative step sizes (ΔL_{ij} and ΔL_{fj}) are selected to have a value of 0.5% and 0.2%, respectively while the capacitor positive step size value is 0.2% of the initial C_{fj} value.

Start

Given Data

P_R, V_{LL}, f_e, Z_s, Supply $V_n\%, \beta_{rms}, \beta_1$, Rectifier $I_n\%$

$L_o\%, L_{ij}, L_{fj}, C_{fj}$, Line THD_I and $\Delta V_o\%$ criteria

Find rated $V_{dc}, I_{dc}, I_{FL}, I_R$ and Z_b

Define L_{ij} and L_{fj} in percentage utilizing Z_b

$C_f = C_f + [\Delta C_f = +0.2\% \times C_{fj}]$

$L_i\% = L_i\% + [\Delta L_i = -0.5\%]$

$L_f\% = L_f\% + [\Delta L_f = -0.2\%]$

Ckt. Analysis @ f_e (Fig. 3.7)

Ckt. Analysis @ nf_e (Fig. 3.8)

Ckt. Analysis @ f_e (Fig. 3.9)

Calculate Performance

Line THD_I from Equation (3.2)

Line PF from Equation (3.6)

$\Delta V_o\%$ from Equation (3.7)

α from Equation (3.11)

$THD_I < THDmax$

$\Delta V_o\% < \Delta Vmax$ Yes → Store Results

No

$L_f\% < L_{fmin}$ No

Yes

$L_i\% < L_{imin}$ No

Yes

$C_f > C_{fmax}$ Yes → Show Results

No

Fig. 3.11 Accurate IBF parameter determination method flowchart.

In the fourth step, within the three nested loops, utilizing the equivalent circuits the system performance is calculated. The total line impedance value (including source impedance Z_s value given) and the shunt branch filter impedance value are calculated at the fundamental and the considered first four dominant current harmonics frequencies for each step variation. These impedance values are utilized to calculate the line current harmonic components (using current sharing formula in parallel impedance branches) at all harmonic frequencies with the knowledge I_{FL} and the rectifier current harmonic content. For the given supply voltage harmonic ratios (V_n %), the corresponding supply current harmonic ratios are calculated by including a voltage harmonic source with V_n % amplitude in the full-load harmonic frequency model (Fig. 3.9). Utilizing the superposition theorem, the harmonic currents due to both sources are calculated. In each element the total harmonic current is selected as the magnitude sum of the individual sources (pessimistic approach). As a result the line current and its harmonic components are calculated. From here, the line current THD_I is calculated.

The fifth step involves enforcing all the constraints (THD_I, PF, ΔV_o %, α) for each step of the nested loop. The most critical two constraints are THD_I and ΔV_o % constraints. A small variation in these constraints results in a large filter parameter change. Most other constraints are implicitly dependent on these two and the optimal parameters are less sensitive to the other constraints. While the line power factor is related to THD_I, the no-load to full-load current ratio α is related to ΔV_o %.

It is observed that the line THD_I value is most sensitive to C_f and L_f values (i.e. f_s) and least sensitive to L_i value. On the other hand ΔV_o % value is sensitive mostly to the L_i value. Therefore, line THD_I and output ΔV_o % strict limits are mandatory to be set (to eliminate the possibility of generating a large number of solutions) and again checked in the sixth step. As a result, the filter parameters that meet the constraints are stored (few combinations ≤ 6). When the nested loops reach limits (15 steps for each reactor and 80 steps for capacitor), the computation procedure will stop and show the optimal results (accurate filter parameters and all constraints). The parameter variation among the available optimal parameter sets is minimal and negligible. Therefore, of the existing solutions sets, those that are closer to the practical component ratings available (by manufacturer datasheets, such as capacitor

71

C value information) or closer to the performance criteria desired available should be selected. This final decision leads to practically optimal parameter sizing.

The method has been tested on ASDs in a wide power range (5.5 kW-500 kW) and the parameters have been calculated. ASD system simulations involving the calculated parameters have been tested in a detailed computer simulation program and the performance results (represented in chapter 4) have accurately met the performance criteria selected during the design (all the evaluated criteria have a deviation less than 8%). Therefore, the accuracy of the method has proven satisfactory.

The performance criteria is based on the performance criteria of recent standards and/or recent industrial products of the same type. The new European standards recommend line current THD criteria less than 10% for many electrical equipment. This implies equipment with worse THD characteristics will not be sold in the European Union. In many power supplies the required input current THD is less than 5%. UPS products are now designed with 3-5% input current THD and 0.99 power factor. Therefore, the same trend continues for ASDs also. It has been observed from the manufacturer datasheets of the IBF system that the line current THD is less than 8% the power factor above 0.97 at full-load. The same manufacturer datasheets state that the maximum output voltage at no load limit is 104.6% implying that ΔV_o % should be less than 5% [6]. Therefore, in this work similar criteria to what is utilized in a similar commercial IBF product has been defined.

In the design considered, the performance criteria is as follows;

ΔV_o= 4%, THD_I =10% and these limits inherently satisfy the other constraints limits ($150 < f_p < 170$, $PF > 0.97$ and $I_{no-load} \leq 50\%$).

Given the power ratings of an ASD and all necessary data, the accurate filter parameters can be obtained. For example, for 50 Hz ASD applications with 5.5 kW, 55 kW, and 500 kW power ratings and related given data, the code has been evaluated. Additional information regarding these commercial ASDs involving the DC bus capacitance, the precharge resistance and L_o values is given in Table 3.5.

From the utility side, the source impedance Z_s values, are shown in Table 3.6. The 5.5kW corresponding values are field estimated (a 500 kVA distribution transformer feeds the local area at METU). The 5.5kW source impedance Z_s values are the base to estimate the source impedance for the other power ratings. It is assumed that the ASD forms a small part of the loads fed from the same distribution transformer. Also a practical utility voltage source with 3% THD_V is considered having dominant voltage harmonic ratios V_n values of 2.2% 5th, 1.3% 7th, 1.1% 11th, 0.9% 13th values. These ratios are selected such that the lower frequency components have larger magnitude and the total distortion is about 3% and found iteratively via computer simulations.

The accurate filter parameters calculated in the MATLAB code for the considered ratings and constraints are shown in Table 3.7.

Table 3.5 ASD parameters for various power ratings

P_R (kW)	5.5	55	500
$R_{precharge}$ (Ω)	20	2.0	0.2
C_{dc} (mF)	1.0	10	90
L_o (4%) mH	3.1	0.31	0.034

Table 3.6 Source impedance parameters for various power ratings

P_R (kW)	5.5	55	500
L_s (μH)	100	10	1.12
R_s (mΩ)	50	5.0	0.55

Table 3.7 Improved broadband filter parameters for various power ratings

P_R (kW)	5.5	55	500
L_i (14.2%) mH	10.8	1.08	0.121
L_f (7.0%) mH	4.9	0.49	0.055
$C_{f\Delta}$ (μF)	20.6	206	1844

In the following, the MATLAB code results for various power ratings are represented. The ASD rated power (P_R), line-to-line supply voltage (V_{LL}), supply fundamental frequency (f_e) and equivalent source impedance components (L_s, R_s) values are entered to the program. The line THD_I and $\Delta V_o\%$ criteria are also entered. The code displays the following results.

```
enter the ASD rated power value in kW:5.5
enter the supply line-to-line rated voltage value in Volts:380
enter the supply frequency value in Hz:50
enter the source equivalent reactance value in μH:100
enter the source equivalent resistance value in milliohms:50
enter the line current THD limit value (THDmax%):10
enter the output voltage regulation limit value (DelVmax%):4
PLEASE WAIT
```

```
'Results'  'Li(mH)'  'Lf(mH)'  'Cf(μF)'    'THD'     'DelVo'    'PF'       'fp'
[    1]   [11.0002] [5.2065]  [20.0837]  [9.9758]  [3.9021]  [0.9668]  [161.0612]
[    2]   [11.0002] [5.2065]  [20.1201]  [9.9259]  [3.9027]  [0.9669]  [160.9155]
[    3]   [11.0002] [5.0513]  [20.5567]  [9.9554]  [3.9104]  [0.9670]  [159.9650]
[    4]   [11.0002] [5.0513]  [20.5931]  [9.9077]  [3.9110]  [0.9671]  [159.8236]
[    5]   [11.0002] [4.8962]  [21.0297]  [9.9638]  [3.9187]  [0.9673]  [158.9257]
[    6]   [11.0002] [4.8962]  [21.0660]  [9.9180]  [3.9194]  [0.9674]  [158.7884]
```

```
enter the ASD rated power value in kW:55
enter the supply line-to-line rated voltage value in Volts:380
enter the supply frequency value in Hz:50
enter the source equivalent reactance value in μH:10
enter the source equivalent resistance value in milliohms:5
enter the line current THD limit value (THDmax%):10
enter the output voltage regulation limit value (DelVmax%):4
```

PLEASE WAIT

'Results'	'Li(mH)'	'Lf(mH)'	'Cf(μF)'	'THD'	'DelVo'	'PF'	'fp'
[1]	[1.1000]	[0.5206]	[200.8369]	[9.9758]	[3.9021]	[0.9668]	[161.0612]
[2]	[1.1000]	[0.5206]	[201.2007]	[9.9259]	[3.9027]	[0.9669]	[160.9155]
[3]	[1.1000]	[0.5051]	[205.5667]	[9.9554]	[3.9104]	[0.9670]	[159.9650]
[4]	[1.1000]	[0.5051]	[205.9305]	[9.9077]	[3.9110]	[0.9671]	[159.8236]
[5]	[1.1000]	[0.4896]	[210.2966]	[9.9638]	[3.9187]	[0.9673]	[158.9257]
[6]	[1.1000]	[0.4896]	[210.6604]	[9.9180]	[3.9194]	[0.9674]	[158.7884]

enter the ASD rated power value in kW:500
enter the supply line-to-line rated voltage value in Volts:380
enter the supply frequency value in Hz:50
enter the source equivalent reactance value in μH:1.12
enter the source equivalent resistance value in milliohms:0.55
enter the line current THD limit value (THDmax%):10
enter the output voltage regulation limit value (DelVmax%):4
PLEASE WAIT

'Results'	'Li(mH)'	'Lf(mH)'	'Cf(μF)'	'THD'	'DelVo'	'PF'	'fp'
[1]	[0.1210]	[0.0573]	[1.8258e+003]	[9.9740]	[3.9028]	[0.9668]	[161.0612]
[2]	[0.1210]	[0.0573]	[1.8291e+003]	[9.9241]	[3.9035]	[0.9669]	[160.9155]
[3]	[0.1210]	[0.0556]	[1.8688e+003]	[9.9536]	[3.9111]	[0.9670]	[159.9650]
[4]	[0.1210]	[0.0556]	[1.8721e+003]	[9.9059]	[3.9118]	[0.9672]	[159.8236]
[5]	[0.1210]	[0.0539]	[1.9118e+003]	[9.9620]	[3.9194]	[0.9673]	[158.9257]
[6]	[0.1210]	[0.0539]	[1.9151e+003]	[9.9162]	[3.9201]	[0.9674]	[158.7884]

3.3.4 Damping Resistor Selection Method

The IBF system along with the rectifier, involve switching transients during turn-on and turn-off of the drive. In an ASD system, the voltage and current overstresses due to the switching transients are manipulated by a DC bus precharge circuit. Generally, this circuit is made of a resistor in parallel with a contactor (or any switch) and the switching transients can be manipulated by controlling this switch according to the DC bus voltage level. If the DC bus voltage is below a preset threshold value, the switch remains off. Otherwise, the switch is turned on and remains on throughout, bypassing the precharge resistor. Therefore, the DC bus voltage capacitor does not

75

experience major overvoltage stress during start-up and line voltage transients. As a result the inverter does not experience any significant overvoltage stress and the DC bus capacitor does not experience either overvoltage or overcurrent stress, leading to economical design. Inclusion of the broadband filter in the system involves introduction of additional dynamics to the system.

An IBF can be directly connected to the ASD terminals with no additional switches. However, a three phase switch or contactor must be placed between the AC line and the IBF terminals. When turning this three-phase switch on or off, additional dynamics are excited. Considering that the precharge circuit manipulates the rectifier and drive side dynamics, the only problematic transients remaining would be on the AC side and related to the IBF components. Therefore the IBF structure and damping characteristics are important in determining the system behavior.

In order to have a high efficiency system, the IBF components are designed and built with high efficiency characteristics (typically 97-99% efficient) and this implies very low damping filter structure. As a result, when enabling the input contactors, the filter experiences voltage and current overstress. Specifically, the capacitor voltage and filter output voltage can become excessively large. In order to damp the switching overvoltages, a damping resistor is necessary. In the IBF structure, as shown in Fig. 3.1, the damping resistor R_d is located across the L_i and L_f total system. Its duty is to specifically damp the turn-on transient overvoltages (reduce the voltage overshoot) across the AC filter capacitors and the rectifier terminals. The choice of R_d involves two criterion, low filter capacitor voltage overshoot and low energy dissipation. While the filter energy efficiency criteria requires high energy efficiency corresponding to large R_d, the voltage overshoot criteria requires low overshoot corresponding to small R_d (high damping). Therefore, a trade-off exists between steady-state and dynamic performance.

In this thesis, major effort has been spent towards obtaining a closed form analytical formula that illustrates the relation between R_d and damping ratio. The results obtained could be evaluated numerically. However, the analysis does not yield a comprehensible closed form formula. Therefore, at this stage detailed computer

simulation based results will be presented and the analysis carried out will be presented in a later stage.

An ASD system with IBF structure has been considered for the detailed system simulation. Three power ratings, 5.5 kW, 55 kW, and 500 kW have been investigated. The filter parameters selected are those listed in table 3.7. Computer simulations have been conducted via Simplorer Student Version (Version 7). In the computer simulations, the inverter drive was modeled with an equivalent DC load in order to simplify the simulations. The simulation involves the start-up transient where the IBF input switch is turned-on and the filter is precharged followed by the DC bus capacitor charging. Further details of the simulation model and simulation software program will be provided in the following chapter. At this stage the damping resistor related results are presented.

For 5.5 kW, as Fig. 3.12 indicates the AC filter capacitor is sensitive to line voltage switching transients, while the DC bus capacitor and the rectifier terminal voltages do not experience major voltage overshoot. Therefore, the voltage overshoot on C_f is what requires attention. The figure illustrates that the capacitor voltage overshoot has a saturation curve, indicating an R_d greater than 300 Ω does not have any damping effect and significant damping is achieved at 100 Ω or less. However, as Fig.3.13 indicates, when R_d is near 100 Ω the input current THD and filter losses increase (system efficiency decreases) significantly. Therefore, a damping resistor with a value less than 100 Ω is prohibitive from the efficiency and THD point of view, while a value greater than 300 Ω is prohibitive from the capacitor voltage overshoot point of view. Depending on whether efficiency or component oversizing related cost is more emphasized in the design, a value in this range must be selected.

Similar to the 5.5 kW case, for 55 kW, and 500 kW ratings, computer simulations have been conducted and the results are shown in Figures 3.14 through 3.17. As a summary the R_d parameter for each power rating can be chosen within the range shown in Table 3.8.
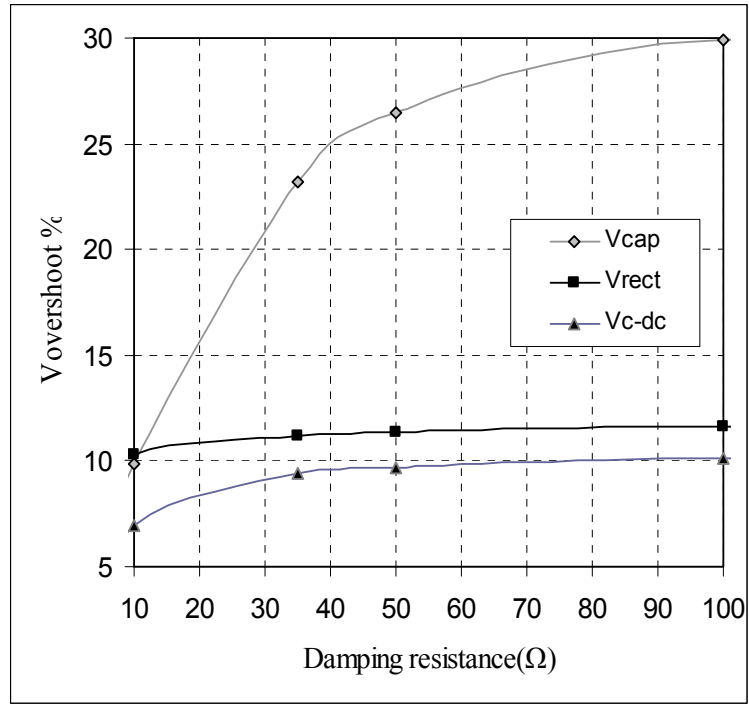
Fig. 3.12 Voltage overshoot for various R_d values (5.5kW system).
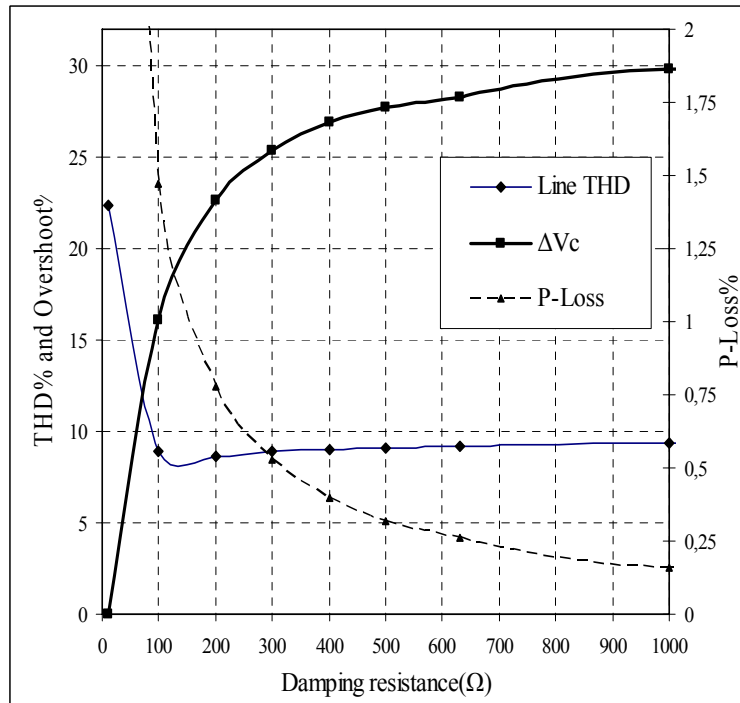
Fig. 3.13 Voltage overshoot, line THD_I and R_d losses for various R_d (5.5kW system).
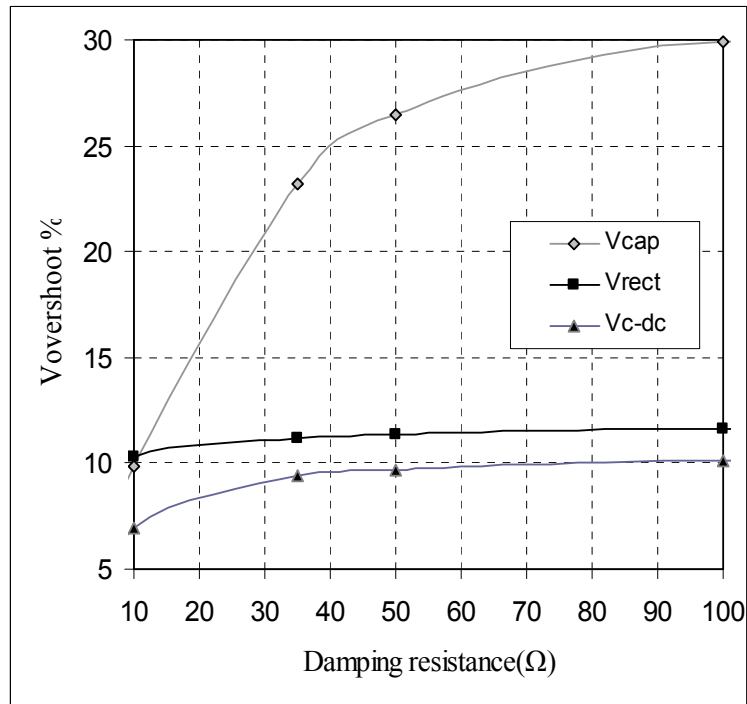
Fig. 3.14 Voltage overshoot for various R_d values (55kW system).
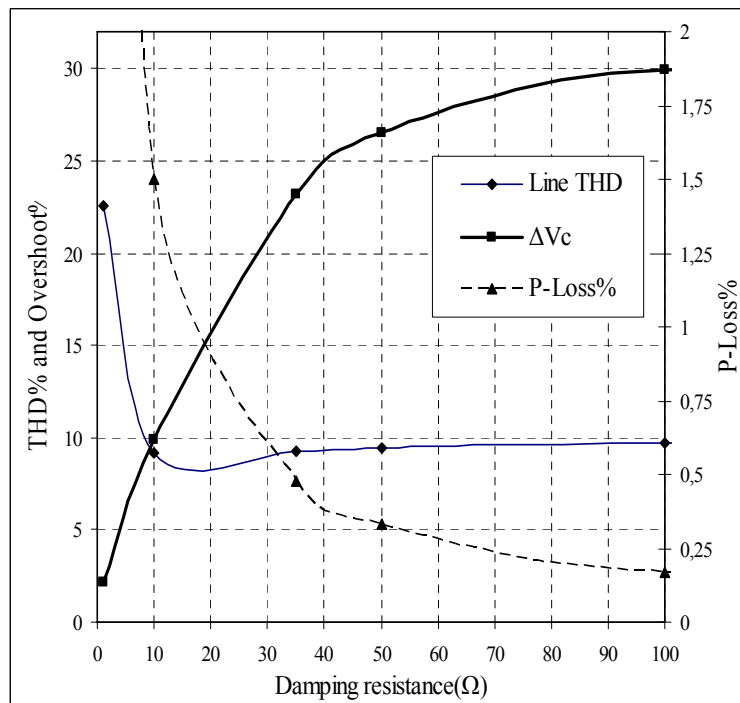
Fig. 3.15 Voltage overshoot, line THD_I and R_d losses for various R_d (55kW system).
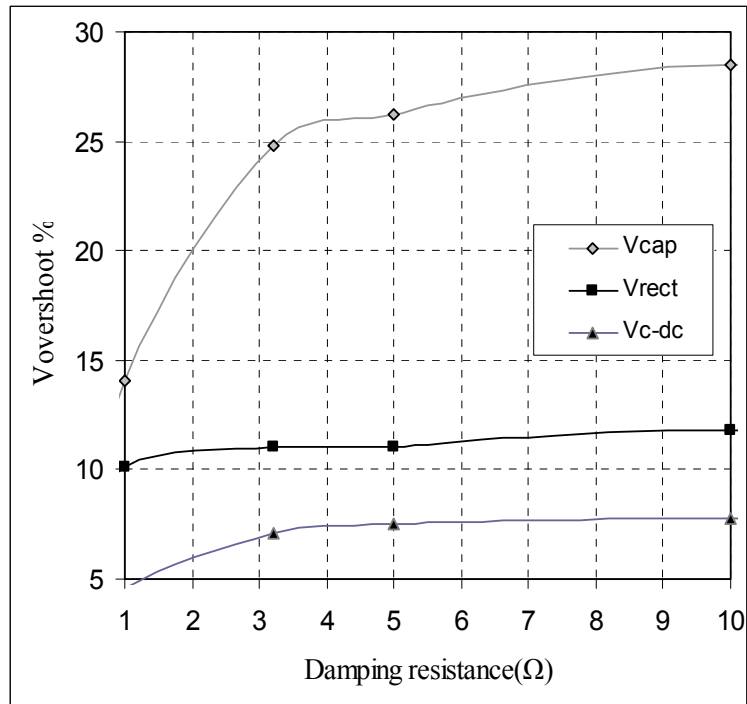
Fig. 3.16 Voltage overshoot for various R_d values (500kW system).
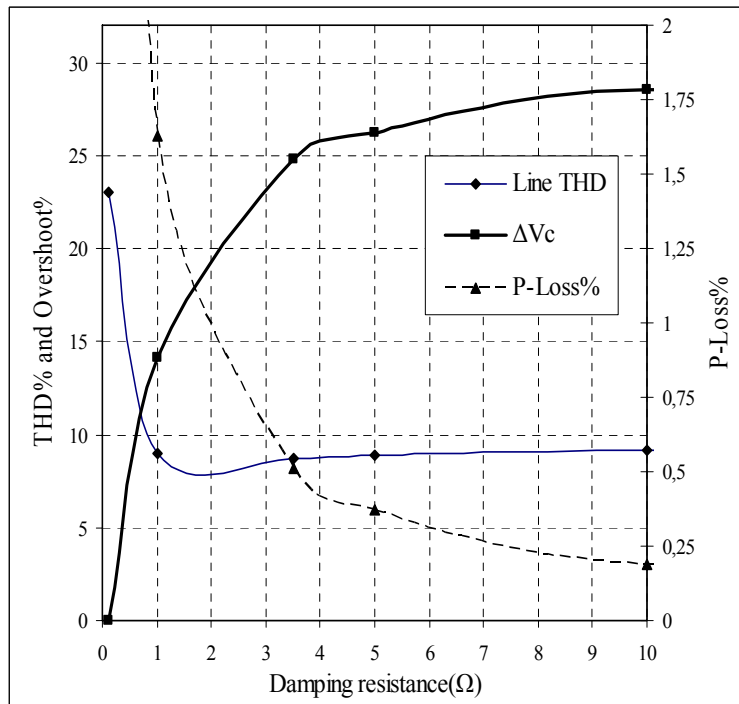
Fig. 3.17 Voltage overshoot, line THD_I and R_d losses for various R_d (500kW system).

Table 3.8 Improved broadband filter damping resistor for various power ratings

P_R (kW)	5.5	55	500
R_d (Ω)	100-300	10- 40	1-5

In the following, the attempt for obtaining closed form analytical formula that illustrates the relation between R_d and damping ratio is presented. As the simulation based results indicate that only the AC filter capacitor voltage is sensitive to line voltage switching transients, the analysis carried out focuses on this specific case.

The closed form method involves analyzing the equivalent circuit of the ASD system with the IBF structure, shown in Fig. 3.18, during the start-up transient. The precharge resistance ($R_{precharge}$) is involved, while the DC-bus capacitor is assumed short-circuited and the source impedance neglected during start-up transients. In the analysis conducted the transfer function $V_c(S)/V_s(S)$ is obtained. The corresponding characteristic equation is analyzed to define the filter damping factor ζ in terms of R_d.
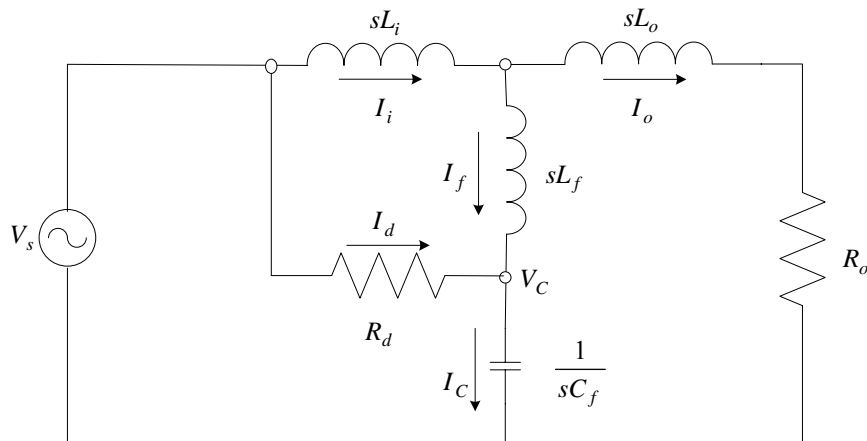
Fig. 3.18 System equivalent circuit under line turn-on transient condition.

The transfer function obtained is given by

$$\frac{V_C}{V_S} = \frac{N_1 s^2 + N_2 s + N_3}{D_1 s^3 + D_2 s^2 + D_3 s + D_4} \qquad (3.44)$$

where

$$N_1 = L_i L_f + L_o L_f + L_o L_i \qquad (3.45)$$

$$N_2 = R_{precharge} L_f + R_{precharge} L_i + R_d L_o \qquad (3.46)$$

$$N_3 = R_{precharge} R_d \qquad (3.47)$$

$$D_1 = C_f R_d \times N_1 \qquad (3.48)$$

$$D_2 = R_{precharge} C_f R_d (L_f + L_i) + N_1 \qquad (3.49)$$

$$D_3 = R_d (L_i + L_o) + R_{precharge} (L_f + L_i) \qquad (3.50)$$

$$D_4 = N_3 \qquad (3.51)$$

where L_i, L_f, L_o and C_f are the filter parameters, while R_d and $R_{precharge}$ are the damping and precharge resistors, respectively.

From this analysis, the obtained transfer function has a complicated characteristic equation and the damping factor ξ can not be explicitly related to the damping resistor R_d. Therefore, for further investigation, utilizing the transfer function the system step response is obtained by MATLAB M-File code for various R_d values and its damping effect on the AC filter capacitor is presented graphically.

The ASD and filter parameters for 5.5 kW power rating in Tables 3.5 and Table 3.7 respectively are selected. The step response plot obtained for various R_d values is

shown in Fig. 3.19, while the corresponding damping factor ξ values are shown in Fig. 3.20. It is clear that the smaller R_d value, the higher AC filter capacitor overvoltage damping is. In contrast, for $R_d > 300$ ohms there is no major difference in the overvoltage damping as the system response in this range is indistinguishable from the plot. Similarly, the damping factor ξ vary in a wide range for $R_d < 300$ ohms and has a negligible variation for the higher R_d range.
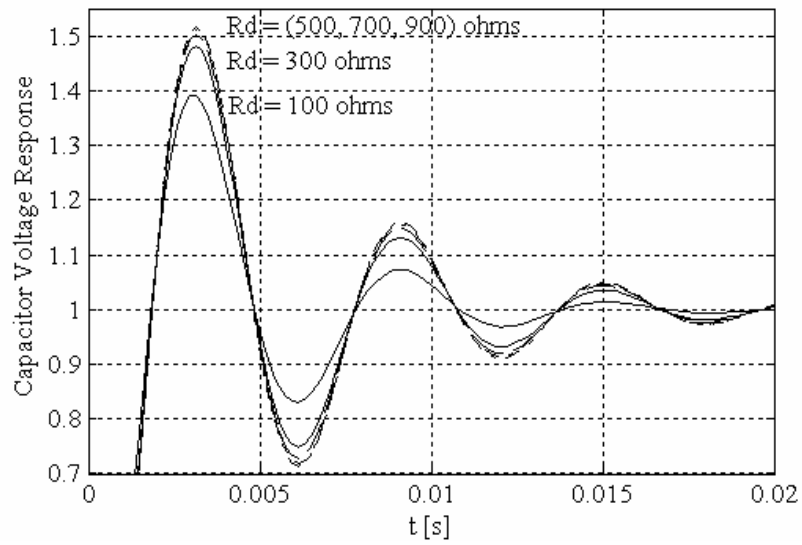
Fig. 3.19 Normalized filter capacitor voltage step response for various R_d (5.5 kW system).
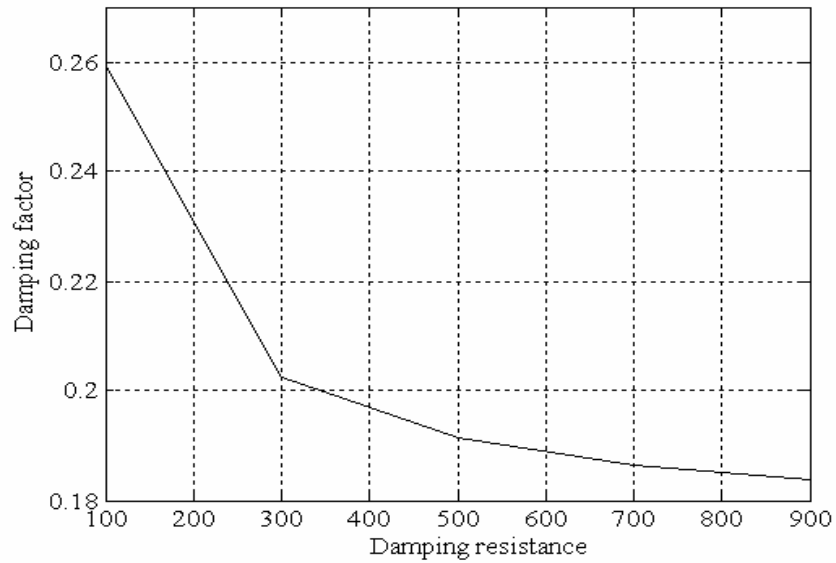
Fig. 3.20 The system damping factor (ξ) variation for various R_d (5.5 kW system).

Similar to the simulation based results, the analytical results favor the same damping resistance R_d range for 5.5kW system. For 55 kW and 500kW ratings, analysis has been conducted in the same way and results validate the R_d range selection shown in Table 3.8.

To verify the single-phase equivalent circuit based analysis, the MATLAB code results obtained are compared to the three-phase computer simulation results (conducted in the previous study). Table 3.9 shows a numerical comparison between the two methods for capacitor voltage damping ratio with various R_d values. In the table, on the left column, the normalized peak value of the V_c/V_s transfer function step response is listed (the analytical approach result, shown in Fig.3.19). On the right column, the three phase full system simulation results are listed. It is observed that the analytical formula based approach and the three-phase simulation results are consistent.

Table 3.9 Code and simulation damping ratio results for various R_d values for 5.5 kW system

R_d (Ω)	V_c / V_s	
	Code	Three-phase Simulation
100	1.39	1.35
300	1.48	1.44
500	1.50	1.47
700	1.51	1.47

Additionally, a single-phase computer simulation has been conducted for the system single-phase (Fig. 3.18) equivalent circuit (with unity step function input) for further comparison. The graphical results, shown in Fig.3.21, also favor the analytical method.
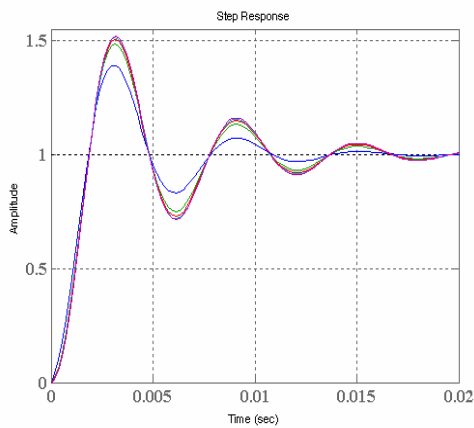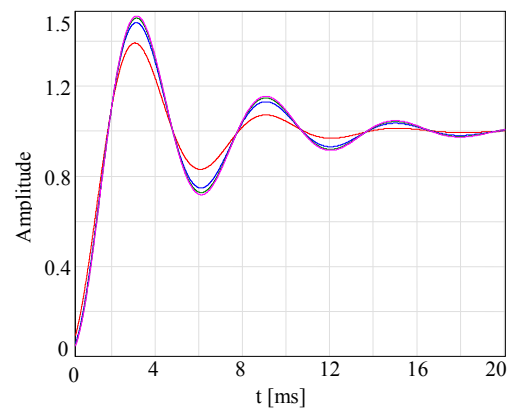
(a)   (b)

Fig. 3.21. AC filter capacitor voltage step response; (a): Code waveform, (b): Simulation waveform (5.5 kW system).

3.4 Summary

In this chapter the improved broadband filter topology has been shown, its operating principle explained, and design method has been established. The IBF design criteria is established and design procedure detailed. The filter employs 4% L_o in all power ratings. The three main filter parameters, L_i, L_f, C_f are first calculated by means of simple formulas via the approximate method. Utilizing the approximate method parameters as initial value, the accurate method further optimizes the three filter parameters with high accuracy leading to the best expected parameters in terms of meeting the cost and performance criteria selected. In the final step, the damping resistor is sized based on the voltage overshoot and energy efficiency criteria selected. All the algorithms are implemented in a MATLAB M-File code. For a given power rating and performance criteria as input, the computer program outputs the optimal improved broadband filter parameters. The code is listed in Appendix A.

With the IBF parameter selection method being established in this chapter, and the other passive filtering method parameter selection methods discussed in the previous chapter, it is possible to design and implement various filter structures for performance evaluation and comparisons.

The next chapter involves detailed computer simulations that evaluate the performance of ASDs with various filter structures (with emphasis on IBF) and provides comparisons among the discussed filtering methods.

CHAPTER 4

COMPUTER SIMULATIONS AND PERFORMANCE ANALYSIS OF ASD SYSTEMS WITH VARIOUS PASSIVE FILTERS

4.1 Introduction

The previous chapters discussed the operating principles and the design methods of conventional passive filters, and developed a method for the design of the recently developed improved broadband filter. In this chapter, the performance of these filters is under investigation. The study will be conducted via detailed modeling of the ASD system through computer simulations. In the study, the focus will be on the steady state performance characteristics. Performance will be evaluated at various operating points, including no-load, half-load, and full-load. Operation under balanced and unbalanced utility grid voltage with or without voltage harmonic distortion will all be considered. Energy efficiency, input power quality (input current THD_I and power factor), filter output voltage regulation, voltage overshoot under switching transients will all be evaluated.

When studying the effects of the utility grid voltage distortion on the filter performance, a 3% THD_V is considered for all filtering topologies investigated. In the study it is assumed that the voltage harmonics (V_n values) are 2.2% 5th, 1.3% 7th, 1.1% 11th, 0.9% 13th all with respect to the fundamental component. These ratios are selected such that the lower frequency components have larger magnitude as it is normally the case in practice. Utility supply of 380V line-to-line voltage and 50Hz frequency is considered. The supply source impedance parameters are shown in Table 3.6, for the various power ratings considered.

The investigation involves three power ratings, low power, medium power, and high power general purpose ASDs with 5.5 kW, 55 kW, and 500 kW ratings respectively. The series inductor filter type filtering study is done with 3% and 6% both. The tuned filter approach involves the 5th and 7th filters. The IBF topology is utilized in full and its parameters are those in Table 3.7.

In the computer simulations the rectifier of the ASD system is modeled with "system level" diodes (reverse recovery effect and switching dynamics neglected). The filter and utility grid are fully modeled with accuracy (including the parasitics and distortion). The inverter side of the ASD system modeled with an equivalent resistor and switch. Since the DC bus capacitor decouples the PWM dynamics of the drive from the rectifier side, this approximation is highly acceptable and does not result in loss of accuracy in filter performance prediction. Based on the data of the recent industrial products, the ASD system DC link capacitor, precharge resistor, and load parameters are given in Table 4.1.

Table 4.1 ASD system parameters for various power ratings

P_R (kW)	5.5	55	500
L_{dc} (2%) mH	1.50	0.152	0.017
$R_{precharge}$ (Ω)	20	2.0	0.2
C_{dc} (mF)	1.0	10	90

For the purpose of modeling, a graphic computer simulation package program Ansoft-Simplorer (student 7th version, SV7) has been utilized [19]. The program is a graphic window based (pick and place) power electronic circuit simulator. The computer simulation software involves a circuit schematic diagram window (ssh file), a graphic view window (view file), and the Day-postprocessor window. In the schematic window the circuit is drawn and simulation parameters are given. The graphic window displays the simulation waveforms as in an oscilloscope. The Day-

postprocessor window provides data processing tools for the purpose of harmonic spectrum, THD, etc. calculation.

In the computer simulation the integration method is trapezoidal integration method. Other related parameters are shown in Fig. 4.1. The shown step size is selected low for high accuracy. The simulation end time is selected such that the modeled system reaches its steady-state conditions. All database results for the selected outputs are saved at the steady-state period (last two cycles). Therefore, the Day-postprocessor processes the saved data and calculates results at steady-state conditions and all transient results are eliminated for high accuracy results. However, for transient analysis the focus is within the first few cycles.

The circuit simulator is based on a modified nodal approach. The trapezoidal algorithm is applied for the solution of the differential equation system. The solution of nonlinear equations is done by the Newton-Raphson method. The calculation of equation systems, linearization in the operating point, takes place by means of LU factorization after applying Gauss method [19].
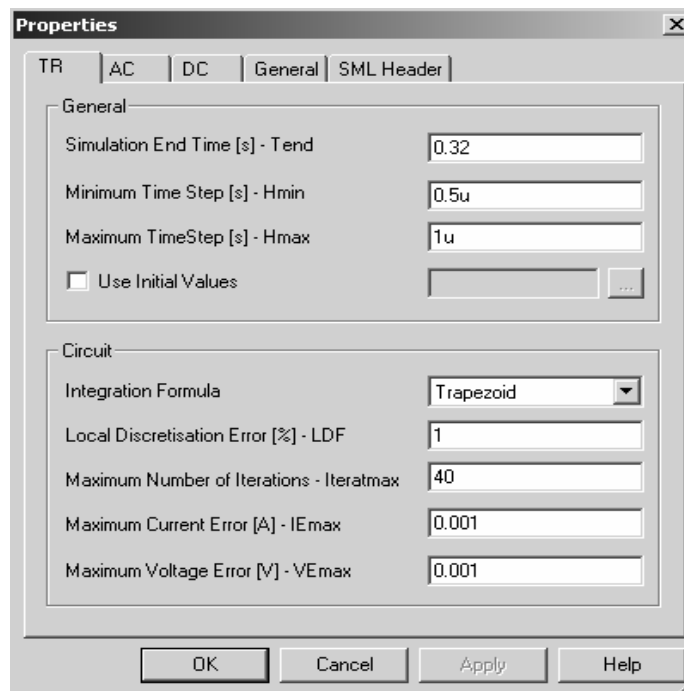
Fig. 4.1 Simulator integration method and its computational parameters.

4.2 AC Line Reactor Filter Based ASD System Simulations

In this section, performance analysis of three-phase 3% and 6% AC line reactor filter based ASD system under balanced and distorted utility (with 3% THD_V) is presented. Simulation current and voltage simulation waveforms are illustrated and analyzed. The AC line reactors are combined with a 2% DC link inductor to increase the effectiveness of the filtering method. The parameter values of the AC line reactances utilized and their equivalent series resistances (R_{ESR}) (using Eqn 3.39) for the 5.5 kW, 55 kW, and 500 kW power ratings are shown in Table 4.2. The table also contains the ASD system DC side equivalent load resistor (R_{dc}) information. Since different AC line reactors result in different DC bus voltage levels, constant load power implies different R_{dc} values. These parameters are implemented in the simulation circuit, shown in Fig. 4.2, for all the power ratings considered.

Table 4.2 Series AC line reactor filter parameters along with the load resistance values

AC Line Reactors	5.5 kW	55 kW	500 kW
L_{ac} (3.0%) mH	2.30	0.229	0.026
R_{ESR} (mΩ)	7.1	0.71	0.079
R_{dc} (Ω)	45	4.5	0.495
L_{ac} (6.0%) mH	4.60	0.458	0.051
R_{ESR} (mΩ)	14.3	1.43	0.16
R_{dc} (Ω)	43.5	4.35	0.483
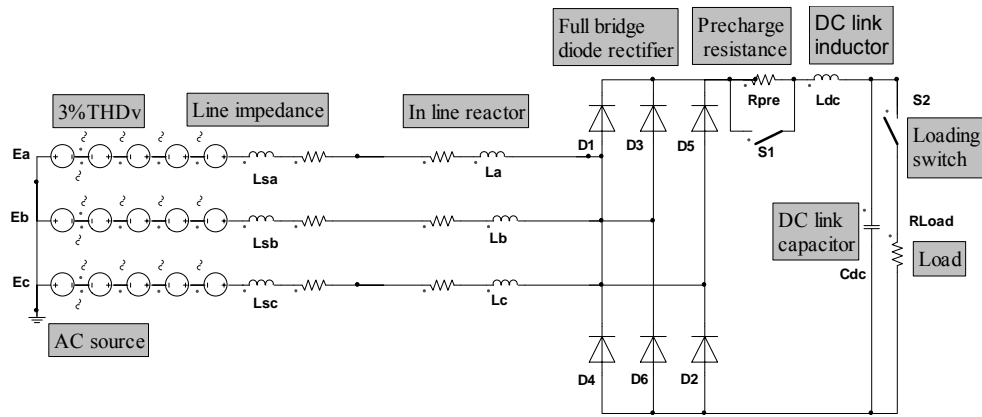
Fig. 4.2 Simulation circuit of the ASD system that utilizes AC line reactor and DC link inductor filter.

4.2.1 Full-Load Simulations of The 5.5kW Rated System

In this section, the simulation results and waveforms for 3% and 6% AC line reactors (Table 4.2) and ASD system (Table 4.1), for 5.5kW ratings are presented. For the 55kW and 500kW rated systems, only the basic results will be summarized due to limited space and significant similarity of the results with the 5.5kW case. The full-load line current and supply voltage simulation waveforms for both 3% and 6% AC line reactors filtering methods for the 5.5kW ASD system are shown in Fig. 4.3 and Fig. 4.4, respectively. In the figure, the current waveform is up-scaled by 10 (implying the actual current is 10 times smaller than that is shown in the figure). Hence 10x. The full-load line current has a 36% and 29% THD$_I$ values for the 3% and 6% AC line reactors, respectively. The line power factor is 0.92 lagging for both.

91
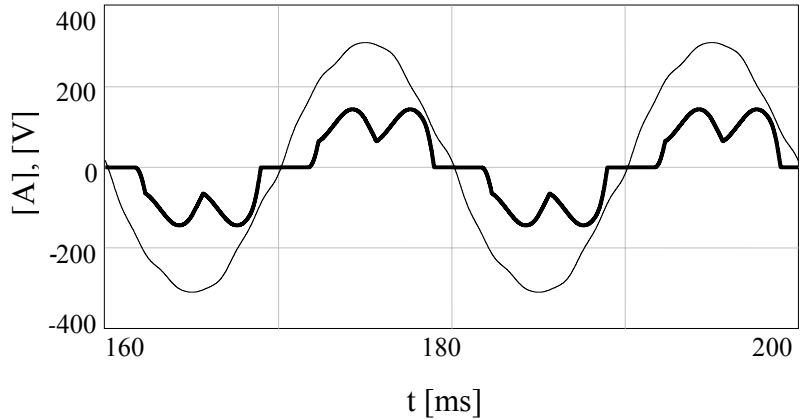
Fig. 4.3 Full-load line current (bold) and supply voltage simulation waveforms for 5.5kW ASD system utilizing 3% L_{ac} and 2% L_{dc} filter (current scale: 10x).
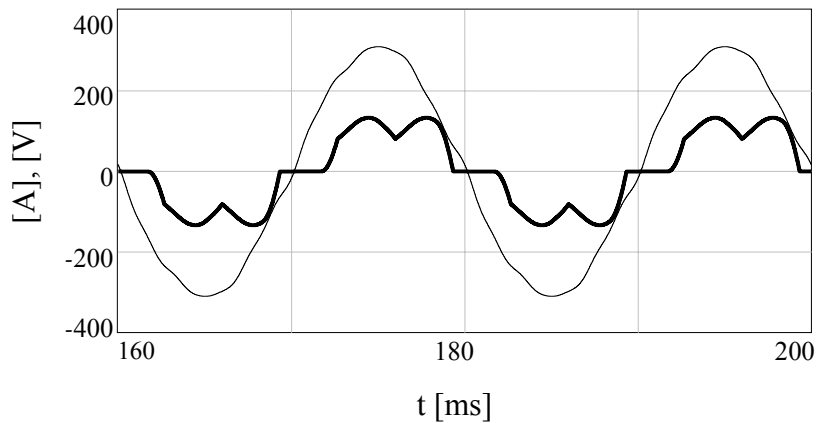
Fig. 4.4 Full-load line current (bold) and supply voltage simulation waveforms for 5.5kW ASD system utilizing 6% L_{ac} and 2% L_{dc} filter (current scale: 10x).

The rated load DC voltage and current simulation waveforms are shown in Fig. 4.5 and Fig. 4.6. It is seen that the 3% AC line reactor filter results in a 502V DC rated output voltage value while the 6% AC line reactor filter results in a lower value of 492V DC rated output voltage. This is due to the larger voltage drop across the 6% reactance.
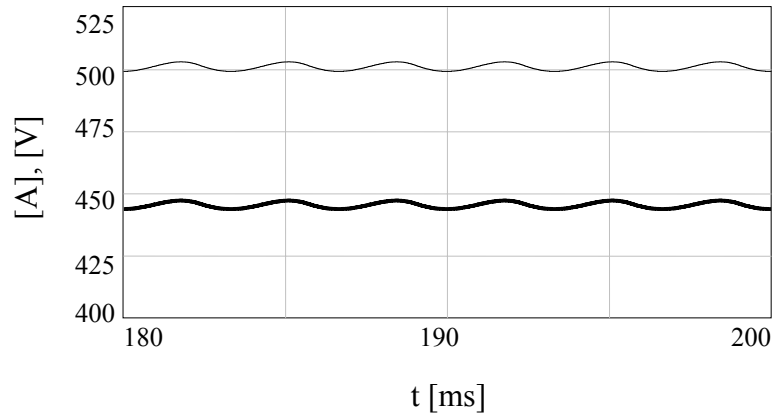
Fig. 4.5 Full-load DC load current (bold) and voltage simulation waveforms for
5.5kW ASD system utilizing 3% L_{ac} and 2% L_{dc} filter (current scale: 40x).
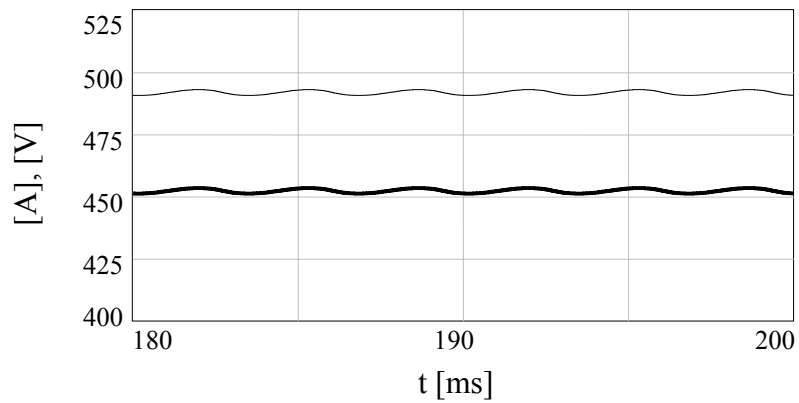
Fig. 4.6 Full-load DC load current (bold) and voltage simulation waveforms for
5.5kW ASD system utilizing 6% L_{ac} and 2% L_{dc} filter (current scale: 40x).

From the above simulation results, it is seen that the reactor filter topology has poor performance at full-load with high line current THD_I values (> 29%) and low line power factor values (0.92). It can be noticed that combining the 2% L_{dc} link inductor slightly improves the line current THD_I values compared with the no DC link inductor case (Table. 3.2). However, the improvement is marginal and for both AC line reactor cases, the line THD_I values are high and do not comply with the modern power quality standards. Further, the topology causes a voltage reduction in the DC

output voltage at full-load. The amount of DC output voltage reduction in both cases is consistent with Equation 2.7 that estimates the DC voltage reduction.

Table 4.3 shows the full-load performance for the selected power ratings for both 3% and 6% AC line reactor combined with the 2% L_{dc} inductance filter. The same conclusions as for the 5.5kW rating can be made for the higher ratings. AC line reactance based filtering (with or without the DC link inductor filtering) is insufficient in terms of modern power quality compliance.

Table 4.3 Full-load performance of 3% and 6% AC line reactor filter for various power ratings

	3% AC Line Reactor			6% AC Line Reactor		
P_R (kW)	5.5	55	500	5.5	55	500
$THD_I\%$	36	36	35	29	29	29
PF	0.92	0.92	0.92	0.92	0.93	0.93
V_{dc} (V)	502	501	499	492	492	491

4.3 Tuned Filter Design and Tuned Filter Based ASD System Simulations

4.3.1 Tuned Filter Design

As discussed in chapter 2, practically single tuned filters are utilized at increasing power levels and the tuned filters are designed for the most dominant harmonics of the rectifier (typically 5 or 5&7). For high performance, a filtering system with the 5th and 7th harmonic shunt filters with added 6% AC input reactor (L_i) and 3% AC rectifier output reactor (L_o) that forms a T-shape topology is designed. In the design of each single tuned filter (5th and 7th), the filter capacitors are sized to also provide full fundamental frequency reactive power compensation (Q_F). This filter reactive power compensation is calculated by

$$Q_F = Q_R - Q_L \tag{4.1}$$

where Q_R is the rated fundamental frequency reactive power the rectifier takes and Q_L is the rated fundamental frequency reactive power of the line. Both reactive power quantities are calculated based on the rated DC output power P_{dc} and the displacement angles between the phase voltage and line current fundamental components at both sides (rectifier and line) as follows

$$Q_F = P_{dc} \times (\tan \phi_R - \tan \phi_L) \tag{4.2}$$

where ϕ_R and ϕ_L are the rectifier and utility line displacement angles, respectively. The rectifier rated displacement angle ϕ_R for the diode bridge rectifier is given by

$$\phi_R = \frac{u}{2} \tag{4.3}$$

where u is the rectifier overlap angle due to current commutation between outgoing and incoming conducting diodes. It is given by

$$\cos u = 1 - \frac{2\omega_e \times L_{ac} \times I_{dc}}{V_{LL} \times \sqrt{2}} \tag{4.4}$$

where L_{ac} is the total AC line reactors utilized (6% and 3%), I_{dc} is the rated DC load current, V_{LL} is the line-to-line voltage and ω_e is the fundamental electrical angular velocity.

For calculated ϕ_R and assumed ϕ_L value to be 0° (unity power factor design criteria), the total demanded fundamental reactive power to be supplied by both shunt single filters (Q_F) are calculated. The 5th filter capacitor is assumed to supply 55% of Q_F while the 7th filter capacitor is assumed to supply 45% of Q_F (could be selected differently). At the fundamental frequency, neglecting the filter reactors (because the reactor impedance is negligible), the tuned filter is purely capacitive. Therefore, each filter capacitor is sized by

$$C_X = \frac{Q_X}{\omega_e \times V_{LL}^2} \tag{4.5}$$

where Q_X is the individual reactive power demand for the corresponding capacitor C_X. The calculated capacitance values assume star connection. Since in practice generally Δ configuration is utilized, these values are converted to Δ connected capacitance values (by dividing by 3) as shown in Table 4.4.

After sizing the 5th and 7th filter capacitors, each filter reactor is calculated for the corresponding harmonic frequency (250Hz and 350Hz for 50 Hz fundamental frequency) value with 4% detuning factor defined in Equation 2.11. The obtained filter parameters and the ASD system DC load equivalent resistance value for the 5.5 kW, 55 kW, and 500 kW ratings are shown in Table 4.4. These parameters are implemented in the simulation circuit, shown in Fig. 4.7, for all power ratings considered. To improve the performance of the method a 2% DC link inductor is added (as included before in the AC line reactor filter case).

Table 4.4 Tuned filter parameters for various power ratings

P_R(kW)	5.5	55	500
L_i (6.0%) mH	4.60	0.458	0.051
R_{ESR} (mΩ)	14.3	1.43	0.16
L_o (3.0%) mH	2.30	0.229	0.026
R_{ESR} (mΩ)	7.1	0.71	0.079
L_5 (mH)	29.6	3.00	0.332
R_{ESR} (mΩ)	400	40	4.4
$C_{5\Delta}$ (μF)	4.94	49.47	441.7
R_{ESR} (mΩ)	80[*]	8.0	0.9
L_7 (mH)	18.5	1.80	0.207
R_{ESR} (mΩ)	210	21	2.3
$C_{7\Delta}$ (μF)	4.04	40.47	361.4
R_{ESR} (mΩ)	72[*]	7.2	0.8
R_{dc} (Ω)	45	4.5	0.5

*lab measurement based
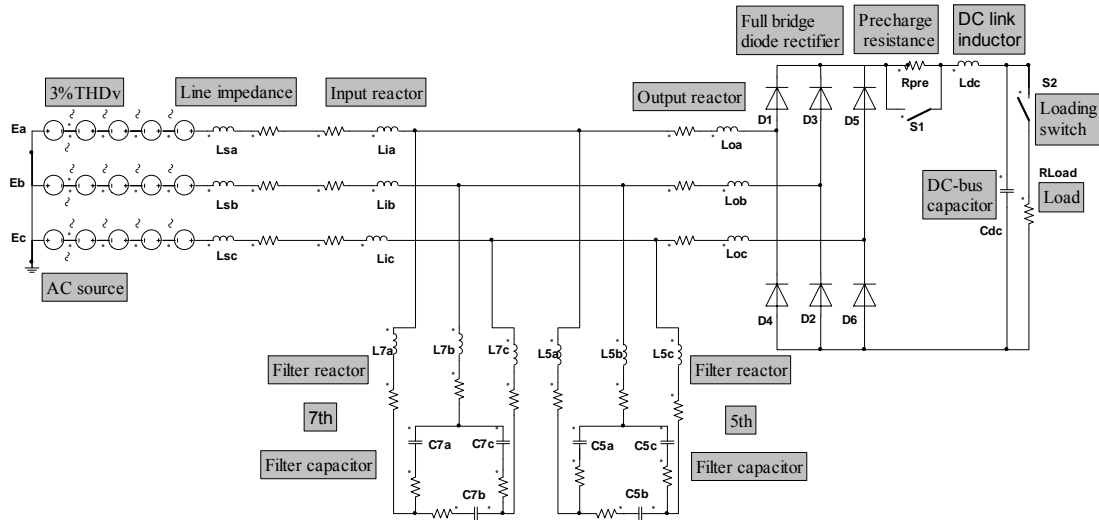
Fig. 4.7 Simulation circuit of the ASD system that utilizes T-shape 5th and 7th single tuned filters and DC link inductor filter.

4.3.2 Full-Load Simulations of The 5.5 kW Rated System

In this section, the simulation results and waveforms for the T-shape 5th and 7th single tuned filters (Table 4.4) and ASD system (Table 4.1), for 5.5kW ratings are presented. In practice low power rating systems such as the presently discussed 5.5 kW rated system do not utilize the tuned filter approach, in particular the utilization of both the 5th and 7th filters at the same time is prohibitive from the cost perspective. At such power ratings if necessary, typically the 5th harmonic filter is utilized and 7th is not. However, for performance evaluation and comparison studies done in this thesis, as the METU University laboratory has limited power capacity, and the project budget is limited, in this study only 5.5 kW rated system could be built and tested. For this reason, the performance for this rating system will also be thoroughy investigated throughout this thesis. The full-load line and rectifier current simulation waveforms are shown in Fig. 4.8. The topology reduces the rectifier current 30% THD_I value to the line current 13% THD_I value at full-load. The full-load line current and supply voltage simulation waveforms are shown in Fig. 4.9. The line power factor is near unity with 0.99 lagging value.

97
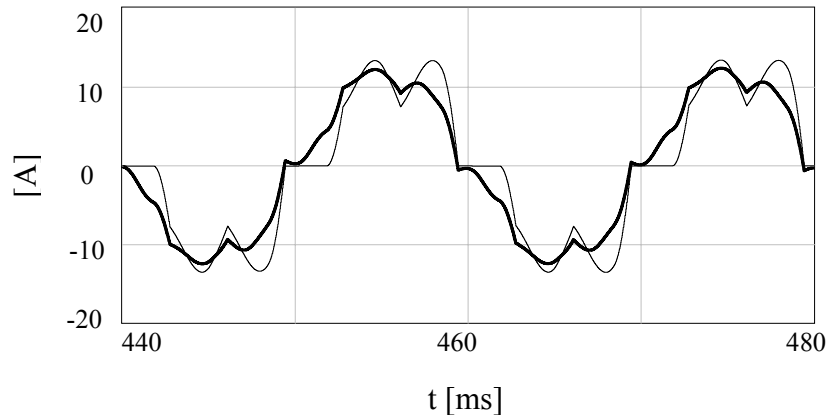
Fig. 4.8 Full-load line (bold) and rectifier current simulation waveforms for 5.5kW ASD system utilizing 5th and 7th tuned and 2% L_{dc} filter.
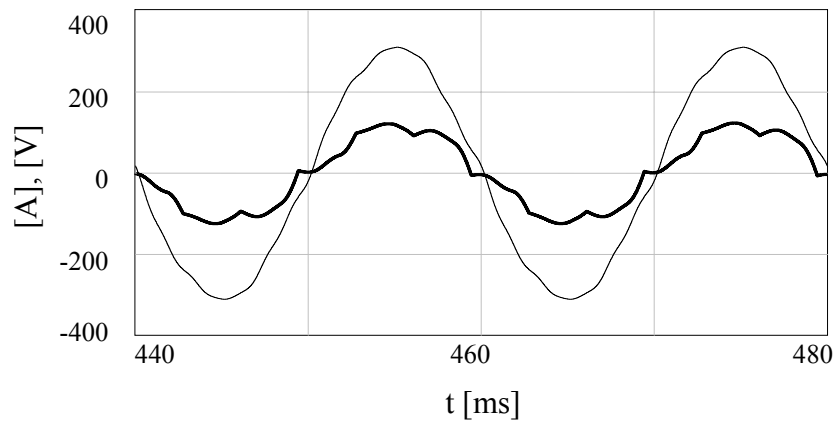
Fig. 4.9 Full-load line current (bold) and supply voltage simulation waveforms for 5.5kW ASD system (current scale: 10x).

The rated load DC voltage and current simulation waveforms are shown in Fig. 4.10. The T-shape 5th and 7th single tuned filter base system results in a 497V DC rated output voltage value. The full-load 5th and 7th tuned filter capacitor current and voltage simulation waveforms are shown in Fig. 4.11 and Fig. 4.12, respectively. The rectifier current and rectifier line-to-line voltage simulation waveforms are shown in Fig. 4.13. It is noticed that the rectifier line-to-line voltage is distorted due to the rectifier current harmonics.
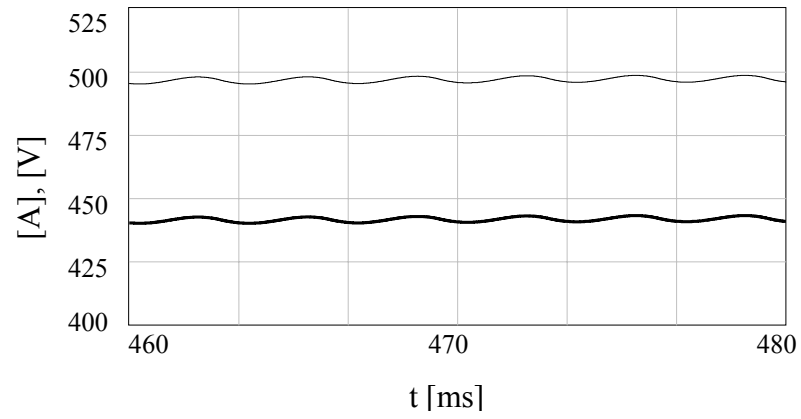
Fig. 4.10 Full-load DC load current (bold) and voltage simulation waveforms for 5.5kW ASD system (current scale: 40x).
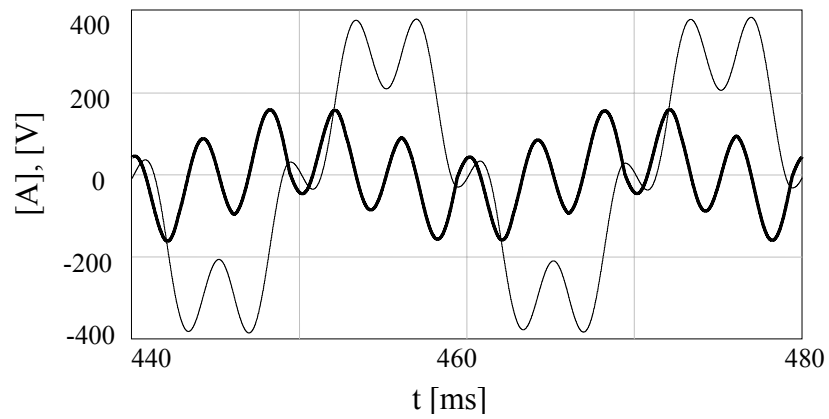
Fig. 4.11 Full-load 5th tuned filter capacitor current (bold) and voltage waveform for 5.5kW ASD system (current scale: 40x).

Fig. 4.12 Full-load 7th tuned filter capacitor current (bold) and voltage simulation waveforms for 5.5kW ASD system (current scale: 40x).

Fig. 4.13 Full-load rectifier current (bold) and line-to-line voltage simulation waveforms for 5.5kW ASD system (current scale: 10x).

From the above simulation results, it is seen that the T-shape 5th and 7th single tuned filters topology has good performance at full-load. The topology decreased the line current THD_I value from 30% to 13% and the line power factor is unity. However, for lower line current THD_I criteria larger AC line reactors and/or AC filter capacitors are required. However, increasing the AC filter capacitor size is limited by the line power factor quality. Larger capacitors result in lower (leading) line power factor. Both solutions increase the topology cost.

100

4.3.3 No-Load Simulations of The 5.5 kW Rated System

In this section, the no-load operating condition simulation results and waveforms are presented. The no-load definition considered involves increasing the rated DC load resistor R_{dc} by a multiplication factor of 100. The no-load line current and supply voltage simulation waveforms are shown in Fig. 4.14. The line current THD_I value increases to 25% as the topology imports the existing utility current harmonics (here represented with the utility line voltage harmonics) at no-load and the line power factor is near zero.
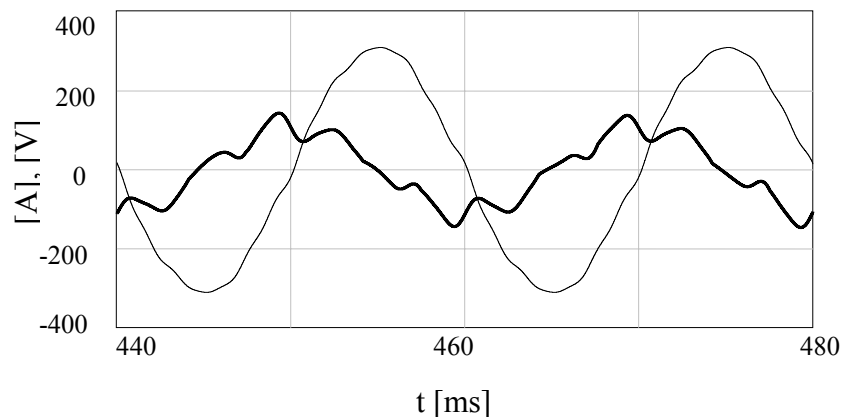
Fig. 4.14.   No-load line current (bold) and supply voltage simulation waveforms for 5.5kW ASD system (current scale: 40x).

The no-load 5th and 7th tuned filter capacitor voltage simulation waveforms compared to the shunt node (between L_i and L_o) voltage simulation waveforms are shown in Fig. 4.15 and Fig. 4.16, respectively. It is seen that each capacitor voltage is approximately equal to the total node voltage. However, both filter capacitor voltage simulation waveforms have higher peak values than the node voltage peak values (more noticeable for 5th single tuned filter).

Fig. 4.15 No-load node (bold) and 5th tuned filter capacitor voltage simulation
waveforms for 5.5kW ASD system.

Fig. 4.16 No-load node (bold) and 7th tuned filter capacitor voltage simulation
waveforms for 5.5kW ASD system.

4.3.4 Full-Load Simulations of The 500 kW Rated System

As the previous section discussed, tuned filters are utilized at power ratings involving
many tens of kilowatts and higher. Since the power ratings considered in this study
are 5.5 kW, 55 kW and 500 kW, the 500 kW rating results will be illustrated in

detail, while the 55 kW results will only be summarized in a table. However, it should be kept in mind that from the low power of 5.5 kW to 500 kW and higher, the behavior of the filter is filter type dependent and performance attributes of the small and large system are essentially the same. Therefore, in this section, as a good representative of the practical tuned filter applications, the high power 500kW ASD system (Table 4.1) utilizing the T-shape 5th and 7th single tuned filters (Table 4.4) is studied. Simulation results and waveforms are presented. The full-load line current and rectifier current simulation waveforms are shown in Fig. 4.17. While the full-load line current and the supply phase voltage simulation waveforms are shown in Fig. 4.18. Similar to the 5.5kW ASD system results, the line current has 12% THD_I value and the line power factor is 0.99 lagging at full-load condition.
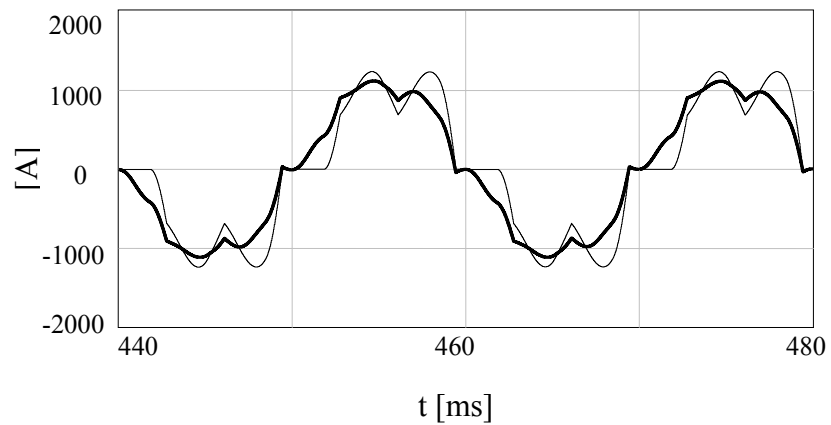
Fig. 4.17 Full-load line (bold) and rectifier current simulation waveforms for 500kW ASD system.
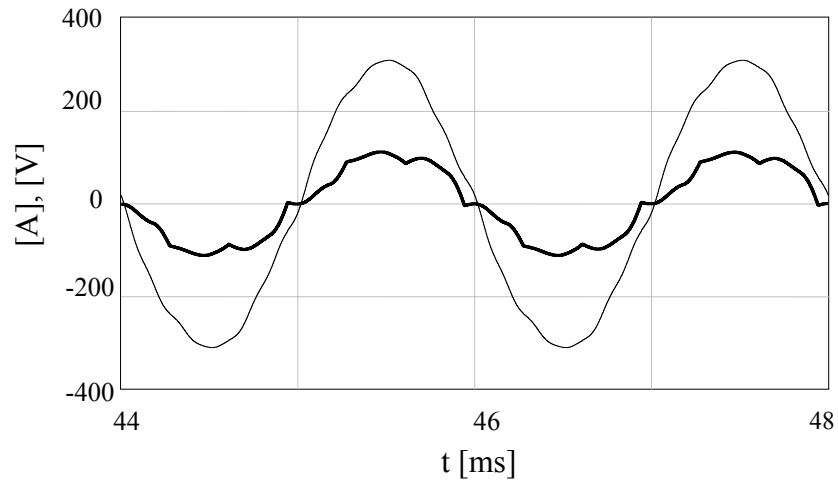
Fig. 4.18 Full-load line current (bold) and supply voltage simulation waveforms for 500kW ASD system (current scale: 0.1x).

The rated load DC voltage and current simulation waveforms are shown in Fig. 4.19. It is seen that the tuned filter topology utilized results in a 495V DC rated output voltage. The full-load 5th and 7th tuned filter capacitor current and voltage simulation waveforms are shown in Fig. 4.20 and Fig. 4.21, respectively.
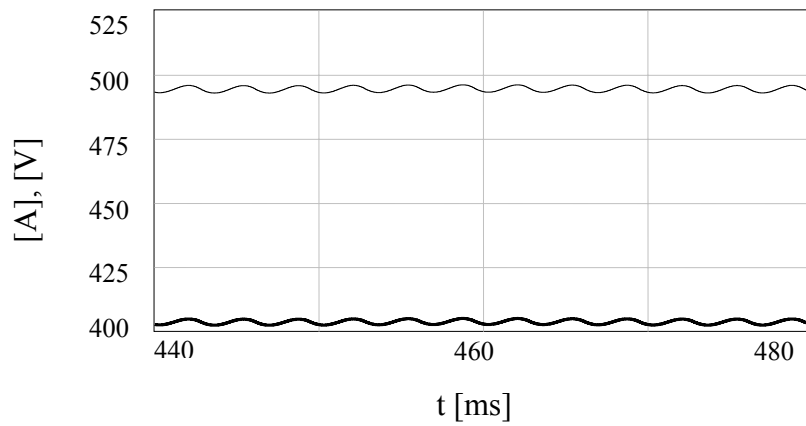
Fig. 4.19 Full-load DC load current (bold) and voltage simulation waveforms for 500kW ASD system (current scale: 0.4x).
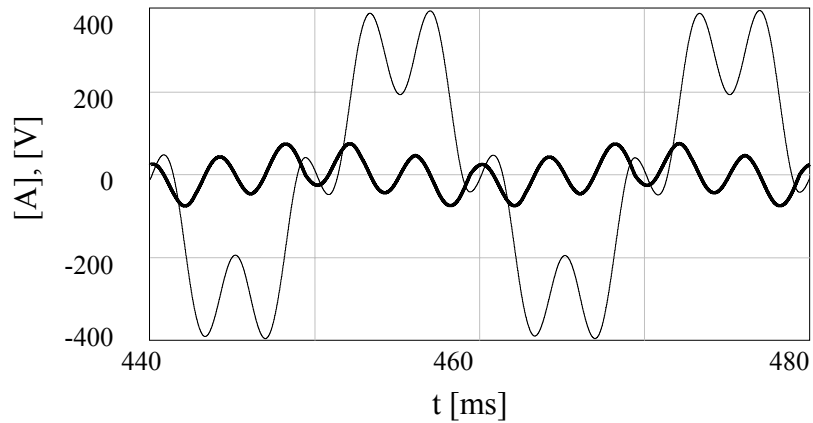
Fig. 4.20 Full-load 5th tuned filter capacitor current (bold) and voltage waveform for 55kW ASD system (current scale: 0.2x).
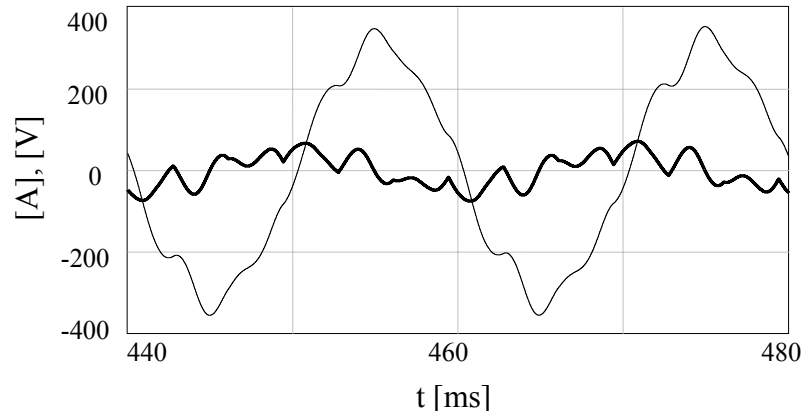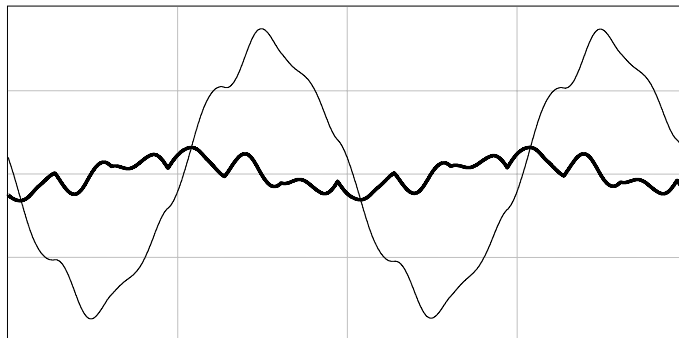

Fig. 4.21 Full-load 7th tuned filter capacitor current (bold) and voltage simulation waveforms for 500kW ASD system (current scale: 0.4x).
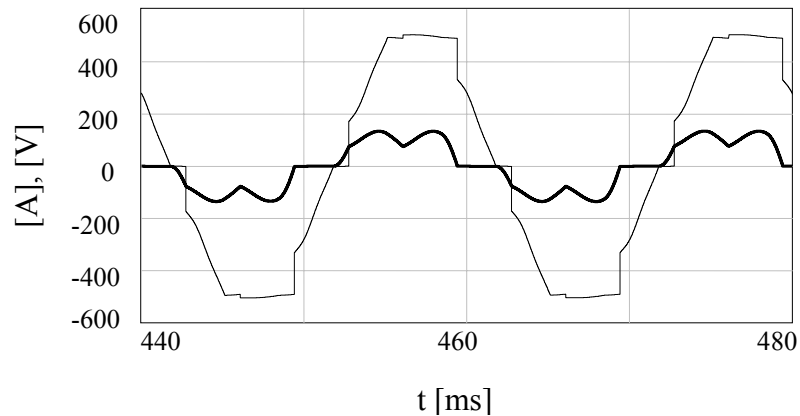
The rectifier current and rectifier line-to-line voltage simulation waveforms are shown in Fig. 4.22. The rectifier voltage is distorted due to the rectifier current harmonics. The same conclusions as for the 5.5kW rating can be made for the higher ratings.

Table 4.5 shows the full-load performance for the various power ratings for the T-shape 5th and 7th single tuned filters (Table 4.4) method combined with the 2% L_{dc}.
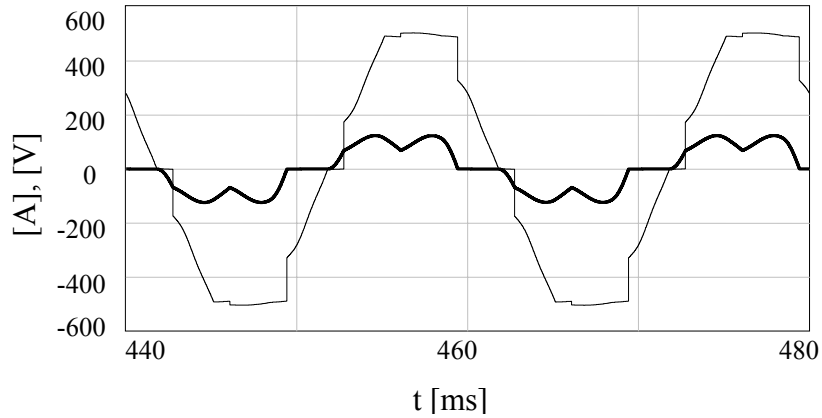
Fig. 4.22 Full-load rectifier current (bold) and line-to-line voltage simulation
waveforms for 500kW ASD system (current scale: 0.1x).

Table 4.5 Full-load performance of the tuned filter for various power ratings

	Tuned Filter		
P_R (kW)	5.5	55	500
THD_I%	13	13	12
PF	0.99	0.99	0.99
V_{dc} (V)	497	496	495

4.3.5 No-Load Simulations of The 500 kW Rated System

The no-load operating condition simulations and performance analysis are presented.
The same no-load definition considered for 5.5kW ASD system is involved. The no-
load line current and supply voltage simulation waveforms are shown in Fig. 4.23.
The line current THD_I value increases to 28% as the topology imports the existing
utility current harmonics at no-load and the line power factor is near zero.

106
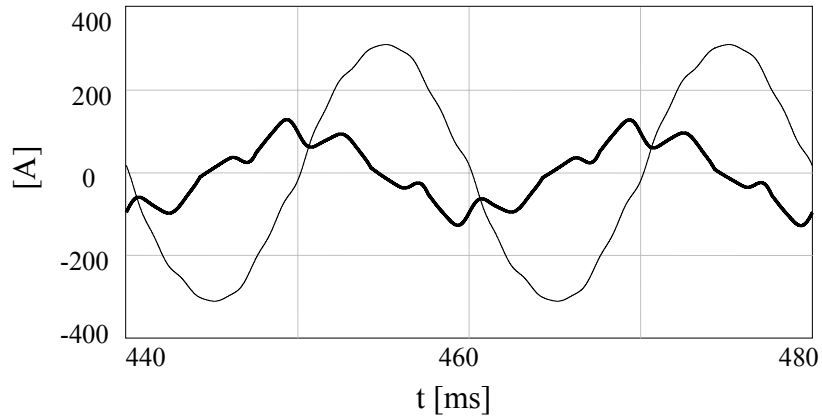
Fig. 4.23 No-load line current (bold) and supply voltage simulation waveforms for 500kW ASD system (current scale: 0.4x).

The no-load 5th and 7th tuned filter capacitor voltage simulation waveforms compared to the defined shunt node voltage simulation waveforms are shown in Fig. 4.24 and Fig. 4.25, respectively. It is seen that each capacitor voltage is approximate equal to the total node voltage.
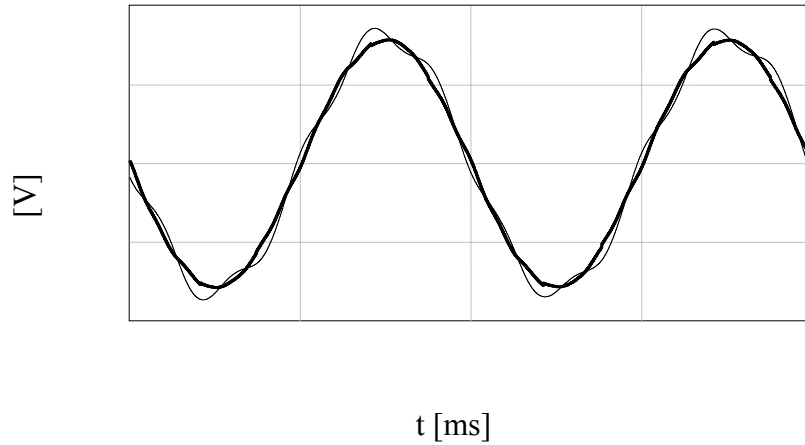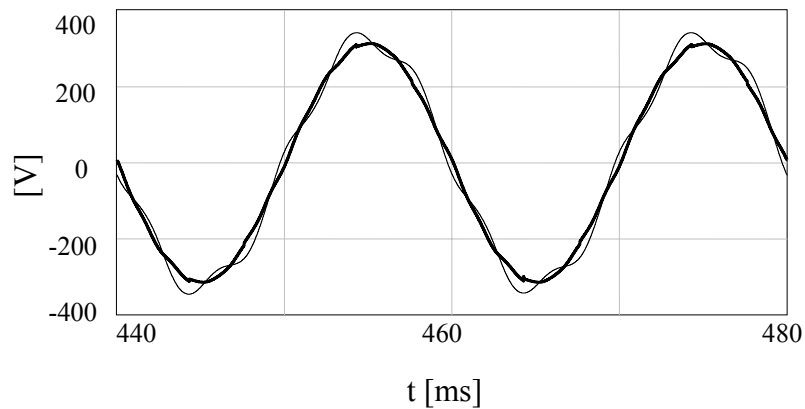

Fig. 4.24 No-load node (bold) and 5th tuned filter capacitor voltage simulation waveforms for 500kW ASD system.
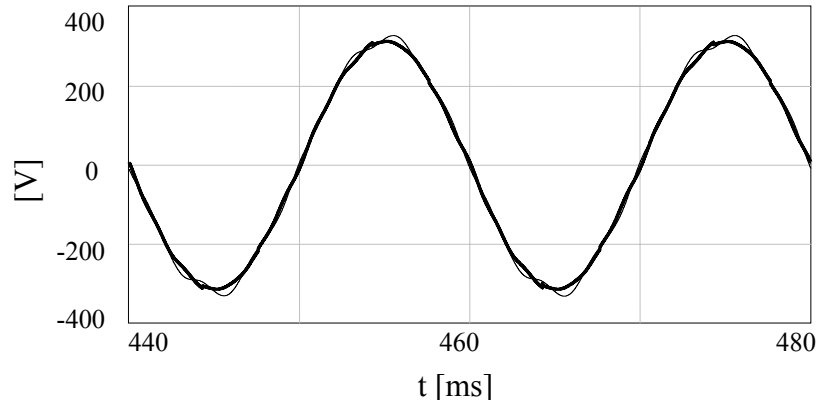
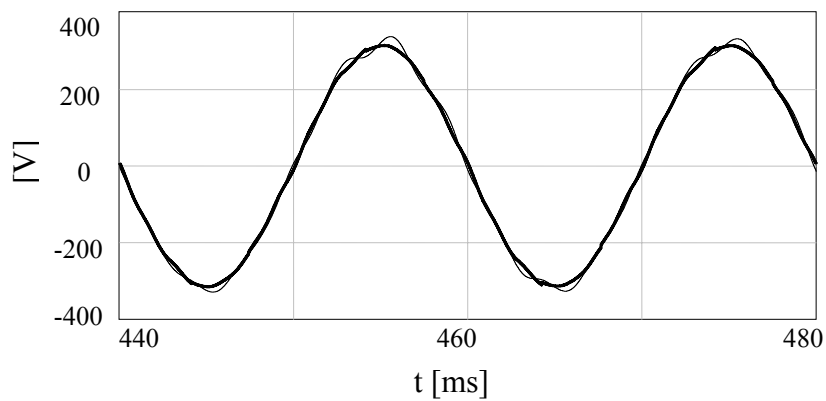Fig. 4.25 No-load node (bold) and 7th tuned filter capacitor voltage simulation waveforms for 500kW ASD system.

4.4 Improved Broadband Filter Based ASD System Simulations

In this section, performance analysis of the IBF based ASD system under balanced and distorted utility (with 3% THD$_V$) is presented. Simulation current and voltage simulation waveforms are illustrated and analyzed. The parameter values of the improved broadband filter utilized and their equivalent series resistances (R$_{ESR}$) for the 5.5 kW, 55 kW, and 500 kW power ratings are shown in Table 4.5. The equivalent series resistances for the filter reactances are estimated by Equation 3.39. The 5.5 kW filter capacitor R$_{ESR}$ value is calculated from the product data sheet information. Other capacitance's R$_{ESR}$ values are estimated based on the 5.5 kW case (scaled proportionally). Table 4.5 also contains the ASD system DC side equivalent load resistor (R$_{dc}$) information. These parameters are implemented in the simulation circuit, shown in Fig. 4.26, for all the power ratings considered.

Table 4.5 IBF parameters for various power ratings

P_R (kW)	5.5	55	500
L_i (mH)	10.8	1.08	0.121
R_{ESR} (mΩ)	34	3.5	0.39
L_f (mH)	4.9	0.49	0.055
R_{ESR} (mΩ)	16	1.6	0.2
$C_{f\Delta}$ (μF)	20.6	206	1844
R_{ESR} (mΩ)	63[*]	6.3	0.69
L_o (mH)	3.1	0.31	0.034
R_{ESR} (mΩ)	10	1.0	0.11
R_d (Ω)	300	40	5
R_{dc} (Ω)	49	4.9	0.54

*product data sheet based estimation
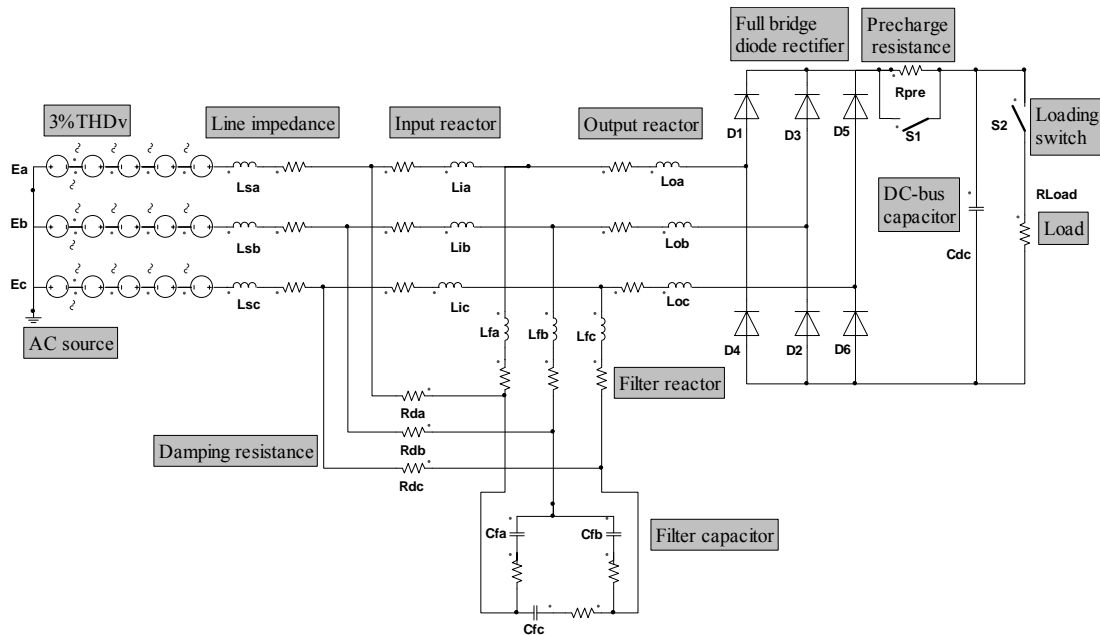
Fig. 4.26 Simulation circuit for ASD system utilizing IBF.

4.4.1 Full-Load Simulations of The 5.5 kW Rated System

For the 5.5kW ASD system, Table 4.6 shows the filter parameters and performance calculated by the accurate design approach described in chapter 3. Simulation performance results obtained will be compared to the accurate design method results. The full-load line current and rectifier current simulation waveforms are shown in Fig. 4.27, while the full-load line current and the supply phase voltage simulation waveforms are shown in Fig. 4.28. The line current has a 9.2% THD_I value and the line power factor is 0.978 leading at full-load conditions. These results are in close correlation with the equivalent circuit based estimation method results shown in Table 4.6. They also verify the accuracy of the parameter determination method. Table 4.6 also points out the difference between the approximate and accurate (optimal) design. In the approximate design, the series resonant frequency was selected as 275 Hz and the parallel resonant frequency was selected 150 Hz. As Table 4.6 indicates, in the optimal design, both frequencies are slightly increased. Therefore, the design increases the frequencies and reduces the passive filter component sizes such that the filter becomes more economical and the performance requirement is still satisfied.

Table 4.6 Accurate design method filter parameters and estimated performance (using the equivalent circuit approach) for 5.5 kW ASD system

Method	L_i (mH)	L_f (mH)	$C_{f\Delta}$ (μF)	L_o (mH)	R_d (Ω)	f_s (Hz)	f_p (Hz)	Line THD_I (%)	Line PF	α	ΔV_o %
Accurate Calculation	10.8	4.9	20.6	3.1	300	287	160	9.94	0.981	0.54	3.91
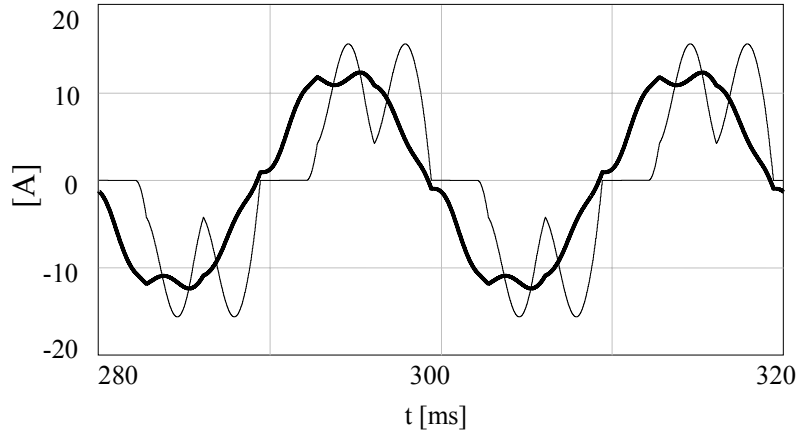
Fig. 4.27 Full-load line (bold) and rectifier current simulation waveforms for 5.5kW ASD system.

Fig. 4.28 Full-load line current (bold) and supply voltage simulation waveforms for 5.5kW ASD system (current scale: 10x).

The rated load DC voltage and current simulation waveforms are shown in Fig. 4.29. It is seen that the IBF system results in a 521V DC rated output voltage. The DC rated output voltage value for the IBF is approximately 5% higher than the previous topologies values. This due to the larger filter capacitor C_f utilized that compensate for the voltage drop across the L_i and L_o reactances. The full-load filter capacitor current and voltage simulation waveforms are shown in Fig. 4.30. While the full-load rectifier current and rectifier line-to-line voltage simulation waveforms are shown in Fig. 4.31.

111

From the above simulation results, it is obvious that the IBF topology has better performance at full-load than the previous filtering topologies. The line current THD_I value is low (<10%) with slightly leading line power factor value (>0.97).

Fig. 4.29 Full-load DC load current (bold) and voltage simulation waveforms for 5.5kW ASD (current scale: 40x).

Fig. 4.30 Full-load filter capacitor current (bold) and voltage waveform for 5.5kW ASD system (current scale: 10x).
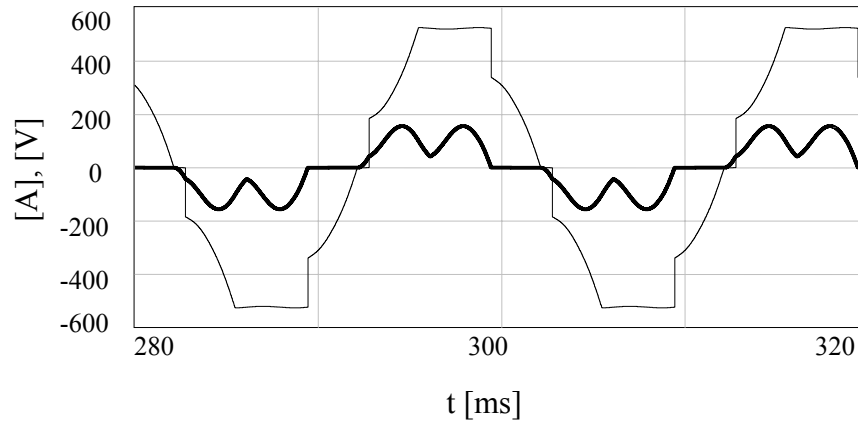
Fig. 4.31 Full-load rectifier current (bold) and line-to-line voltage simulation waveforms for 5.5kW ASD system (current scale: 10x).

4.4.2 No-Load Simulations of The 5.5 kW Rated System

In this section, the no-load operating condition simulation results and waveforms are presented. The same no-load definition applied to the tuned filter topology is considered. The no-load line current and the supply phase voltage simulation waveforms are shown in Fig. 4.32. On contrast to the tuned filter method (25% line THD_I), the line current THD_I value has a low value of 6.5% at no-load and the filter blocks the utility current harmonics. However, the no-load current of IBF is nearly twice the no-load current of TF. The line power factor is near zero at no-load condition.

Fig. 4.32 No-load line current (bold) and supply voltage simulation waveforms for 5.5kW ASD system (current scale: 20x).

The no-load node P and filter capacitor voltage simulation waveforms are shown in Fig. 4.33. It seen that the filter capacitor voltage at no-load has all the node P voltage. Therefore, both voltage are equal and are indistinguishable from the waveform.
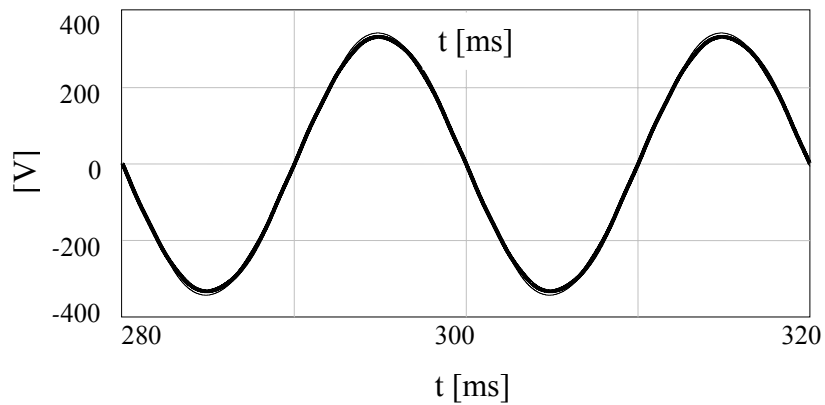
Fig. 4.33 No-load node P (bold) and filter capacitor voltage simulation waveforms for 5.5kW ASD system.

4.4.3 Full-Load Simulations of The 55 kW Rated System

Similar to the 5.5 kW case, for the 55kW ASD system, Table 4.7 shows the filter parameters and full-load performance calculated by the accurate design approach described in chapter 3. Simulations waveforms and performance results implementing the calculated parameters are presented. Performance comparison with the accurate design method results is investigated.

The full-load line current and rectifier current simulation waveforms are shown in Fig. 4.34. While the full-load line current and the supply phase voltage simulation waveforms are shown in Fig. 4.35. The line current has a 9.34% THD_I value and the line power factor is 0.979 leading at full-load conditions. Again results are consistent with Table 4.7.

Table 4.7 Accurate design method filter parameters and estimated performance
(using the equivalent circuit approach) for 55 kW ASD system

| Method	L_i (mH)	L_f (mH)	$C_{f\Delta}$ (µF)	L_o (mH)	R_d (Ω)	f_s (Hz)	f_p (Hz)	Line THD_I (%)	Line PF	α	ΔV_o %
Accurate Calculation	1.08	0.49	206	0.31	40	287	160	9.94	0.981	0.54	3.91
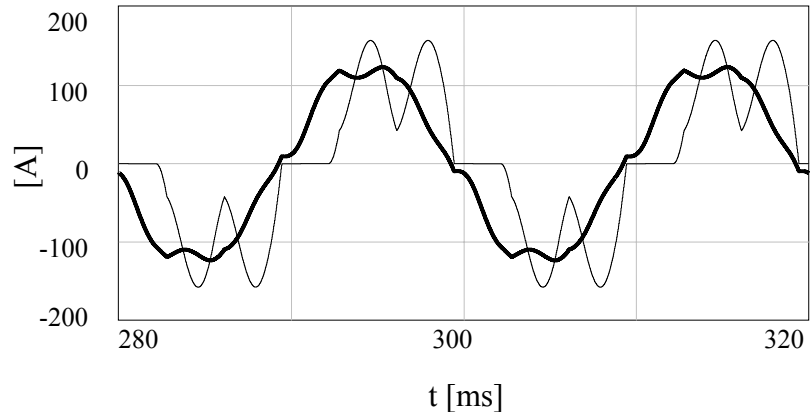
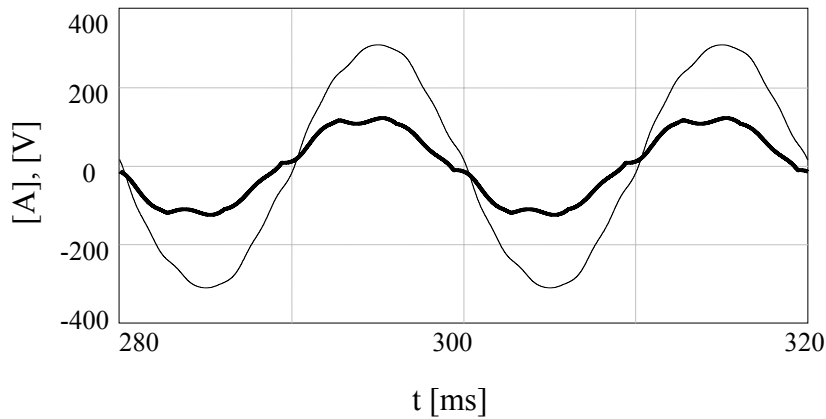Fig. 4.34 Full-load line (bold) and rectifier current simulation waveforms for 55kW ASD system.
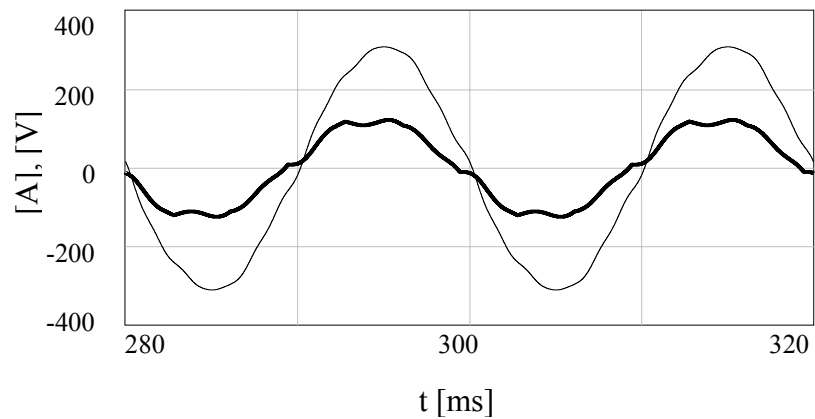
Fig. 4.35 Full-load line current (bold) and supply voltage simulation waveforms for 55kW ASD.

The rated load DC voltage and current simulation waveforms are shown in Fig. 4.36. The IBF topology utilized results in a 521V DC rated output voltage. The full-load filter capacitor current and voltage simulation waveforms are shown in Fig. 4.37. While the rectifier current and rectifier line-to-line voltage simulation waveforms are shown in Fig. 4.38.
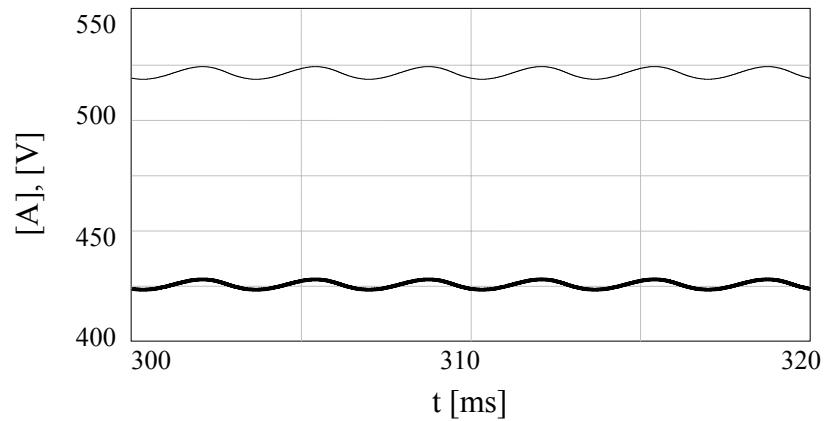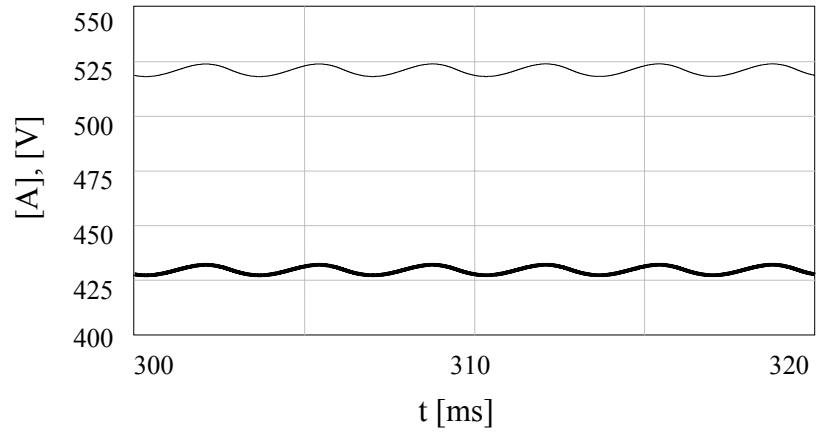
Fig. 4.36 Full-load DC load current (bold) and voltage simulation waveforms for 55kW ASD system (current scale: 4x).
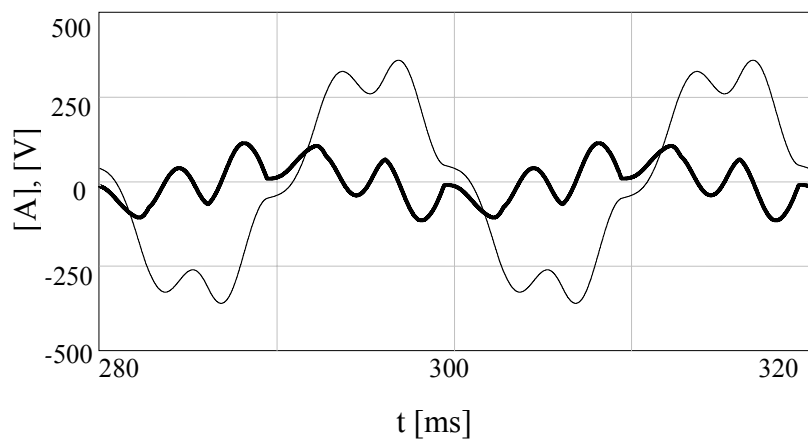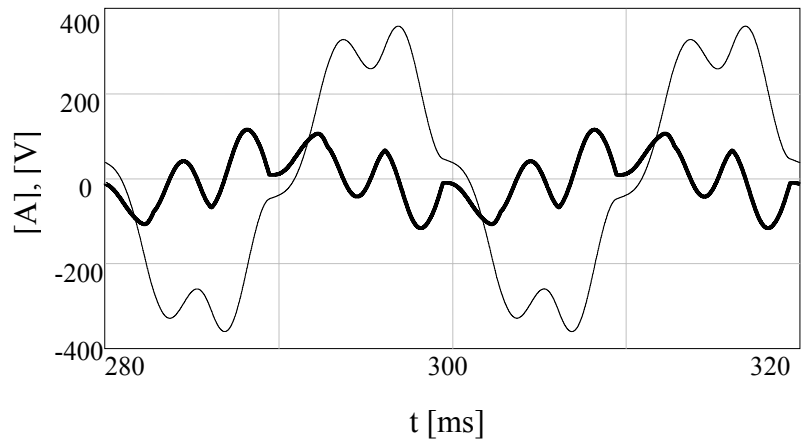

Fig. 4.37 Full-load filter capacitor current (bold) and voltage waveform for 55kW ASD system.
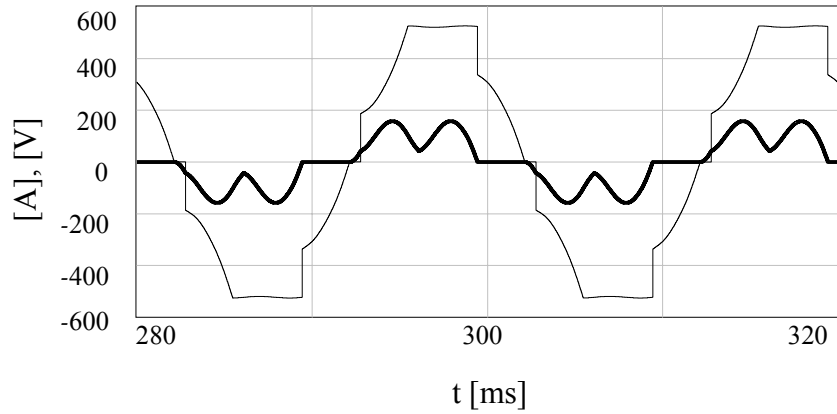
Fig. 4.38 Full-load rectifier current (bold) and line-to-line voltage simulation waveforms for 55kW ASD system.

4.4.4 No-Load Simulations of The 55 kW Rated System

The no-load operating condition simulation results and waveforms for 55 kW power rating are presented in this section. The no-load line current and the supply phase voltage simulation waveforms are shown in Fig. 4.39. The line current THD_I value has a low value of 7.7% at no-load and the filter eliminates importing the utility current harmonics. The line power factor is zero at no-load condition.
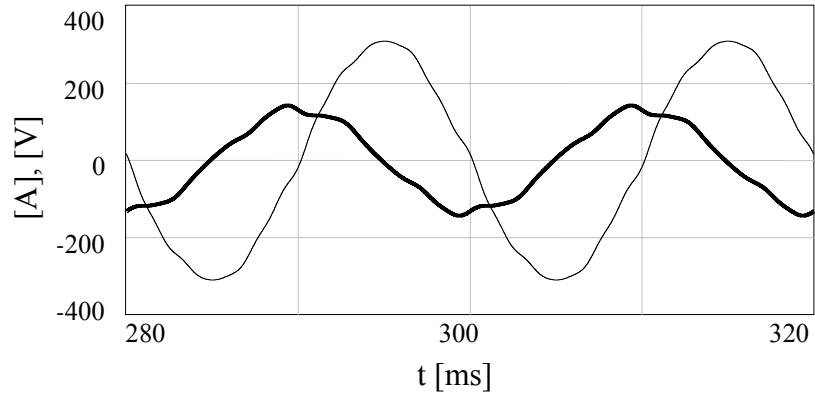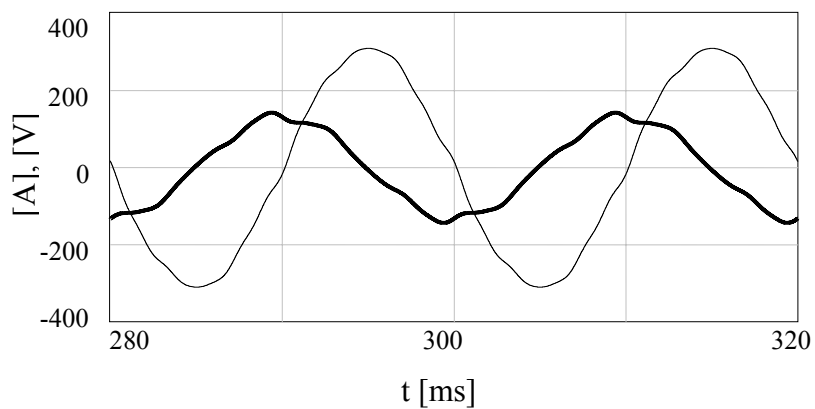

Fig .4.39 No-load line current (bold) and supply voltage simulation waveforms for 55kW ASD system (current scale: 2x).

118

The no-load node P and filter capacitor voltage simulation waveforms are shown in Fig. 4.40. Likewise the 5.5 kW power rating results, It seen that the filter capacitor voltage at no-load has all the node P voltage. Therefore, they are indistinguishable from the waveform.
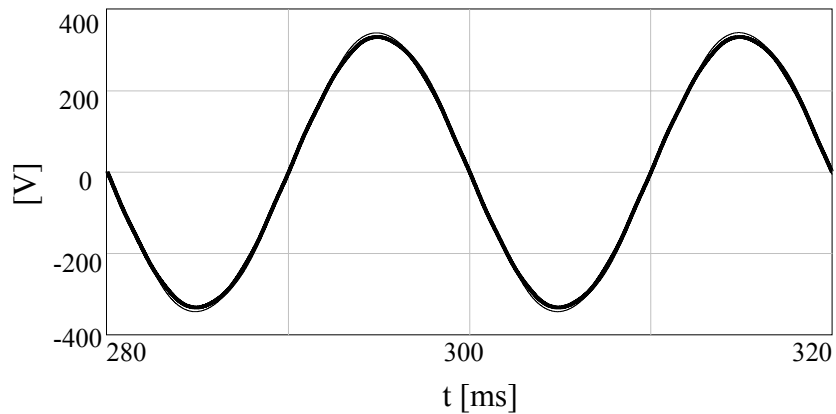
Fig. 4.40 No-load node P (bold) and filter capacitor voltage simulation waveforms for 55kW ASD system.

4.4.5 Full-Load Simulations of The 500 kW Rated System

In the same way that the 5.5 kW and 55 kW rated ASD systems simulation results and performance are presented, the 500kW ASD system is investigated. Table 4.8 shows the filter parameters and performance calculated by accurate design approach.

The full-load line current and rectifier current simulation waveforms are shown in Fig. 4.41. While the full-load line current and the supply phase voltage simulation waveforms are shown in Fig. 4.42. The line current has a 9.3% THD_I value and the line power factor is 0.979 leading at full-load conditions.

Table 4.8 Accurate design method filter parameters and estimated performance
(using the equivalent circuit approach) for 500 kW ASD system

Method	L_i (mH)	L_f (mH)	$C_{f\Delta}$ (μF)	L_o (mH)	R_d (Ω)	f_s (Hz)	f_p (Hz)	Line THD$_I$ (%)	Line PF	α	ΔV_o %
Accurate Calculation	0.121	0.055	1844	0.034	5.0	288	160	9.93	0.981	0.54	3.91
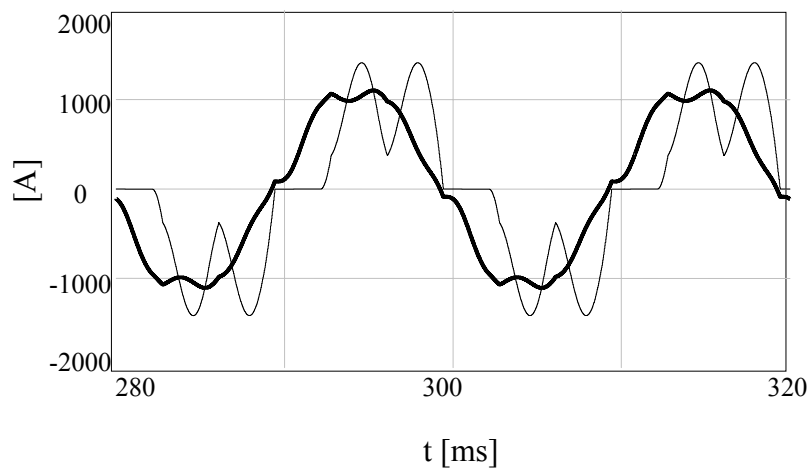
Fig. 4.41 Full-load line (bold) and rectifier current simulation waveforms for 500kW ASD system.
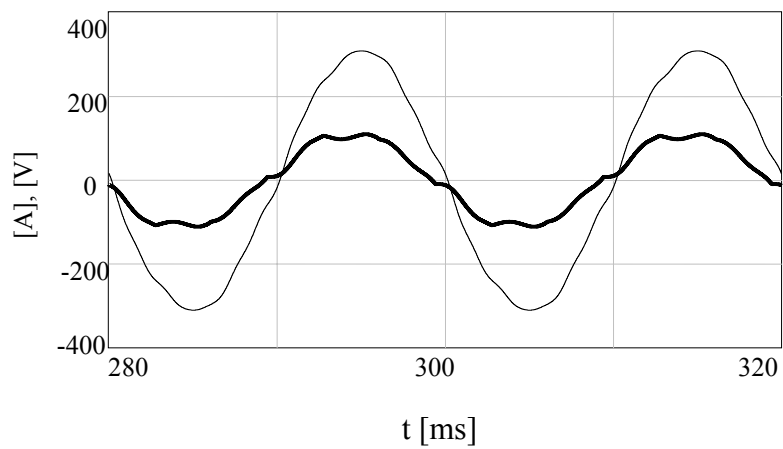
Fig. 4.42. Full-load line current (bold) and supply voltage simulation waveforms for 500kW ASD system (current scale: 0.1x).

The rated load DC voltage and current simulation waveforms are shown in Fig. 4.43. Similarly to 5.5 kW and 55 kW power ratings the IBF topology utilized results in a 520V DC rated output voltage. The full-load filter capacitor current and voltage simulation waveforms are shown in Fig. 4.44. While the rectifier current and rectifier line-to-line voltage simulation waveforms are shown in Fig. 4.45.
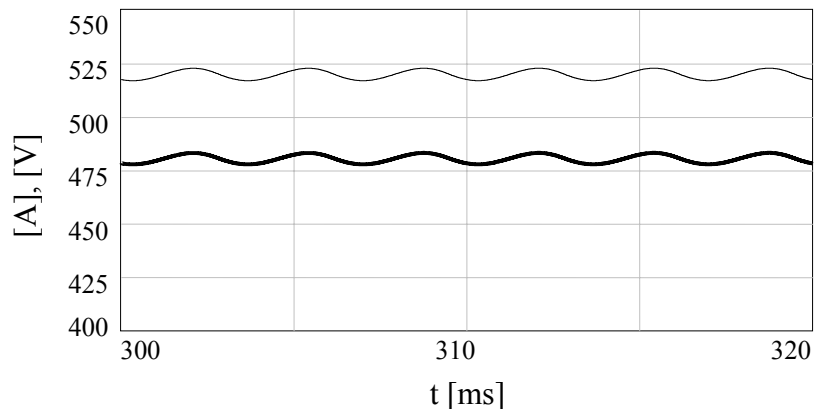
Fig. 4.43 Full-load DC load current (bold) and voltage simulation waveforms for 500kW ASD system (current scale: 0.5x).
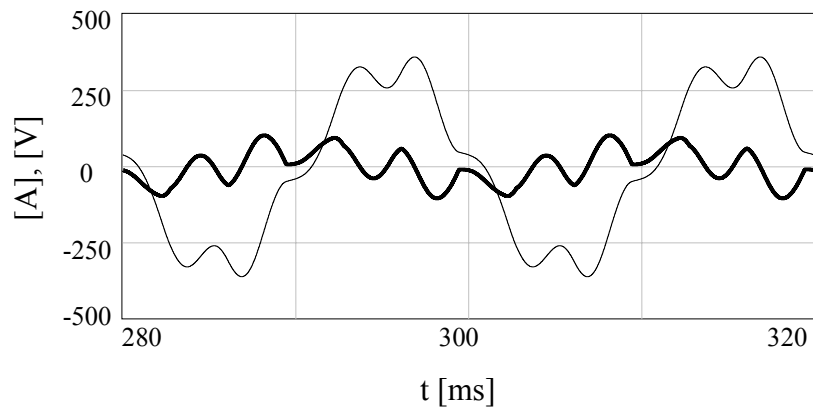
Fig. 4.44 Full-load filter capacitor current (bold) and voltage waveform for 500kW ASD system (current scale: 0.1x).
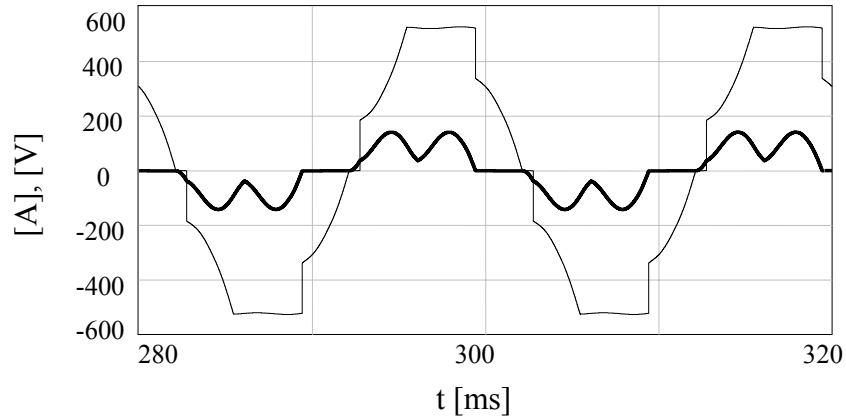
Fig. 4.45 Full-load rectifier current (bold) and line-to-line voltage simulation waveforms for 500kW ASD system (current scale: 0.1x).

4.4.6 No-Load Simulations of The 500 kW Rated System

Similar to the previous power rated ASD systems, in this section, the no-load operating condition simulation results and waveforms are presented with the same no-load definition applied. The no-load line current and the supply phase voltage simulation waveforms are shown in Fig. 4.46. The line current THD_I value has a low value of 7.5% at no-load. On the contrary, the line current THD_I value increased to 28% at no-load for the tuned filter case.
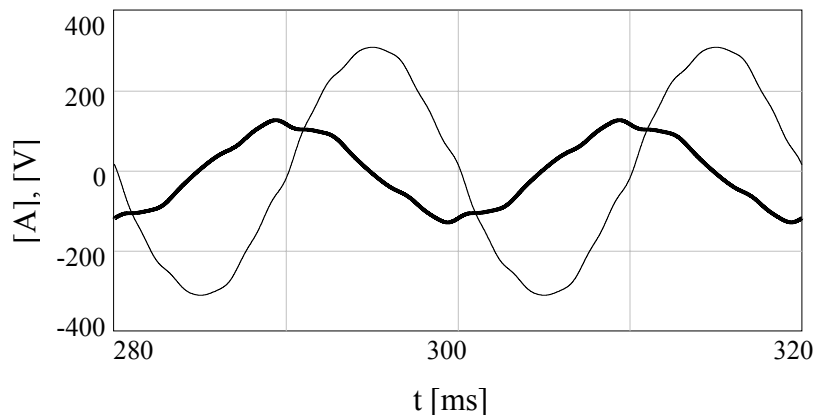
Fig. 4.46 No-load line current (bold) and supply voltage simulation waveforms for 500kW ASD system (current scale: 0.2x).

The no-load node P and filter capacitor voltage simulation waveforms are shown in Fig. 4.47. Likewise the presented lower rated ASD systems, the filter capacitor voltage at no-load has all the node P voltage.
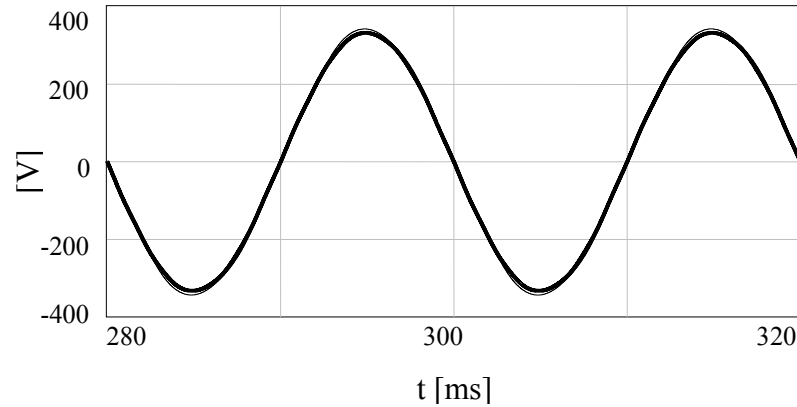
Fig. 4.47 No-load node P (bold) and filter capacitor voltage simulation waveforms for 500kW ASD system.

To summarize, Table 4.9 shows the topology performance obtained by the accurate design method and by detailed computer simulations for all power ratings considered. It is seen that the simulation results are consistent with the analytical results. Accuracy of the results is high with the maximum deviation being 8% in the THD_I and usually with most variables it has much higher accuracy.

Table 4.9 IBF equivalent circuit based and detailed computer simulation based performance prediction comparison for various power rating ASD systems

$P_R(kW)$	5.5			55			500		
Power Quality Constraint	Line THD_I %	Line PF	ΔV_o %	Line THD_I %	Line PF	ΔV_o %	Line THD_I %	Line PF	ΔV_o %
Accurate Method	9.94	0.981	3.91	9.94	0.981	3.91	9.93	0.981	3.91
Computer Simulation	9.20	0.978	3.82	9.34	0.979	3.86	9.30	0.979	3.80
Deviation (%)	8.0	0.4	2.3	6.4	0.2	1.3	6.7	0.2	2.3

4.5 Improved Broadband Filter Performance Characteristics

In this section the IBF performance characteristics are obtained based on the detailed computer simulations investigated. More data points than what has been demonstrated in the above sections have been taken and the results shown in the performance characteristic curves in this section. The improved broadband filter line current THD_I, line power factor and efficiency performance characteristics, from no-load to full-load, are shown in Fig. 4.48 to Fig. 4.50 for all power ratings considered. From nearly 50% load to full-load, over a wide range the IBF based system provides high overall performance. In particular the input current THD_I has satisfactory performance in the full operating range. The IBF based drive does not emit any harmonics to the environment, making the drive environment friendly and candidate for extremely low emission system.
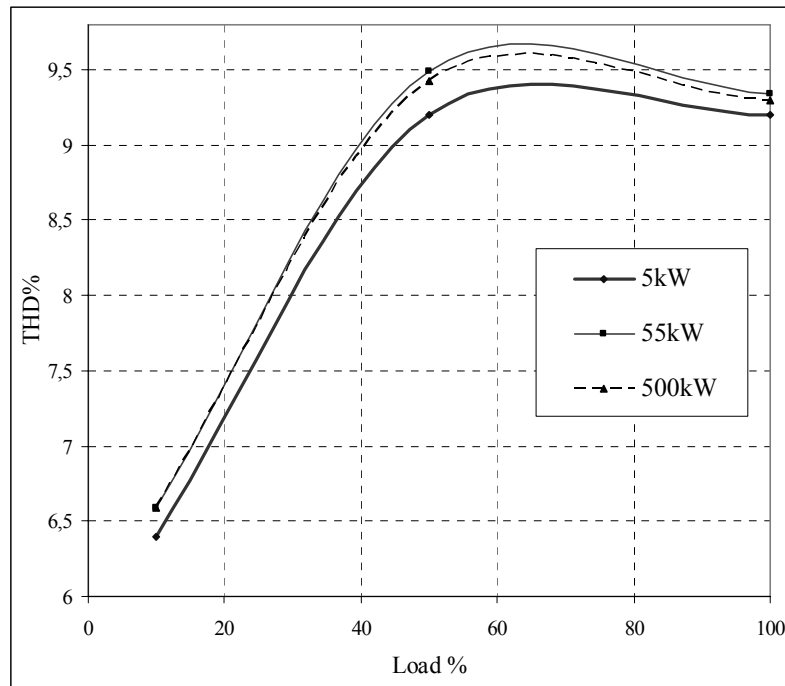
Fig. 4.48 The load current dependency of the IBF line current THD_I.
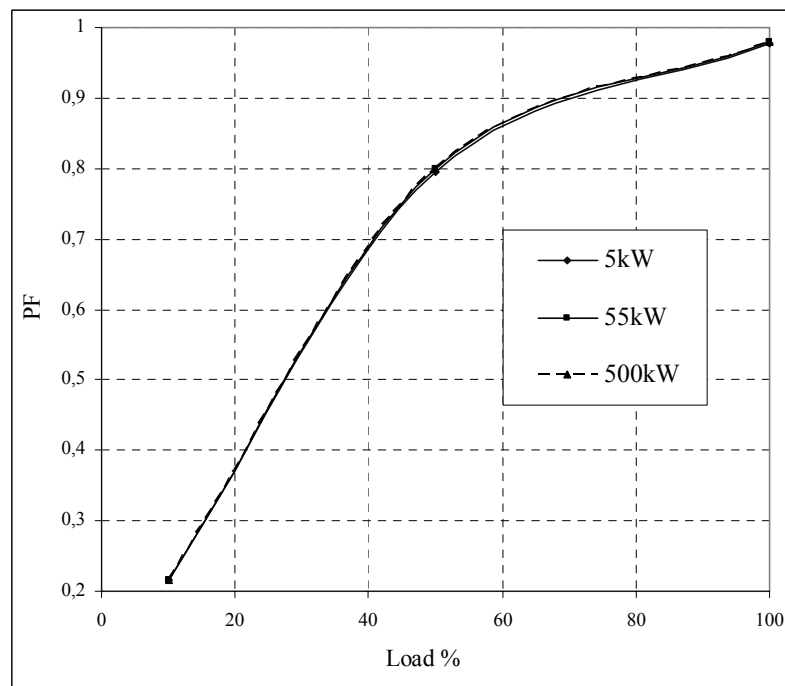
Fig. 4.49 The load current dependency of the IBF input power factor.
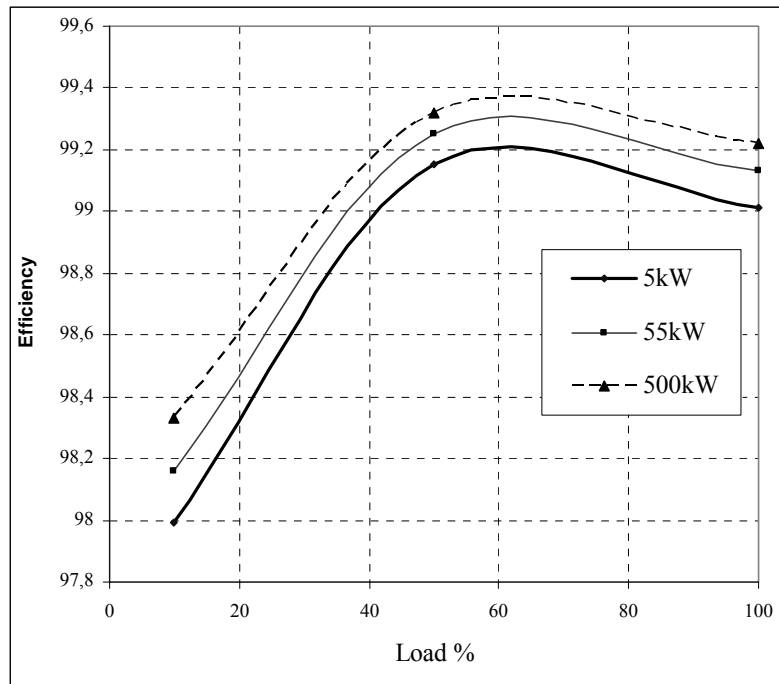
Fig. 4.50 The load current dependency of the IBF efficiency.

4.6 Improved Broadband Filter Switching Transient Simulations

As discussed in the previous chapter (section 3.3.4), the duty of the damping resistance R_d is to specifically damp the turn-on transient overvoltages (reduce the voltage overshoot) across the AC filter capacitors. While it has no major affect on the rectifier terminals and the DC bus voltage. In this section, for 5.5 kW ASD system, the AC line switching transients are investigated by means of detailed computer simulations. The AC filter capacitor voltages and the rectifier terminal voltages along with the DC bus voltage simulation waveforms (with and without damping) are presented. Due to the significant performance/behavior similarity observed for all the power ratings investigated, only the 5.5kW rated system (Fig. 3.12 to Fig. 3.17) results are presented.

The line side switch closure modeling simulation involves the start-up transient where the IBF input switch is turned-on at t=20ms (with respect to phase "a") and the AC filter capacitors are precharged followed by the DC bus capacitor charging. In Table 3.8 it was shown a damping resistor of 100Ω would provide the highest

126

practical damping. Therefore, this resistor value has been utilized in the computer simulation.   Also a simulation is run with the damping resistor removed and both cases are compared in Fig. 4.51. It is clear that the 100Ω damping resistor provides noticeable voltage stress reduction on the AC filter capacitor compared to the no-damping case. On the other hand, rectifier line-to-line voltage waveforms, shown in Fig. 4.52, and DC bus capacitor voltage waveforms, shown in Fig. 4.53, have negligible peak overvoltage reduction.
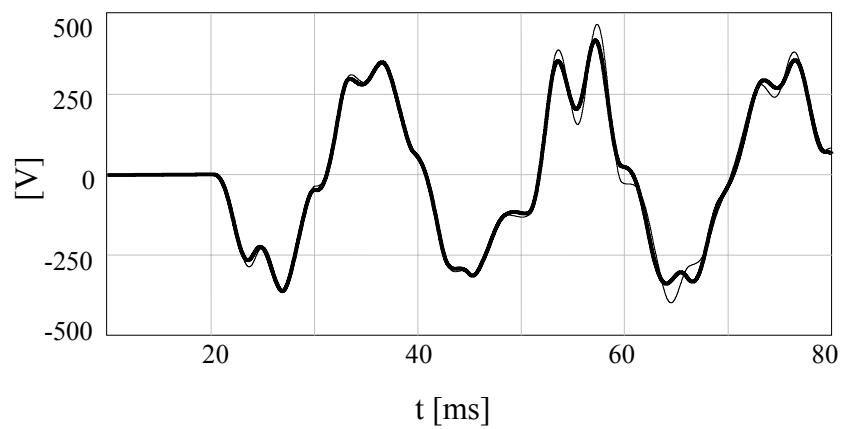
Fig. 4.51 AC filter capacitor turn-on (t=20ms) transient voltage simulation waveforms with 100Ω R_d (bold) and without damping for 5.5kW ASD system.
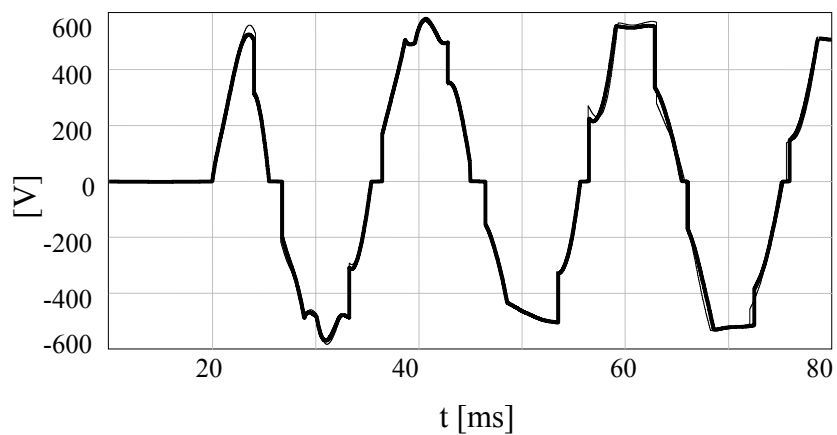
Fig. 4.52 AC rectifier terminals turn-on (t=20ms) transient voltage simulation waveforms with 100Ω R_d (bold) and without damping for 5.5kW ASD system.
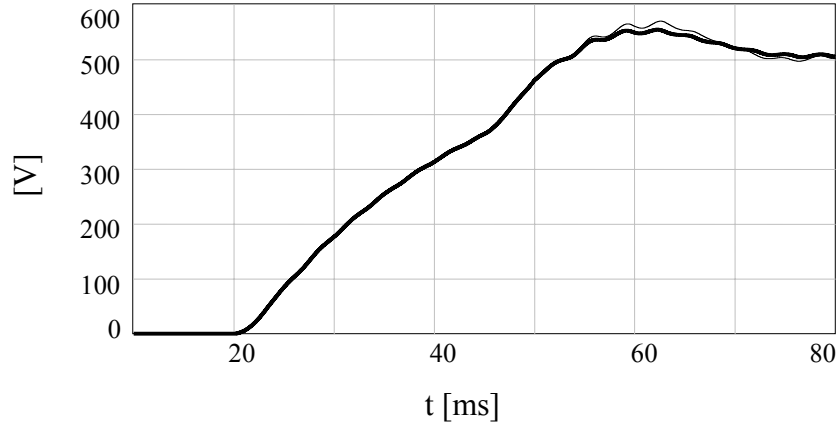
Fig. 4.53 DC bus capacitor turn-on (t=20ms) transient voltage simulation waveforms with 100Ω R_d (bold) and without damping for 5.5kW ASD system.

4.7 Simulation Results Under Unbalanced Utility Grid Voltage

In this section, performance of the various passive filtering methods is investigated under unbalanced utility grid voltage conditions. The utility grid is considered to be without voltage harmonic distortion. The line current THD_I values for all phases are investigated. The investigation involves various utility unbalanced voltage values for the improved broadband filter for all power ratings considered. For comparison purpose, a 5.5 kW power rating is considered for the three different passive filtering topologies discussed. The line current THD_I value and the DC load output voltage ripple variations are presented.

The National Electrical Manufacturers Association of USA (NEMA) standard voltage unbalance definition applied in the study is given by [20]

$$\text{Voltage unbalance} = \frac{\text{Maximum deviation from mean of } \{V_{ab}, V_{bc}, V_{ca}\}}{\text{Mean of } \{V_{ab}, V_{bc}, V_{ca}\}} \tag{4.6}$$

where the voltages utilized are the line-to-line values.

For instant, according to this definition, 1% voltage unbalance is equivalent to 2% voltage value reduction in phase "a". Computer simulations were run for all the

128

power ratings and unbalance conditions considered and the results are summarized in tables. Table 4.10 to Table 4.12 show the line current THD_I values at full-load and half-load for the various power ratings considered. The analysis involves three different voltage unbalance values compared to the nominal balanced line current THD_I values. It is seen that the line current THD_I values at full-load do not have significant variation for all power ratings. Under significant line voltage unbalance (3%) and half-load, the worst line current THD_I can be nearly 12% which is considered as a fairly low value compared to the results of most other filtering methods under balanced conditions! Therefore, the IBF topology is not sensitive to line voltage unbalances and even under severe line voltage unbalances the line current THD_I remains low for all phases.

Table 4.10 IBF performance under unbalanced line voltage for 5.5kW ASD system

Voltage Unbalance (%)	% THD_I at 100% Load	% THD_I at 50% Load
0	7.67	7.85
1	7.82 -7.86	7.92 – 7.98
2	8.10 – 8.47	8.43 – 9.71
3	8.44 – 9.45	9.02 – 11.67

Table 4.11 IBF performance under unbalanced line voltage for 55kW ASD system

Voltage Unbalance (%)	% THD_I at 100% Load	% THD_I at 50% Load
0	7.62	7.82
1	7.77 – 7.81	8.01 – 8.32
2	8.04 – 8.42	8.40 – 9.68
3	8.38 – 9.38	8.99 – 11.62

Table 4.12 IBF performance under unbalanced line voltage for 500kW ASD system

Voltage Unbalance (%)	% THD$_I$ at 100% Load	% THD$_I$ at 50% Load
0	7.54	7.76
1	7.70 – 7.73	7.95 – 8.26
2	7.96 – 8.34	8.34 – 9.61
3	8.30 – 9.30	8.94 – 11.55

The unbalanced line voltage and unbalanced output performance attributes of the various filtering methods discussed is also investigated in detail. As an unbalanced operating condition, 5% voltage reduction in phase "a" of the three-phase AC utility grid (50 Hz, 380V line-to-line) resulting in 2.5% line voltage unbalance has been considered. Table 4.13 indicates that the improved broadband filter is not sensitive to line voltage unbalance. Over a wide operating range the IBF filter characteristics are stable and the input current THD$_I$ is low.

Table 4.13 Full-load performance under 2.5% input voltage unbalance for a 5.5 kW ASD system[*]

Filter Type		3% Line Reactor	6% Line Reactor	Tuned Filter	Improved Broadband Filter
Nominal Line THD$_I$(%)		36	29	11.6	8.90
Line THD$_I$ (%)	Phase a	45.16	32.92	13.13	9.47
	Phase b	46.59	32.75	14.78	9.61
	Phase c	31.39	26.33	11.72	9.50
ΔV_{dc} (V$_{pp}$)		3.2%	1.6%	1.3%	1.0%

*supply THD$_V$ = 0.0%

The three-phase supply voltage and line current waveforms are investigated under balanced and 2.5% unbalanced utility grid for IBF and 3% AC line reactor filter for the purpose of comparison. As shown in Fig. 4.54 and Fig. 4.55, the line currents are

stable under both utility grid operating conditions for IBF. In contrast, as shown in Fig. 4.56 and 4.57, the line currents are highly distorted under the 2.5% unbalanced utility grid compared to the balanced case waveforms for the 3% AC line reactor filter.
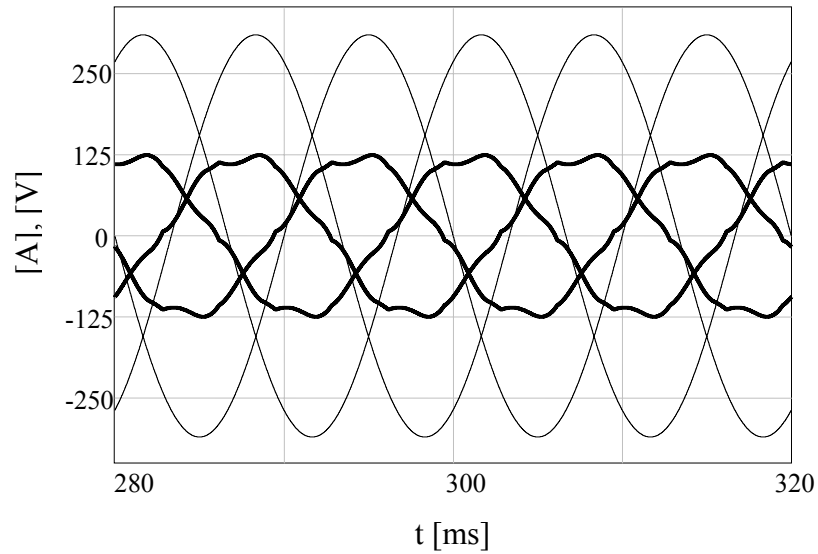
Fig. 4.54 Full-load three-phase supply voltage and current (bold) waveforms for balanced utility grid for 5.5kW ASD system utilizing IBF (current scale: 10x).
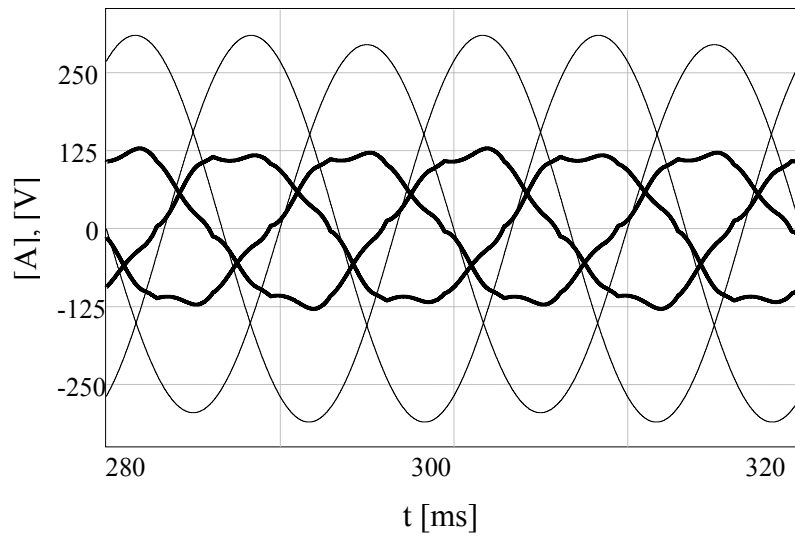
Fig. 4.55 Full-load three-phase supply voltage and current (bold) waveforms for 2.5% unbalanced utility grid for 5.5kW ASD system utilizing IBF (current scale: 10x).
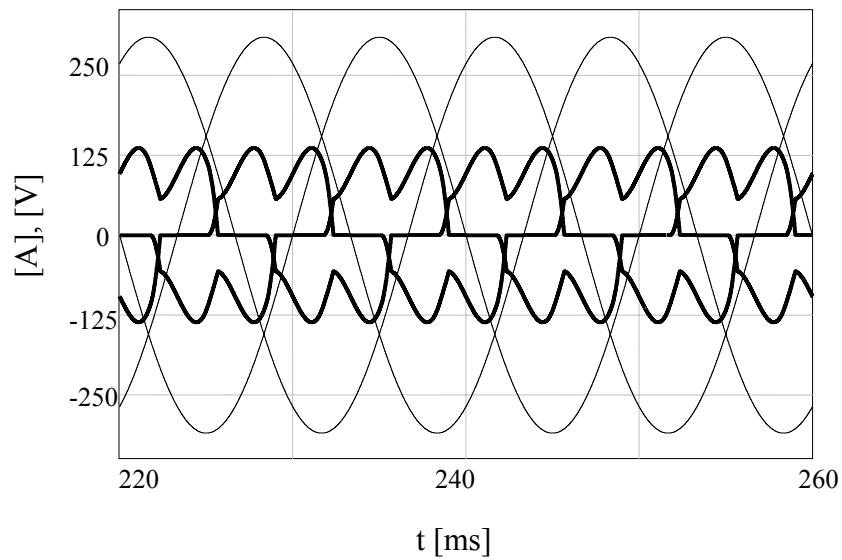
Fig. 4.56 Full-load three-phase supply voltage and current (bold) waveforms for balanced utility grid for 5.5kW ASD system utilizing 3% AC line reactor (current scale: 10x).
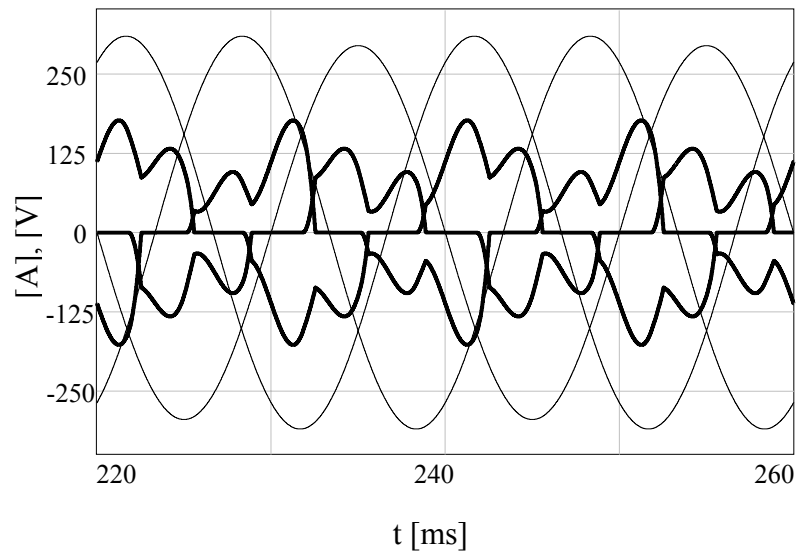
Fig. 4.57 Full-load three-phase supply voltage and current (bold) waveforms for 2.5% unbalanced utility grid for 5.5kW ASD system utilizing 3% AC line reactor (current scale: 10x).

For the DC side, as shown in Fig. 4.58, the DC bus voltage at the rectifier output is stable and no significant second harmonic is present for IBF. On the contrary, as shown in Fig. 4.59, the 3% AC line reactor filter is highly sensitive to the line voltage unbalance and large second harmonic voltage exists on the DC bus capacitor voltage.
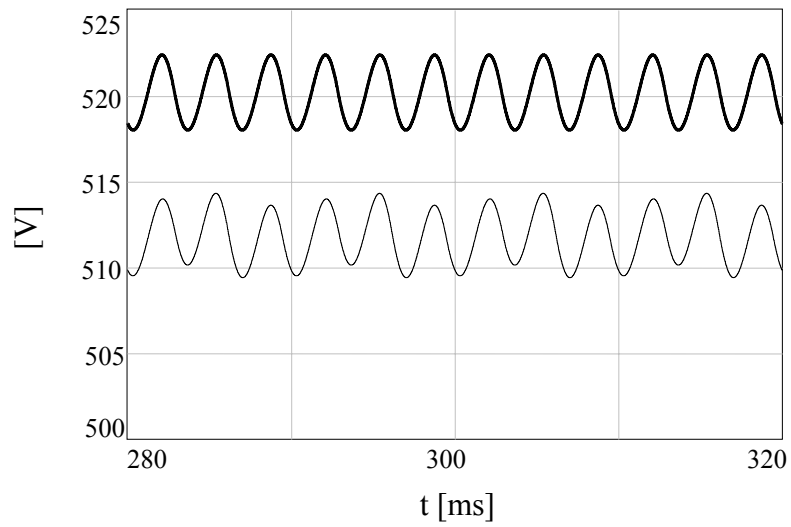
Fig. 4.58 Full-load DC bus capacitor voltage waveforms for balanced (bold) and
2.5% unbalanced utility grid for 5.5kW ASD system utilizing IBF.
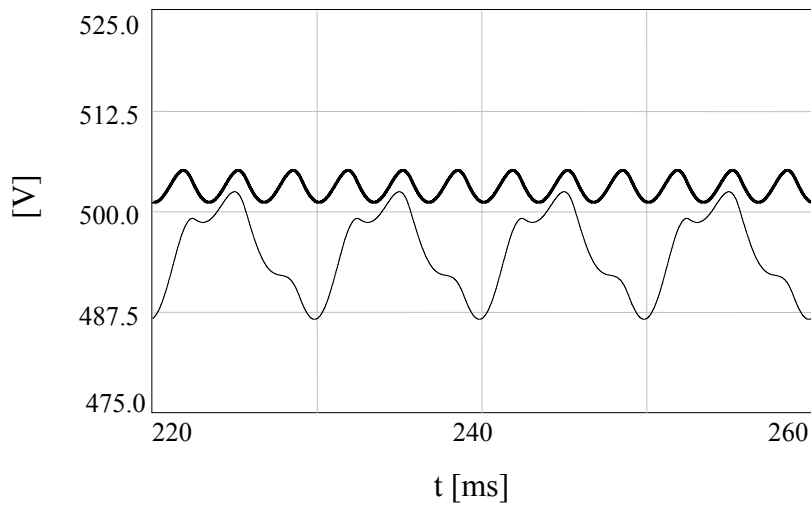
Fig. 4.59 Full-load DC bus capacitor voltage waveforms for balanced (bold) and
2.5% unbalanced utility grid for 5.5kW ASD system utilizing 3% AC line reactor.

Investigation of the AC line current harmonic spectrum for the IBF (Table 4.14) and
the 3% AC line reactor (Table 4.15) reveals another advantage of the IBF system. As
well known, due to line voltage unbalance a second harmonic voltage is generated in
the rectifier output voltage. This in turn results in a third harmonic current on the AC

134

line. As Table 4.14 indicates under the line voltage unbalance, the third harmonic current generated in the IBF system is less than 2% of the fundamental component. However, with the 3% line reactor filter, as Table 4.15 shows, nearly 20% third harmonic current exists in the line current. This results in additional distortion in the AC line current. The reason that the IBF structure is more forgiving to line voltage unbalances is due to the fact that the IBF input inductance L_i is quite large and it blocks the effect of line voltage unbalances. Therefore, in the IBF structure stable and low distortion input and output characteristics are obtained, while the other configurations exhibit poor performance.

Table 4.14 Line current harmonic spectrum under 2.5% voltage unbalance for 5.5kW ASD system utilizing IBF

	f [Hz]	L1.I [A]	Phi [rad]	Phi [deg]	%(Max)
Minimum	50	0.15197	1.0784	61.785	1.2775
Maximum	0.55k	11.895	6.1272	0.35106k	0.1k
0	50	11.895	3.3512	0.19201k	0.1k
1	0.15k	0.22861	1.0784	61.785	1.9218
2	0.25k	0.8131	1.7641	0.10107k	6.8355
3	0.35k	0.15197	6.118	0.35053k	1.2775

Table 4.15 Line current harmonic spectrum under 2.5% voltage unbalance for 5.5kW ASD system utilizing 3% AC line reactor

	f [Hz]	L4.I [A]	Phi [rad]	Phi [deg]	%(Max)
Minimum	50.001	93.806m	0.46769	26.797	1.0127
Maximum	1.45k	9.2625	6.233	0.35712k	0.1k
0	50.001	9.2625	3.0793	0.17643k	0.1k
1	0.15k	1.8093	1.2979	74.366	19.534
2	0.25k	3.7617	5.0906	0.29167k	40.612
3	0.35k	0.89101	0.46769	26.797	9.6195

4.8 Filter Performance Comparisons

This section presents the performance comparison of various passive harmonic filters for three-phase diode rectifier front-end type adjustable speed drives. The comparison is based on the simulation results obtained in this chapter. The filter full-load performance characteristics are listed in Table 4.16. The table indicates that the improved broadband filter THD_I and power factor performance is superior to the other filter configurations. The DC bus voltage of IBF is slightly higher (4%) than the alternatives and this is not considered as a drawback.

Only the tuned filter performance is comparable to IBF. However, even the tuned filter has about 3% higher THD_I therefore the performance difference is significant. Therefore, IBF provides higher input power quality than the other passive filtering methods. At the output it also provides stable output voltage with high voltage regulation.

As Table 4.16 indicates, the efficiency of the IBF based system is comparable to the tuned filter based system due to the fact that both filters involve similar number of components with similar ratings. The 3% and 6% AC line reactors have higher efficiency, due to the minimal component count, however at the expense of poor overall performance.

Table 4.16 Full-load performance of various filters for 5.5-500 kW ASD systems[*]

Filter Type	3% line Reactor	6% line Reactor	Tuned Filter	IBF
Full-load Input	36	29	12-13	9.2-9.4
Input Power Factor	0.92 (lag.)	0.93 (lag.)	0.99 (lag.)	0.98 (lead.)
Full-load DC Voltage (V)	499-502	491-492	495-497	520-521
Efficiency(%)	99.96-99.97	99.39-99.94	98.8-99.4	99.0-99.2

* Supply $THD_V = 3\%$.

Table 4.17 provides additional performance data on the investigated filters. The data involves the voltage regulation at node P (ΔV_o %) for the TF and IBF along with the line current no-load to full-load ratio. The voltage regulation at the rectifier terminals (ΔV_{rect}%) and at the DC bus ΔV_{dc}(%) are investigated for all filters.

Evaluation of voltage regulation of the ASD system at various locations indicates that IBF has the poorest voltage regulation among all. However, the amount of voltage variation is not significant (6-7% more than the alternative methods) and practically not problematic. Also the filter performance at no-load is compared for the discussed filters. The IBF structure involves about twice no-load current as the tuned filter. This is due to the filter structure. However, one advantage of the IBF topology is that the larger no-load current improves the line current THD_I at the expense of operating with near zero leading power factor. This may be favorable in installations where the demand for reactive power is not met by the compensation systems. Otherwise, IBF should be mainly considered for inverter drive applications with high operating duty cycle in order to avoid poor leading PF and problems associated with it.

Table 4.17 Additional performance of various filters for 5.5-500 kW ASD systems

Filter Type	3% Line Reactor	6% Line Reactor	Tuned Filter	IBF
ΔV_o(%)	------	------	1.4-1.6	3.8-3.9
ΔV_{rect}(%)	0.58-0.60	1.06-1.07	1.7-1.9	4.2-4.3
ΔV_{dc}(%)	5.7-6.0	6.0-7.0	7.5-8.0	13.0-14.0
$I_{no-load}/I_{full-load}$	0.0	0.0	0.22-0.23	0.54-0.56

In attempt to compare the current harmonic mitigation effectiveness of the tuned filter and the IBF filter, the following several results are discussed concerning the 5.5kW tuned filter and IBF systems presented. The frequency domain analysis of the

filter impedance reveals some important results regarding the performance of the improved broadband filter and tuned filter.

Figure 4.60 shows the filter impedance seen from the rectifier side (towards the line side) for the tuned filter and IBF. The figure shows the parallel resonance frequency of the broadband filter is slightly above 150 Hz. In the dominant harmonic frequency range (5th and 7th) both filters have similar low impedance values. However, looking at the shunt filter path of the improved broadband and the tuned filters shown in Fig. 4.61 reveals the fact that the improved broadband filter has a higher impedance ratio compared to the tuned filter. The impedance ratio is given by

$$R_Z = \frac{Z_i + Z_s}{Z_f} \tag{4.6}$$

where Z_i is the input line impedance, Z_s is the source impedance and Z_f is the total shunt branch filter impedance (of L_f and C_f).

In the tuned filter, although the impedance at the tuning frequencies is lower than the broadband filter, the relatively small line side reactance provides a low impedance path to the dominant harmonics and a significant amount of harmonic current leaks to the AC line. If the tuning frequency increases and drifts from the characteristic harmonic frequency, the performance of the tuned filter degrades further. However, in the improved broadband filter, the impedance ratio is higher (5 in IBF compared to 2 of tuned filter at 250Hz) and most of the characteristic harmonics are trapped in the broadband filter LC parallel filter path (L_f, C_f) and a little amount of harmonics leak to the AC line. With the input inductance filter behaving as band-stop filter to the rectifier harmonics, the line current THD_I of IBF is significantly lower than the THD_I of the comparable size tuned filter. Also as important is the quite low possibility of parallel resonance with other loads connected to the point of common coupling. While the broadband filter exhibits only a slightly above third harmonic resonance point (which is highly unlikely to be excited), the tuned filter may fall into resonance with the 5th, 7th harmonic sources in the power network and result in overstresses on the filter components, hence harmonic resonance hazard risk.
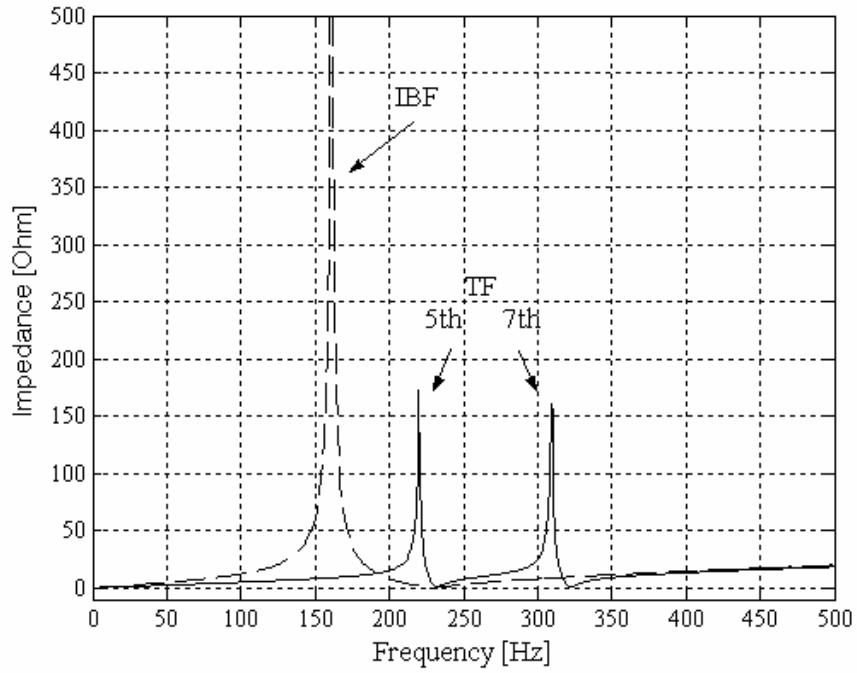
Fig. 4.60 TF and IBF output impedance characteristics (5.5 kW ASD system).
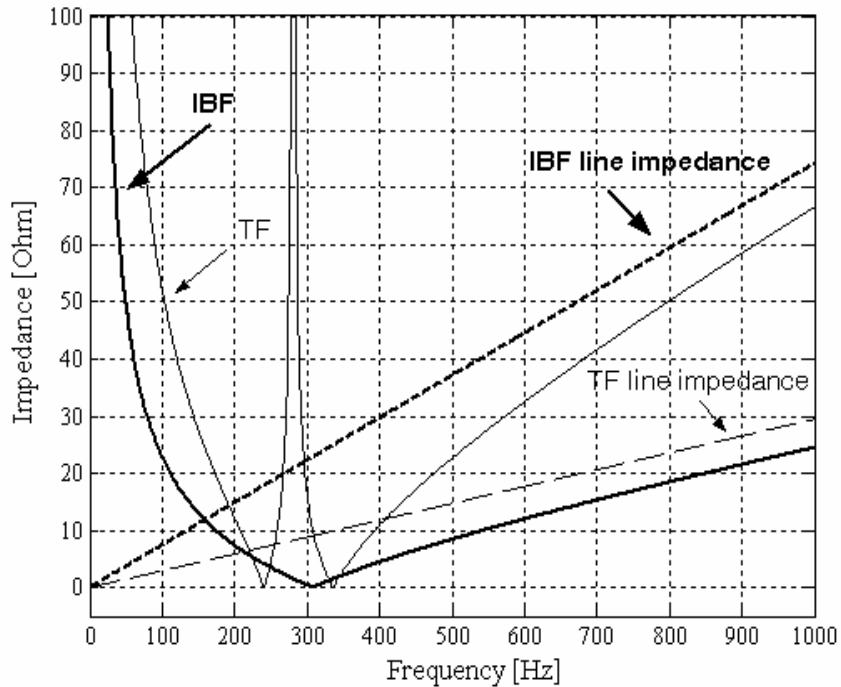
Fig. 4.61 TF and IBF shunt impedance and line impedance characteristics illustrating the impedance ratio differences (5.5 kW ASD system).

Figure 4.62 shows the tuned filter and IBF impedance seen from the supply (towards the rectifier side) at no-load. For both filters the output reactor L_o is not considered and the no-load equivalent impedance consists of the input reactor L_i connected in series with the single shunt branch filter (L_f-C_f) for IBF and the parallel equivalent of the 5th and 7th shunt filter for TF. The figure emphasizes the fact that the improved broadband filter has higher impedance values compared to the tuned filter at the dominant harmonics frequency at no-load. Therefore, the IBF structure minimizes the effect of the line voltage harmonics on the shunt filter. The overall results favor the IBF as high performance passive harmonic filtering method.
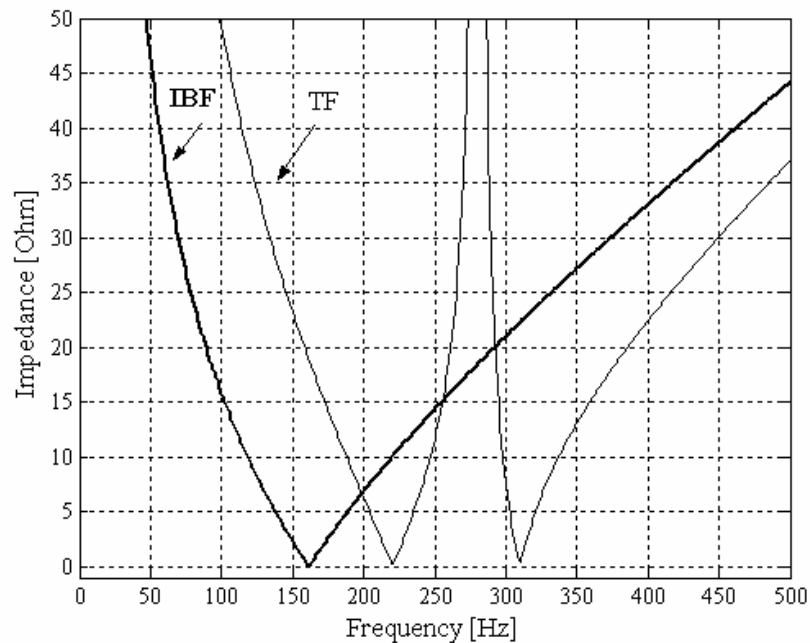
Fig. 4.62 No-load TF and IBF input impedance characteristics (5.5 kW ASD system).

4.9 Summary

In this chapter the performance of various filter structures (with emphasis on IBF) have been discussed. Performance evaluation of the discussed filtering methods was presented and a detailed comparison provided. The steady-state performance characteristics at various operating points were in focus. Balanced and unbalanced utility grid with or without voltage harmonic distortion operating conditions were considered. The main power quality parameters (line current THD_I and power factor, filter output voltage regulation) and energy efficiency attributes have been investigated. Concerning the transient conditions, the voltage overshoot at various locations of IBF based system was presented and the effectiveness of the appropriately selected damping resistor in suppressing the transients was shown.

With the computer simulation based study supporting the theoretical performance prediction and illustrating the accuracy of IBF filter parameter optimization method, the next step involves laboratory implementation of the investigated systems. The next chapter addresses the practical implementation issues and shows the performance results.

CHAPTER 5

EXPERIMENTAL RESULTS AND PERFORMANCE EVALUATION OF A RECTIFIER SYSTEM WITH VARIOUS PASSIVE FILTERS

5.1 Introduction

The previous chapter presented the computer simulations and performance analysis of a rectifier system with various passive filters. In this chapter, for the considered filters, the experimental performance characteristics are extracted. In the experimental study, the focus will be on the steady state performance characteristics. Performance will be evaluated from no-load to full-load operating points and under the practical distorted voltage supply. Main input and output power quality characteristics will be presented.

For the purpose of laboratory evaluation, an experimental rectifier system with 380V, 50 Hz, 5.5 kW ratings is designed and built in the laboratory for all filters discussed in the previous chapter (3% and 6% AC line reactors, T-shape 5th and 7th tuned filter, and IBF). The laboratory 50 Hz frequency line-to-line voltage supply varies between 385 and 395V rms range with voltage total harmonic distortion THD$_V$ value of 1.8–2.5% range. The harmonic spectrum and THD of the laboratory supply voltage measured at a specific instant is shown in Fig. 5.1. The supply phase voltage waveforms are shown in Fig. 5.2. The measurement is done with the Fluke 434 power quality analyzer [21].
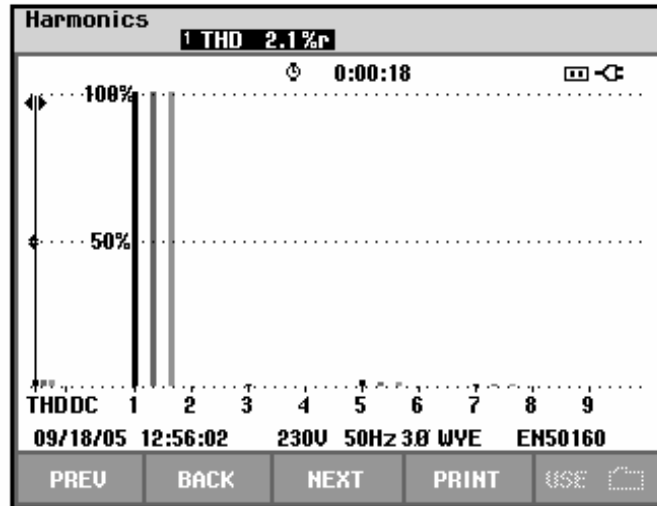
Fig. 5.1 Three-phase laboratory supply voltage harmonic spectrum.
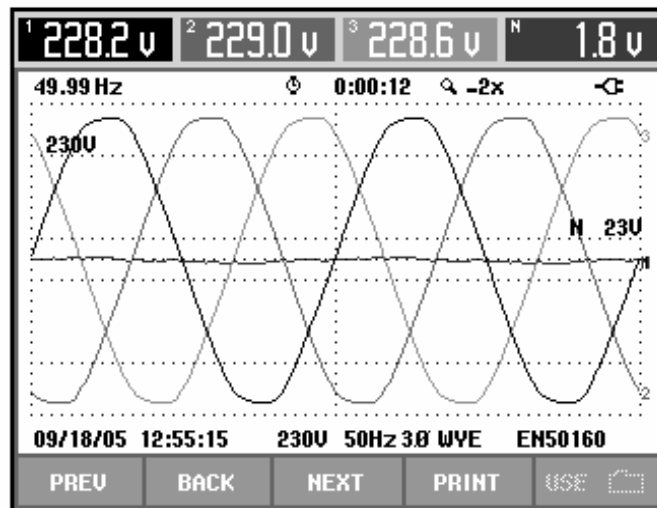
Fig. 5.2 Three-phase laboratory supply voltage waveforms.

The laboratory system is not a motor drive system, but it is a three-phase diode bridge rectifier feeding an RC load that emulates the ASD behavior. The rectifier system DC link capacitor, precharge resistor, DC link inductor and load parameters of the laboratory system are shown in Table 5.1. The resistive load (R_L) is connected in parallel with the DC link capacitor bank via a 20A automatic loading switch, while the DC link inductor is connected in series with the total RC load. The DC bus capacitor bank is formed from four capacitors. As shown in the figure, two pairs of

143

parallel connected capacitors (each 1mF) are connected in series to form a 1 mF equivalent capacitance with sufficient voltage and high current ratings.

The precharge resistor is connected to L_{dc} and shorted by means of a manual switch after limiting the inrush currents. A single fast fuse (32A) is connected to the rectifier output in series for shoot-through protection. The 100A, 1600V FUJI three-phase full diode bridge rectifier module utilized is connected to the AC side terminals through three-phase fast fuses (32A). The passive harmonic filter implemented is connected to the AC side to the three-phase fast fuses and to the grid lines via a 20A circuit breaker utilizing an emergency stop set, as shown in Fig. 5.3.

Table 5.1 Experimental setup rectifier system parameters

Component	Quantity	Specifications
$R_{precharge}$	2	10Ω, 40W
L_{dc}	1	1.50mH, 20A, 50Hz
C_{dc}	4	1000μF, 450VDC, 5.5A
Load resistance	3	240V, (2-20Amps) variable resistor
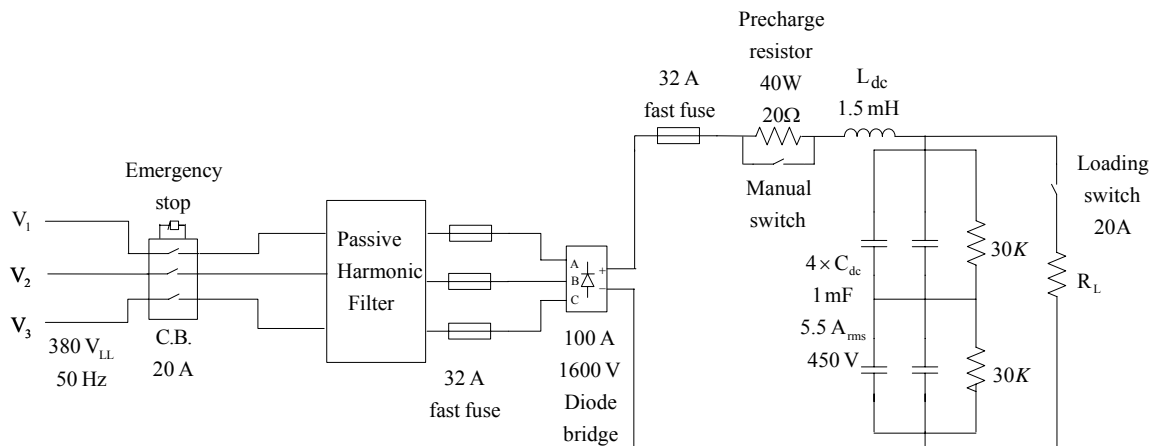
Fig. 5.3 The laboratory rectifier system elementary circuit diagram.

For the purpose of current and voltage measurements and power quality analysis, listed in Table 5.2, Agilent 54624A oscilloscope [22], and three-phase power quality analyzer Fluke 434 were utilized.

Table 5.2 Laboratory measurement equipment

	Agilent 54624A Mixed-Signal Oscilloscope	FLUKE 434 Power Quality Analyzer
Differential voltage probe measurement range	0-600V(rms)	0-1000V(rms)
Current probe measurement range	0-100A (rms)	0.5-40A(rms)

5.2 AC Line Reactor Filter Based Rectifier System Experimental Results

In this section the experimental performance characteristics of a three phase 3% and 6% AC line reactor filter based rectifier system under the laboratory practical distorted voltage supply operating conditions are presented. Experimental current and voltage waveforms are illustrated and analyzed. The AC line reactors are combined with a 2% DC link inductor in the DC side. The three phase AC line reactors are designed for 5.5kW power rating with the reactance parameters shown in Table 4.2.

5.2.1 Three Phase 3% AC Line Reactors Filter Based Rectifier System Experimental Results

In this section, the experimental results for the designed 3% AC line reactors and rectifier system (Table 5.1) are presented. The 3% AC line reactors are implemented as shown in Fig. 5.4.

145
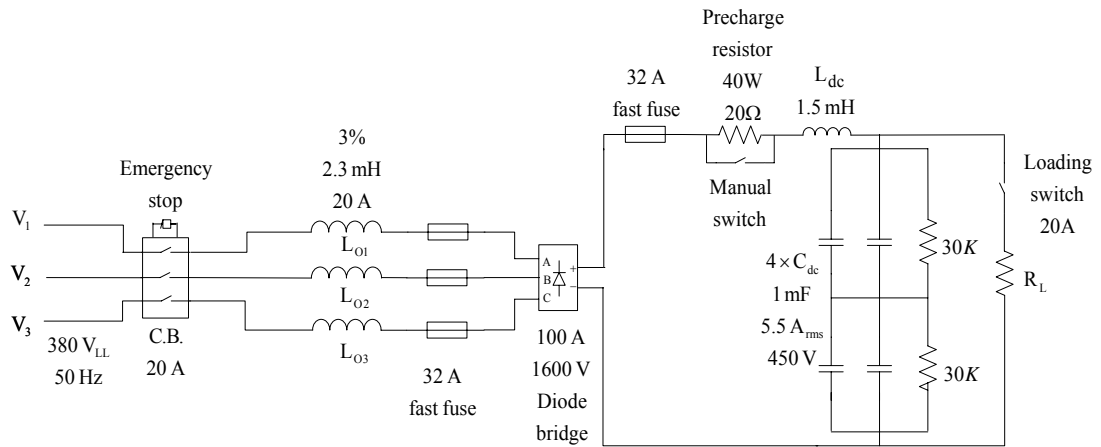
Fig. 5.4 Laboratory setup for 5.5kW rectifier system utilizing 3% AC line reactor.

The experimental full-load line current and supply voltage waveforms for 3% AC line reactors filtering method for the 5.5kW rectifier system are shown in Fig. 5.5. The full-load three-phase line current harmonic spectrum with 38.9% THD_I is shown in Fig. 5.6(a). In Fig. 5.6(b) the line current harmonic spectrum for phase "a" is shown including the higher frequency current harmonics. The power quality analyzer three-phase line terminal data representing the line power factor 0.90 lagging value is shown in Fig. 5.6(c). As the oscillograms and the data illustrate, the filter exhibits poor power quality characteristics, insufficient for the modern power quality requirements.

Fig. 5.5 Full-load line current and supply voltage experimental waveforms for 5.5kW rectifier system utilizing 3% L_{ac} and 2% L_{dc} filters (scales: 100V/div, 5A/div, 2.5ms/div).

Fig. 5.6 (a): Three-phase line current harmonic spectrum (b): single-phase line "a" current harmonic spectrum (c): three-phase line terminal data for the 5.5 kW rectifier system utilizing 3% L_{ac} and 2% L_{dc} filters at full-load.

The rated load DC voltage and current experimental oscilloscope waveforms are shown in Fig. 5.7. The full-load rectifier line-to-line voltage and the rectifier current waveforms are shown in Fig. 5.8. The estimated filter efficiency is greater than 98.6%. Due to the limited performance of the power quality analyzer Fluke 434, the power measurement at the filter output (rectifier input) terminals is inaccurate. The rectifier input terminal voltage is discontinuous (due to diode commutation and discontinuous mode operation), and the current waveform includes harmonics. As a result the power quality analyzer can not measure the rectifier input power accurately. However, the line voltage has low distortion and is continuous. Also the line current is continuous (though it has steep segments). As a result the filter input power can be measured with reasonable accuracy while the filter output power can

147

not be measured within reasonable accuracy. Therefore, measuring the filter efficiency directly is impossible with the existing measurement equipment. For this reason, the DC load power that is the only accurately measurable power is considered. With this choice, the total efficiency of the filter and rectifier (diode rectifier + DC bus capacitor) can be measured to a sufficient degree of accuracy. The efficiency value obtained with this measurement gives the minimum efficiency and the results imply that the filter will provide better efficiency than the measurement. Thus, the result can be considered as pessimistic efficiency value. Nevertheless the estimated total efficiency values are approximate quantities.
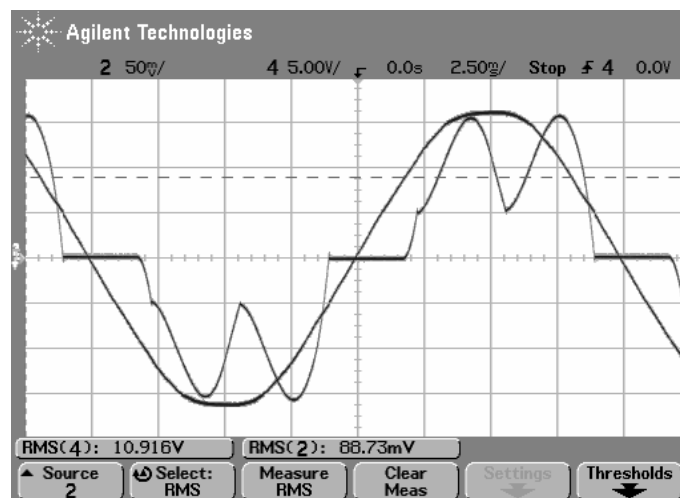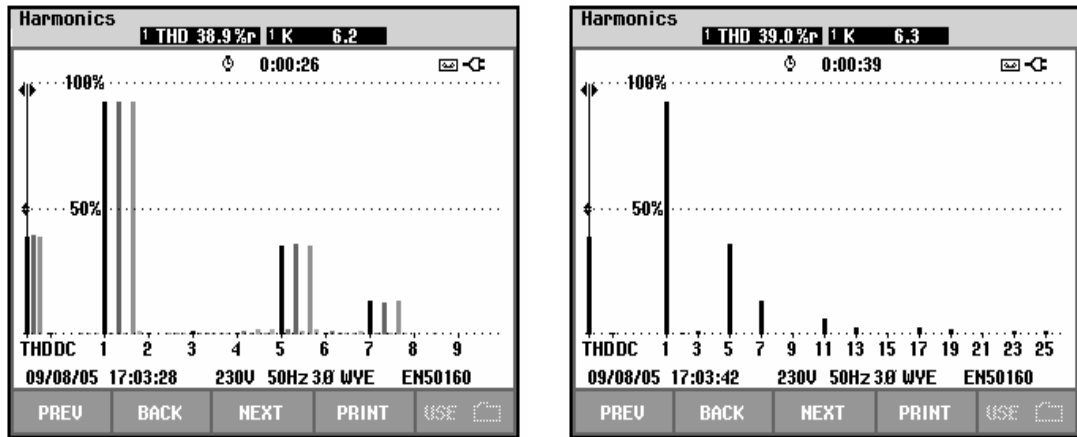

Fig. 5.7 Full-load DC load current and voltage experimental waveforms for 5.5kW rectifier system utilizing 3% L_{ac} and 2% L_{dc} filters (scales: 200V/div, 5A/div, 2.5ms/div).

Fig. 5.8 Full-load rectifier current and rectifier line-to-line voltage experimental waveforms for 5.5kW rectifier system utilizing 3% L_{ac} and 2% L_{dc} filters (scales: 200V/div, 5A/div, 2.5ms/div).

5.2.2 Three Phase 6% AC Line Reactors Filter Based Rectifier System Experimental Results

In this section, the experimental results for the designed 6% AC line reactors and rectifier system (Table 5.1) are presented. The 6% AC line reactors are implemented as shown in Fig. 5.9.
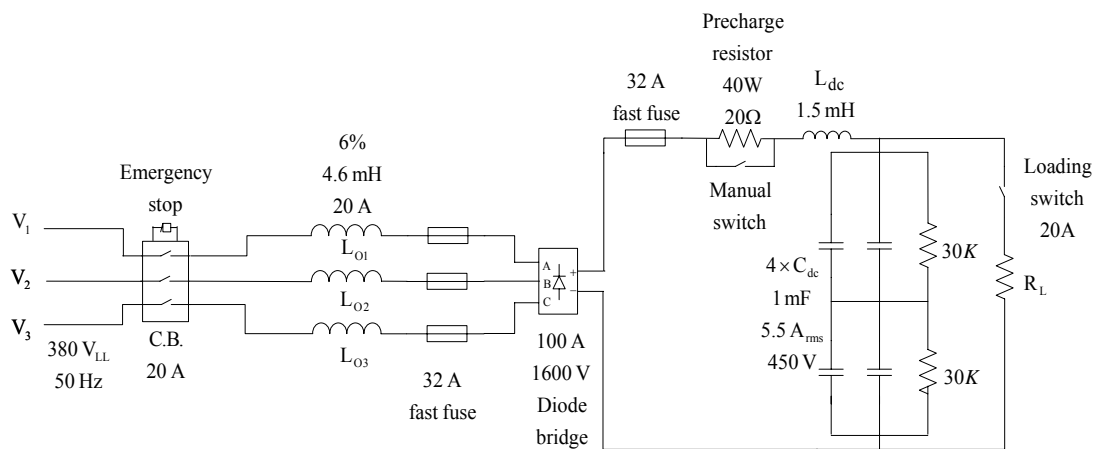
Fig. 5.9 Laboratory setup for 5.5kW rectifier system utilizing 6% AC line reactor.

The experimental full-load line current and supply voltage waveforms for 6% AC line reactors filtering method for the 5.5kW rectifier system are shown in Fig. 5.10. The full-load line current harmonic spectrum with 30.2% THD$_I$ is shown in Fig. 5.11(a). In Fig. 5.11(b) the line current harmonic spectrum for phase "a" is shown including the higher frequency current harmonics. The power quality analyzer three-phase line terminal data representing the line power factor 0.92 lagging value is shown in Fig. 5.11(c). Similarly to the 3% AC line reactor filter, the filter shows poor power quality performance at the utility.
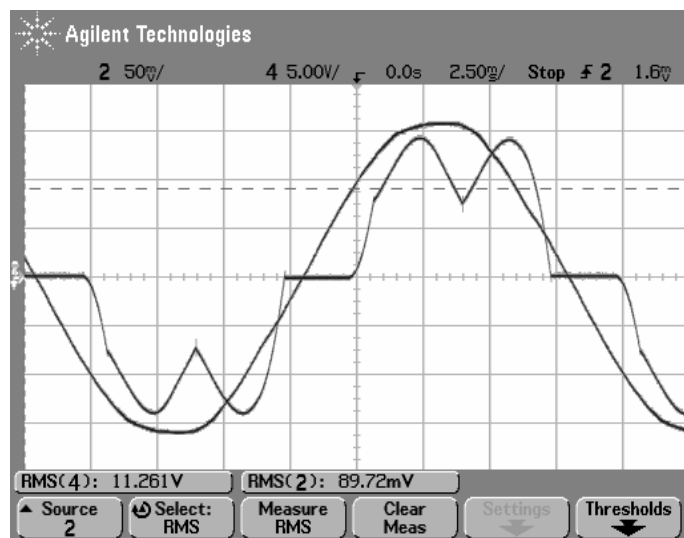
Fig. 5.10 Full-load line current and supply voltage experimental waveforms for 5.5kW rectifier system utilizing 6% L$_{ac}$ and 2% L$_{dc}$ filters (scales: 100V/div, 5A/div, 2.5ms/div).

(a)

(b)
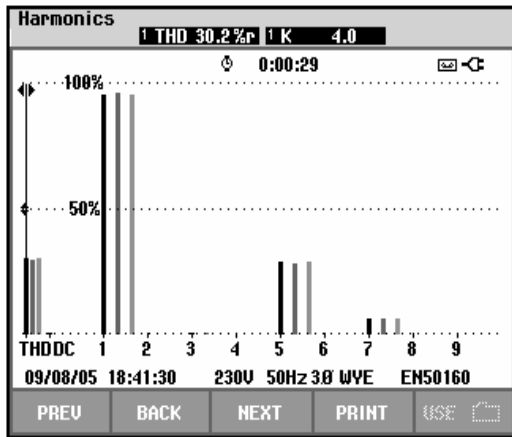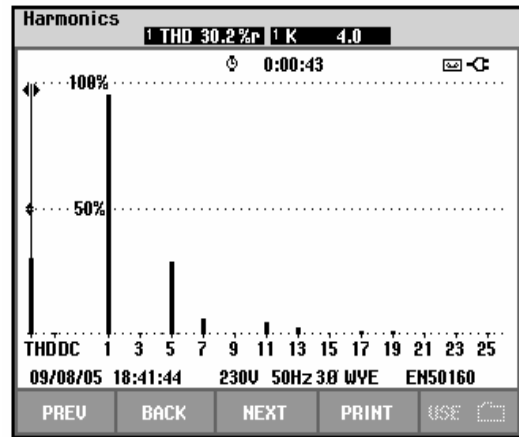
(c)

Fig. 5.11 (a): Three-phase line current harmonic spectrum (b): single-phase line "a" current harmonic spectrum (c): three-phase line terminal data for the 5.5 kW rectifier system utilizing 6% L_{ac} and 2% L_{dc} filter at full-load.

The rated load DC voltage and current experimental oscilloscope waveforms are shown in Fig. 5.12. The full-load rectifier line-to-line voltage and the rectifier current waveforms are shown in Fig. 5.13. The estimated filter efficiency is greater than 98.7%.
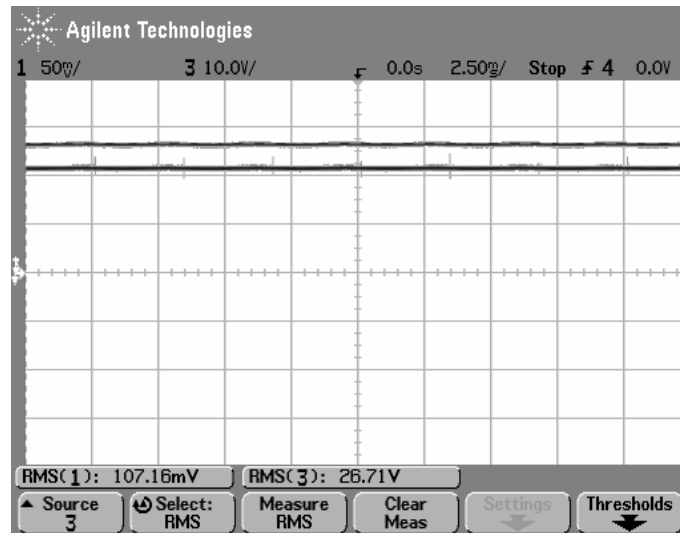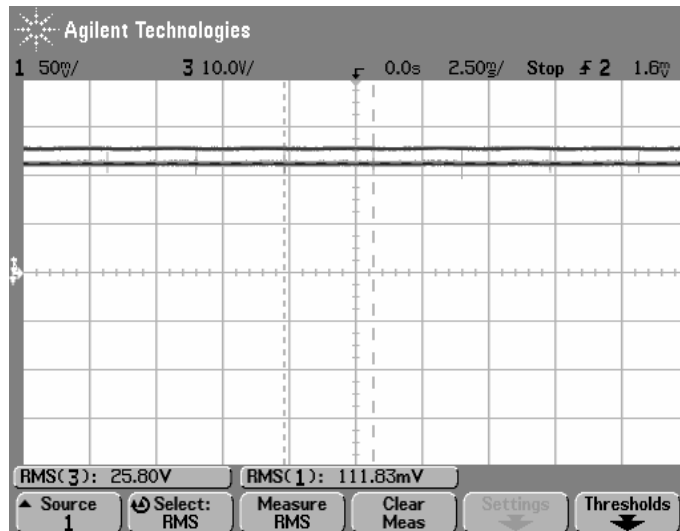
Fig. 5.12 Full-load DC load current and voltage experimental waveforms for 5.5kW rectifier system utilizing 3% L_{ac} and 2% L_{dc} filters (scales: 200V/div, 5A/div, 2.5ms/div).
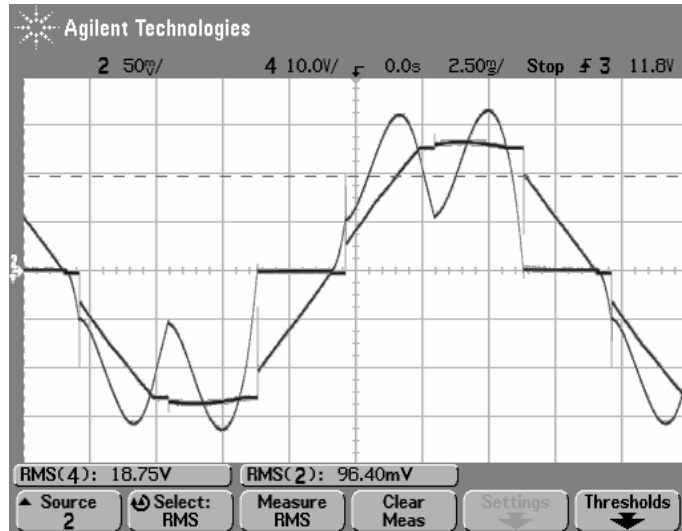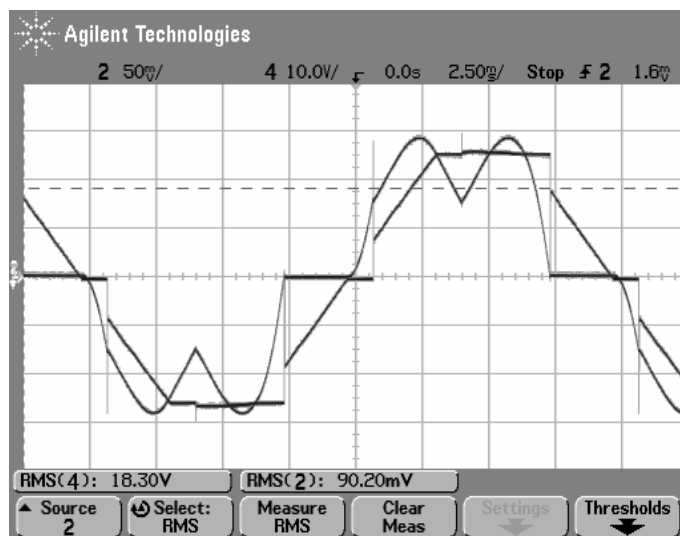

Fig. 5.13 Full-load rectifier current and rectifier line-to-line voltage experimental waveforms for 5.5kW rectifier system utilizing 6% L_{ac} and 2% L_{dc} filters (scales: 200V/div, 5A/div, 2.5ms/div).

From the above experimental results for the AC line reactor filtering topology considered cases, it is seen that the line current THD_I has high values (>30) for both utilized AC line reactors, meanwhile the line power factor has low values ($\leq$0.92). Further improvement of the line current THD_I and line power factor values can be

achieved by utilizing larger line reactors with the cost of lower DC rated output voltage values.

5.3 Tuned Filter Based Rectifier System Experimental Results

In this section the experimental performance characteristics of the T-shape 5th and 7th single tuned filter based rectifier system combined with a 2% DC link inductor are presented. The rectifier system parameters of Table 5.1 are utilized. However, for the 5th and 7th single tuned filter design, modified parameters different from those presented in Table 4.4 for 5.5kW power rating are utilized. This is due to the fact that the practical AC filter capacitors available in the manufacture's datasheets do not exactly match the theoretical 5th and 7th AC capacitor filter designed values. Therefore, selecting the nearest value capacitors available in the datasheets to the required specifications is considered. Consequently, the corresponding AC 5th and 7th filter reactor modified parameters are calculated according to the same design method discussed in section 4.3.1 utilizing the same detuning factor value. Therefore, the modified tuned 5th and 7th single tuned filter parameters are shown in Table 5.3 with the original filter simulation parameters. These modified 5th and 7th single tuned filter parameters and the rectifier system parameters (Table 5.1) are implemented in the laboratory setup as shown in Fig. 5.14.

Table 5.3 Tuned filter parameters for 5.5 kW power rating

	Original Value (Simulation)	Modified Value (Experimental)
$C_{5\Delta}$ (µF)	4.94	5.0
L_5 (mH)	29.6	29.3
$C_{7\Delta}$ (µF)	4.04	3.5
L_7 (mH)	18.5	20.4
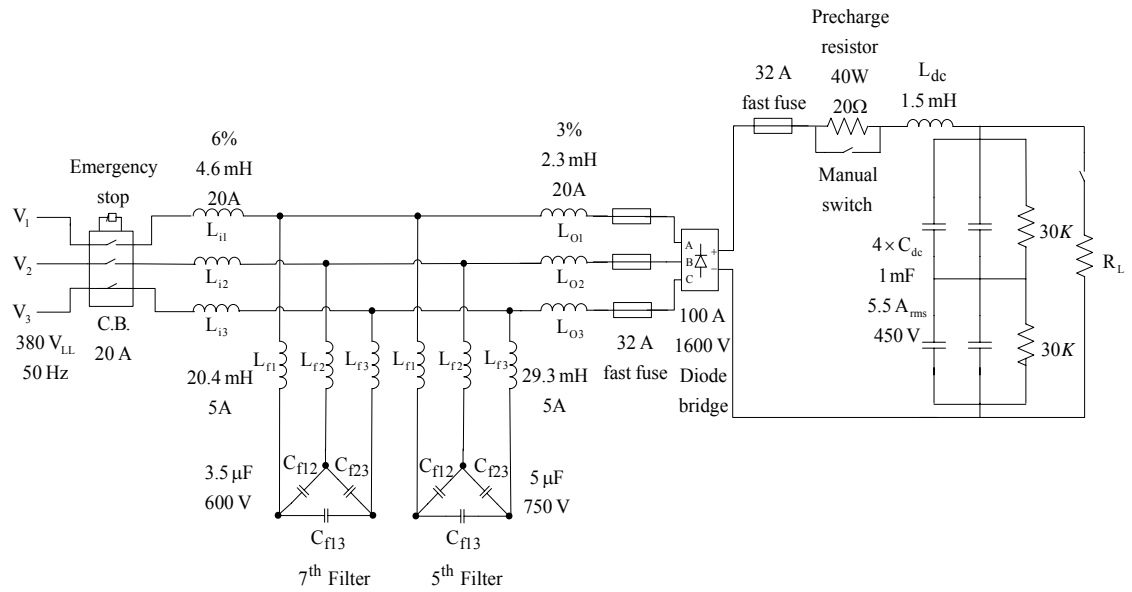
Fig. 5.14 Laboratory setup for 5.5kW rectifier system utilizing T-shape 5th and 7th single tuned filter.

5.3.1 Full-Load Experimental Results of The Tuned Filter Based Rectifier System

The experimental full-load line current and rectifier current waveforms for the T-shape 5th and 7th single tuned filtering method for the 5.5kW rectifier system are shown in Fig. 5.15 (a). The three-phase full-load line current harmonic spectrum with 14.4% THD$_I$ is shown in Fig. 5.15(b), while the three-phase full-load rectifier current harmonic spectrum with 34.8% THD$_I$ is shown in Fig. 5.15(c). The single-phase full-load line current and rectifier current harmonic spectrum for phase "a" are shown in Fig. 5.16, respectively. The tuned filter topology reduces the rectifier current 34.8% THD$_I$ value to the line current 14.4% THD$_I$ value at full-load.

154
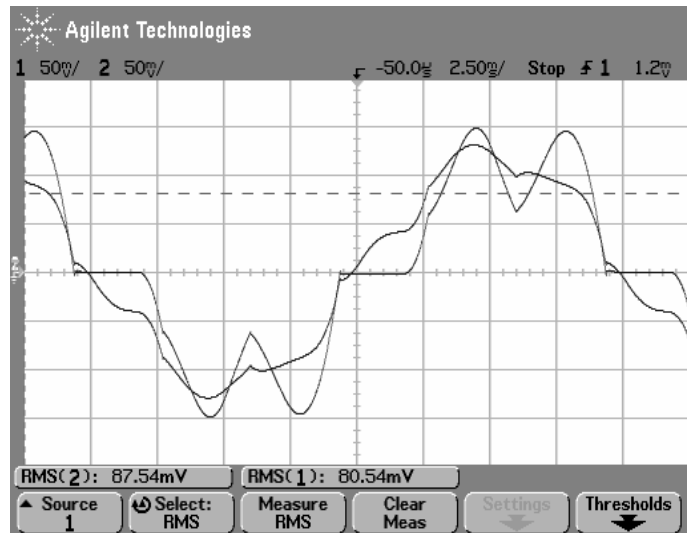
(a)
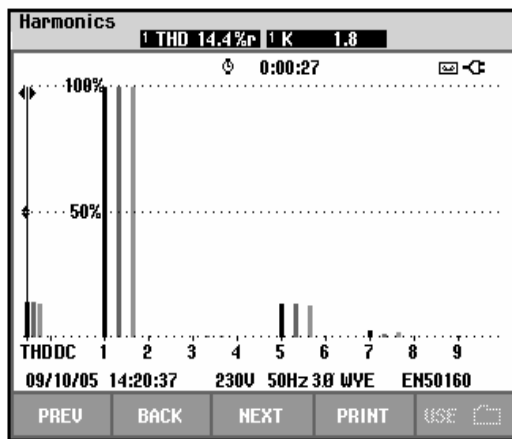
(b)
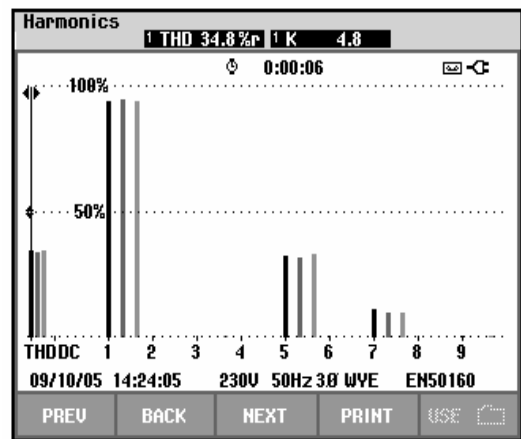
(c)

Fig. 5.15. (a): Full-load line and rectifier current experimental waveforms (scales: 5A/div, 2.5ms/div) (b): line current harmonic spectrum, (c): rectifier current harmonic spectrum for the 5.5 kW rectifier system utilizing T-shape 5th and 7th single tuned and 2% L_{dc} filters.
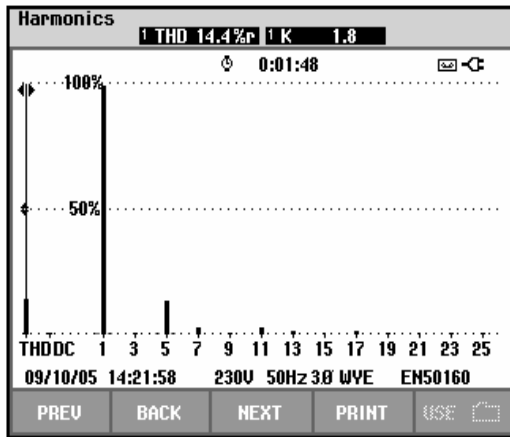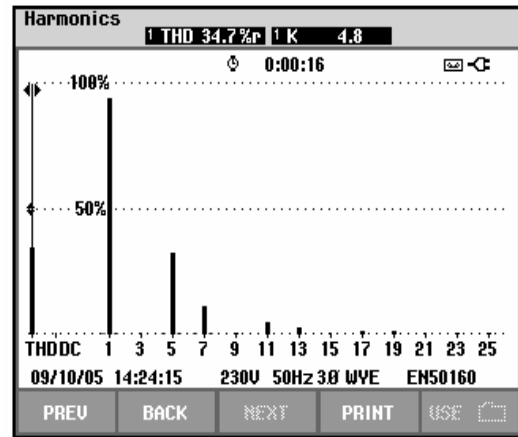
(a)   (b)

Fig. 5.16 (a): Single-phase line current harmonic spectrum (phase "a"), (b): single-phase rectifier current harmonic spectrum (phase "a") for the 5.5 kW rectifier system utilizing T-shape 5th and 7th single tuned and 2% L_{dc} filters.

The full-load line current and supply voltage waveforms are shown in Fig. 5.17(a) while the power quality analyzer three-phase line terminal data is shown in Fig. 5.17(b). The line power factor represented has a 0.99 lagging value. Compared to the AC line reactors discussed, the tuned filtering method exhibits better full-load performance. However, as the line power factor is near unity the line current THD_I value is still high (>14%) and can not be accepted by the power quality modern standards.

156

(a)

(b)

Fig. 5.17 (a): Full-load line current and supply voltage experimental waveforms (scales: 100V/div, 5A/div, 2.5ms/div) (b): three-phase line terminal data for the 5.5 kW rectifier system utilizing T-shape 5th and 7th single tuned and 2% L_{dc} filters.

The rated load DC voltage and current experimental oscilloscope waveforms are shown in Fig. 5.18 and the rectifier current and rectifier line-to-line voltage waveforms are shown in Fig. 5.19 at full-load. Due to the rectifier current harmonics the rectifier line-to-line voltage is distorted. The full-load node P phase voltage and the 5th and 7th tuned filter capacitor current waveforms are shown in Fig. 5.20.

Fig. 5.18 Full-load DC load current and voltage experimental waveforms for 5.5kW rectifier system utilizing T-shape 5th and 7th single tuned and 2% L_{dc} filters (scales: 200V/div, 5A/div, 2.5ms/div).
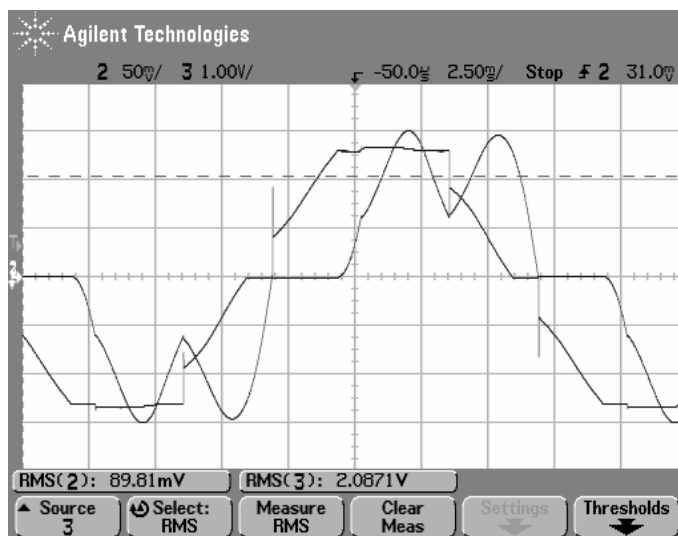
Fig. 5.19 Full-load rectifier current and rectifier line-to-line voltage experimental waveforms for 5.5kW rectifier system utilizing T-shape 5th and 7th single tuned and 2% L_{dc} filters (scales: 200V/div, 5A/div, 2.5ms/div).
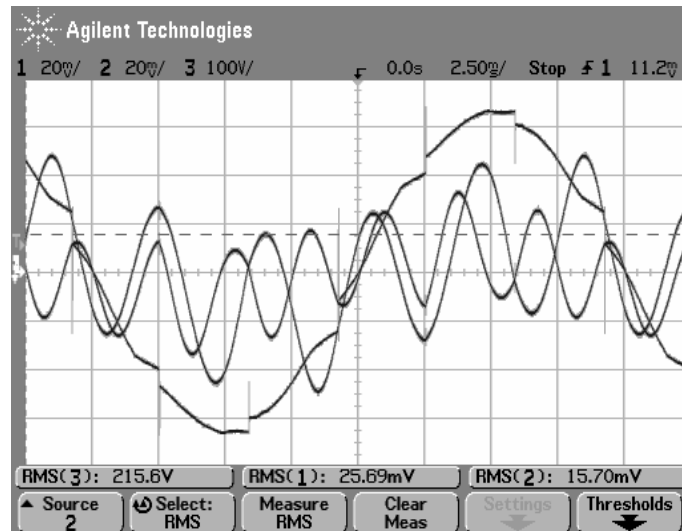
Fig. 5.20 Full-load node P phase voltage and 5th and 7th tuned filter capacitor current waveforms for the 5.5 kW rectifier system utilizing T-shape 5th and 7th single tuned and 2% L$_{dc}$ filters (scales: 100V/div, 1A/div, 2.5ms/div).

The full-load 5th and 7th tuned filter capacitor current and voltage waveforms are shown in Fig. 5.21 (a) and Fig. 5.21 (b), respectively. The approximate filter efficiency including the three-phase rectifier bridge at full-load is 98.6%.
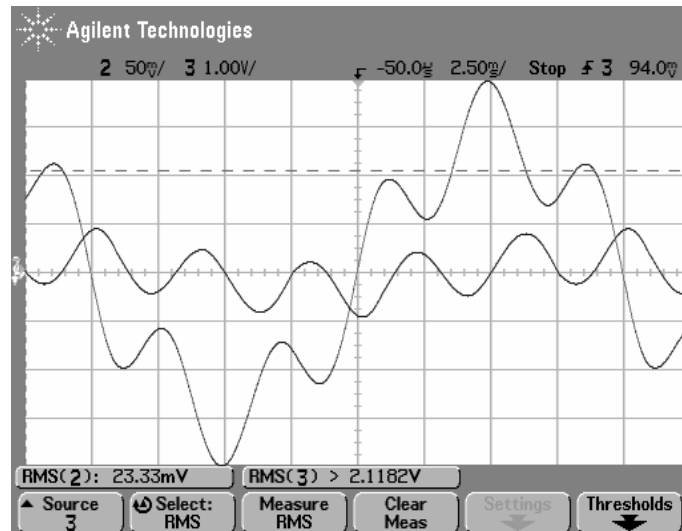
(a)
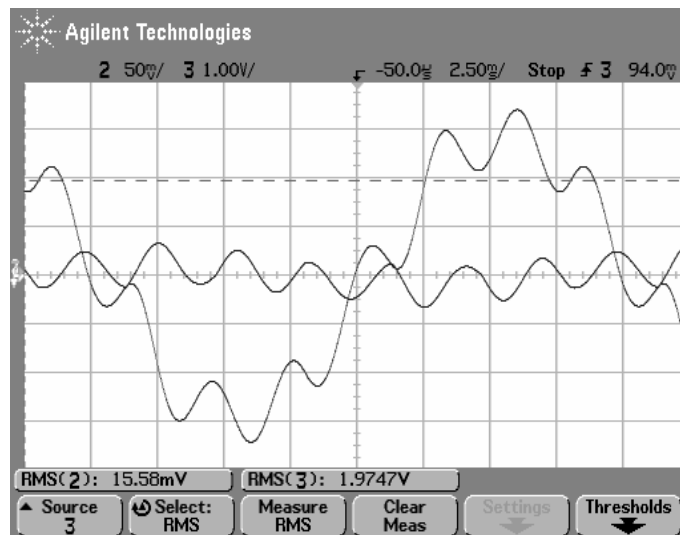
(b)

Fig. 5.21 (a) Full-load 5th tuned filter capacitor current and voltage experimental waveforms, (b) Full-load 7th tuned filter capacitor current and voltage experimental waveforms for 5.5kW rectifier system utilizing T-shape 5th and 7th single tuned and 2% L$_{dc}$ filters (scales: 200V/div, 2.5ms/div, 5A/div)

5.3.2 No Load Experimental Results of The Tuned Filter Based Rectifier System

In this section, the no-load operating condition experimental results are presented. The load resistors are not connected to the system and the loading switch is kept open during the test. The no-load line current and supply voltage waveforms are

shown in Fig. 5.22. The no-load line current harmonic spectrum is shown in Fig. 5.23(a). The power quality analyzer three-phase line terminal data is shown in Fig. 5.23(b). The line current THD_I value increases to 21.7% as the tuned filter imports the existing utility current harmonics at no-load and the line power factor is near zero. The no-load 5th and 7th tuned filter capacitor current and voltage waveforms are shown in Fig. 5.24 (a) and Fig. 5.24 (b), respectively.
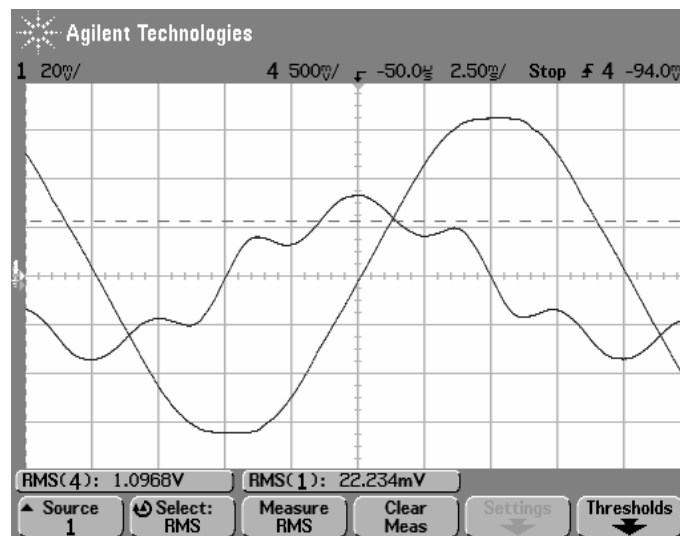
Fig. 5.22 No-load line current and supply voltage experimental waveforms for 5.5kW rectifier system utilizing T-shape 5th and 7th single tuned and 2% L_{dc} filters (scales: 100V/div, 2A/div, 2.5ms/div)
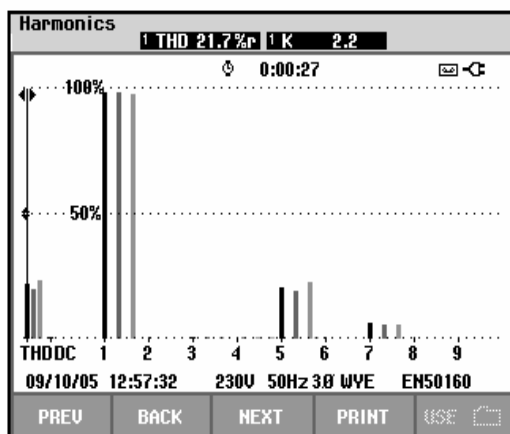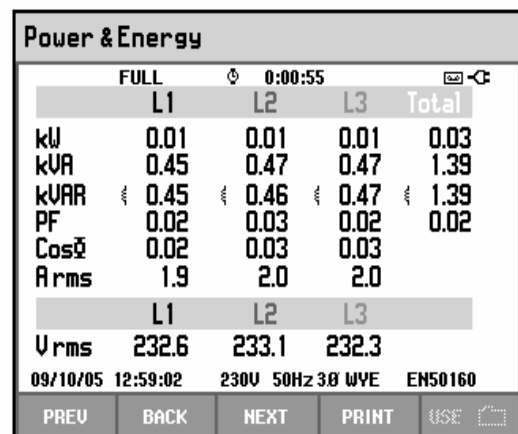
| | (a) | | (b) | |

Fig. 5.23 (a): No-load line current harmonic spectrum (b):no-load three-phase line terminal data for the 5.5 kW rectifier system utilizing T-shape 5th and 7th single tuned and 2% L_{dc} filters.
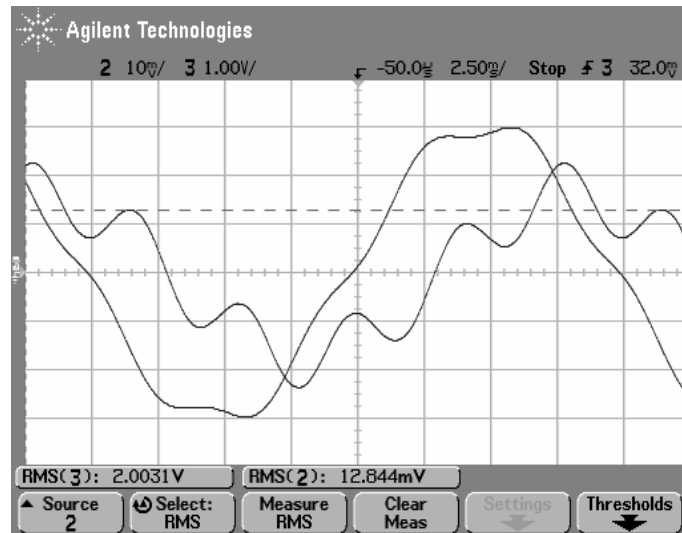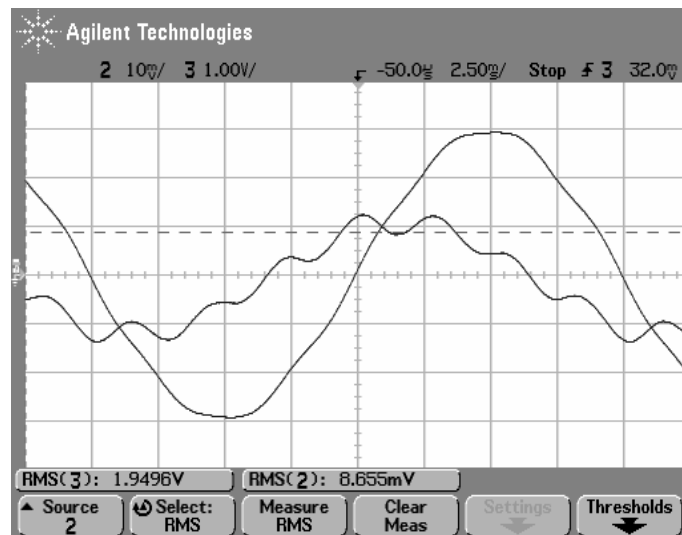
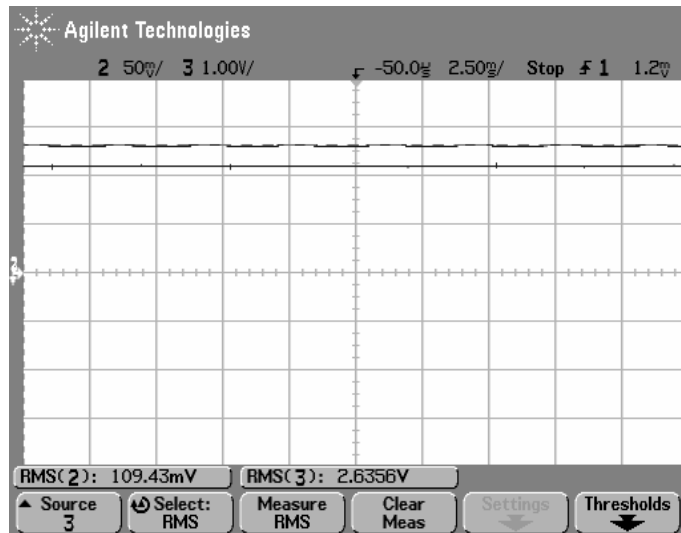Fig. 5.24 (a) No-load 5th tuned filter capacitor current and voltage experimental waveforms, (b) No-load 7th tuned filter capacitor current and voltage experimental waveforms for 5.5kW rectifier system utilizing T-shape 5th and 7th single tuned and 2% L_{dc} filters (scales: 200V/div, 1A/div, 2.5ms/div).

The no-load node P phase voltage and the 5th and 7th tuned filter capacitor current waveforms are shown in Fig. 5.25. It seen that the node P voltage variation from no-load to full-load for the tuned filter is confined to 2.8% (utilizing the rms measured values by the oscilloscope). However, it is observed that the rms measured values are approximated quantities. Therefore, the voltage regulation estimation is carried out by a digital multi-meter (Brymen BM805) to improve the accuracy of the measurement

162

results for all the case studies considered. The final results will be represented later in this chapter.

Fig. 5.25 No-load node P phase voltage and 5th and 7th tuned filter capacitor current waveforms for the 5.5 kW rectifier system utilizing T-shape 5th and 7th single tuned and 2% L_{dc} filters (scales: 100V/div, 1A/div, 2.5ms/div).

5.4 Improved Broadband Filter Based Rectifier System Experimental Results

In this section the experimental performance characteristics of the improved broadband filter based rectifier system are presented. The test was conducted under the laboratory practical distorted voltage supply operating conditions. Experimental current and voltage waveforms are illustrated and analyzed.

Similar to the tuned filter case, the designed capacitor value was not available as a standard product by any major capacitor manufacturer. Therefore, capacitors that are closest in value to the designed value were selected. The AC filter capacitors selected from the EPCOS capacitor product line (ordering code B32340C4032A310, 400V rating and -5 +10% capacitance tolerance) [23] have a 66.5µF star connected capacitance (22.3 µF delta connected) with approximately 9% larger value than the

optimal design value (which is 20.6 µF delta connected). The filter reactor L_f is designed for 4.4mH reactance value while the input and output reactors are designed with their original values (L_i = 10.8mH and L_o=3.1mH). The damping resistor R_d utilized has a 220Ω resistance value. The designed filter is implemented as shown in Fig. 5.26.
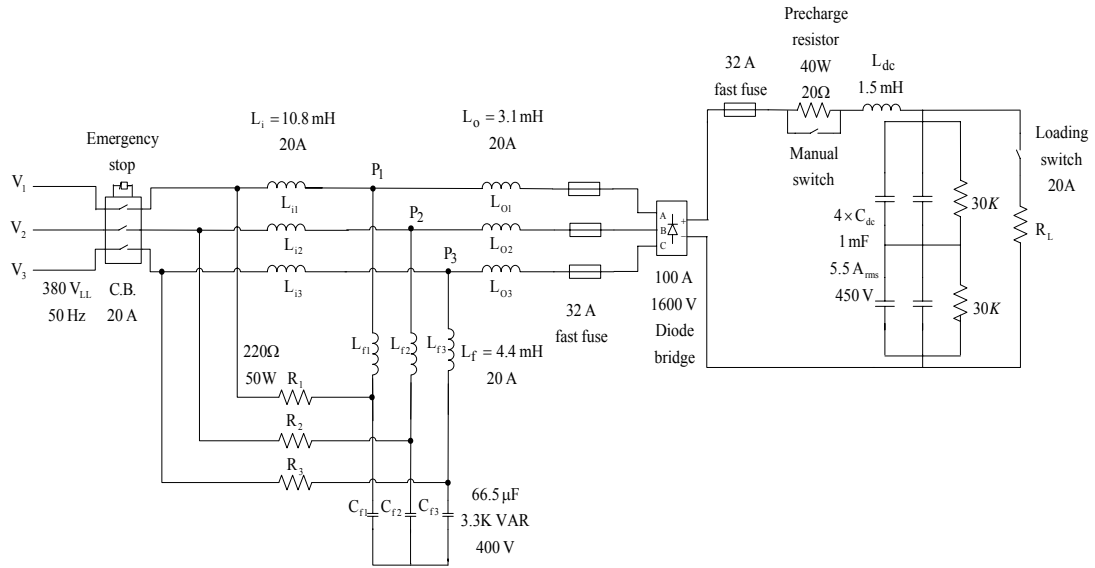
Fig. 5.26 Laboratory setup for 5.5kW rectifier system utilizing IBF.

5.4.1 Full-Load Experimental Results of The Improved Broadband Filter Based Rectifier System

The experimental full-load line current and rectifier current waveforms for the improved broadband filtering method for the 5.5kW rectifier system are shown in Fig. 5.27 (a). The full-load line current harmonic spectrum with 5.5% THD_I is shown in Fig. 5.27(b), while the full-load rectifier current harmonic spectrum with 42% THD_I is shown in Fig. 5.27(c). As the oscillograms indicate, the IBF filter topology dramatically reduces the rectifier current 42% THD_I value to the line current 5.5% THD_I value at full-load.

The single-phase full-load line for phase "b" current and rectifier for phase "c" current harmonic spectrum are shown in Fig. 5.28, respectively. It is observed that the IBF topology effectively eliminates the wide range of the rectifier current harmonics, while the TF topology utilized reduces the 5th and 7th rectifier current harmonics (Fig. 5.16).
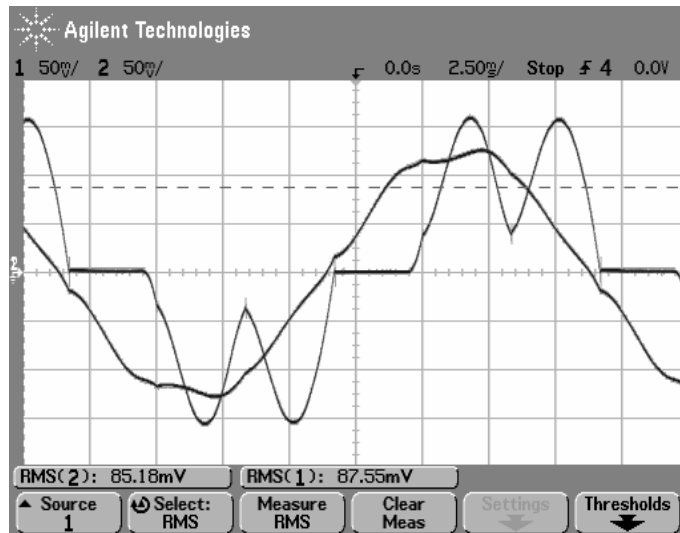
(a)
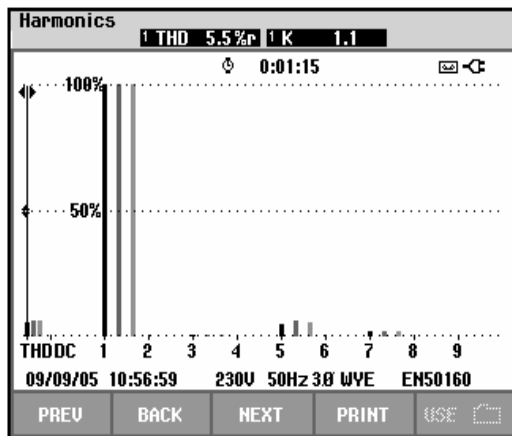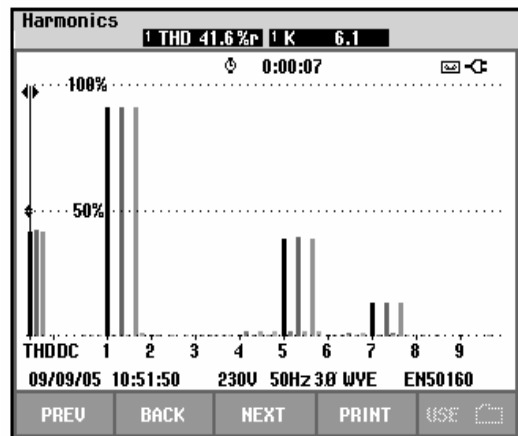
(b)   (c)

Fig. 5.27 (a): Full-load line and rectifier current experimental waveforms (scales: 5A/div, 2.5ms/div) (b): Line current harmonic spectrum, (c): rectifier current harmonic spectrum for the 5.5 kW rectifier system utilizing IBF. (EU standard phase colors)
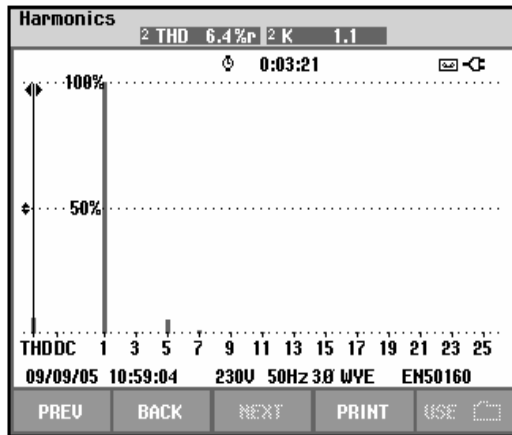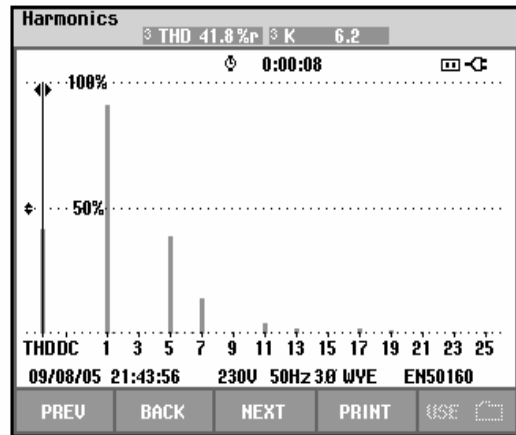
(a)   (b)

Fig. 5.28 (a): Single-phase line current harmonic spectrum (phase "b"), (b): single-phase rectifier current harmonic spectrum (phase "c")for the 5.5 kW rectifier system utilizing IBF.

The full-load line current and supply voltage waveforms are shown in Fig. 5.29(a) while the power quality analyzer waveforms for the full-load line current and supply voltage are shown in Fig. 5.29(b). The line power factor represented has a 0.94 leading value due to the larger available AC filter capacitor value than the optimal design value. As the experimental data indicates, the improved broadband filtering method has better performance at full-load than the previous filtering methods. The line current THD_I value is low (<6%) with leading line power factor value of 0.94. Although the design is not highly sensitive to the tuning frequency (unlike the TF), the very large difference between the designed and available capacitor (9%) result in better line current THD_I and slightly poorer PF than the computer simulation.

(a)

(b)

Fig. 5.29 (a): Full-load line current and supply voltage experimental waveforms (scales: 100V/div, 5A/div, 2.5ms/div) (b): three-phase line terminal data for the 5.5 kW rectifier system utilizing IBF. (EU standard phases colors)

The rated load DC voltage and current experimental oscilloscope waveforms are shown in Fig. 5.30 and the rectifier current and rectifier line-to-line voltage waveforms are shown in Fig. 5.31 at full-load. It is seen that the rectifier current harmonics result in distorted rectifier line-to-line voltage likewise the tuned filter case. The full-load node P phase voltage and the filter capacitor current waveforms are shown in Fig. 5.32.
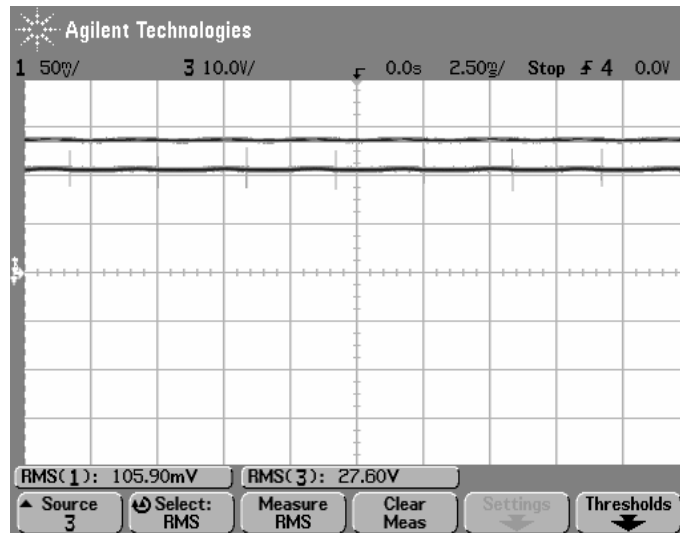
Fig. 5.30 Full-load DC load current and voltage experimental waveforms for 5.5kW rectifier system utilizing IBF (scales: 200V/div, 5A/div, 2.5ms/div).
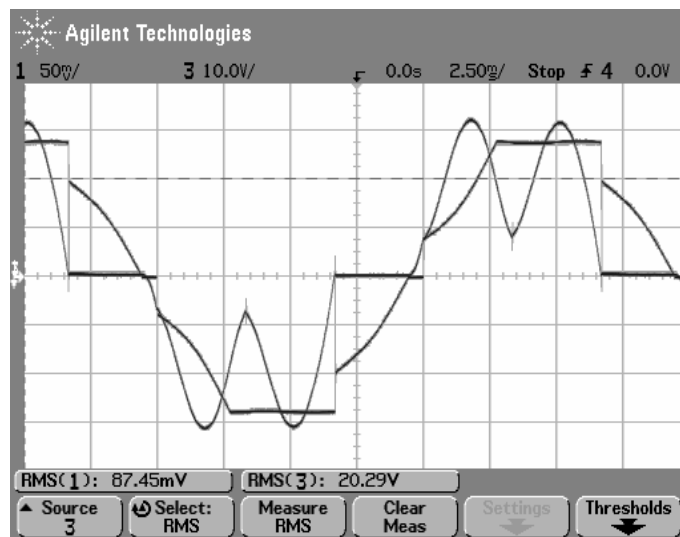
Fig. 5.31 Full-load rectifier current and rectifier line-to-line voltage experimental waveforms for 5.5kW rectifier system utilizing IBF (scales: 200V/div, 5A/div, 2.5ms/div).
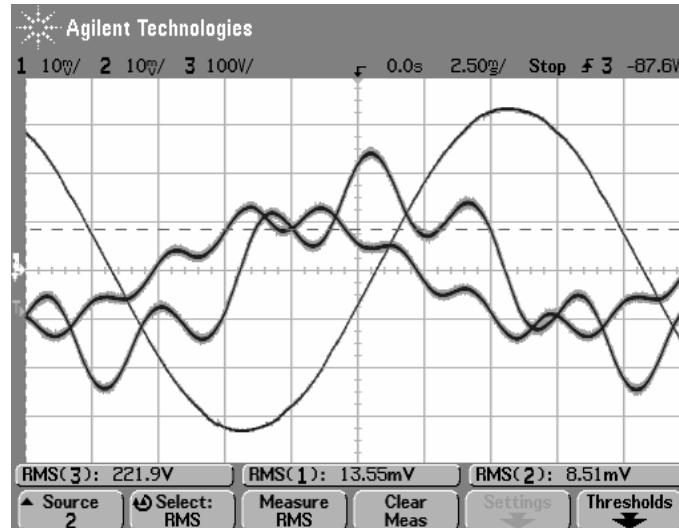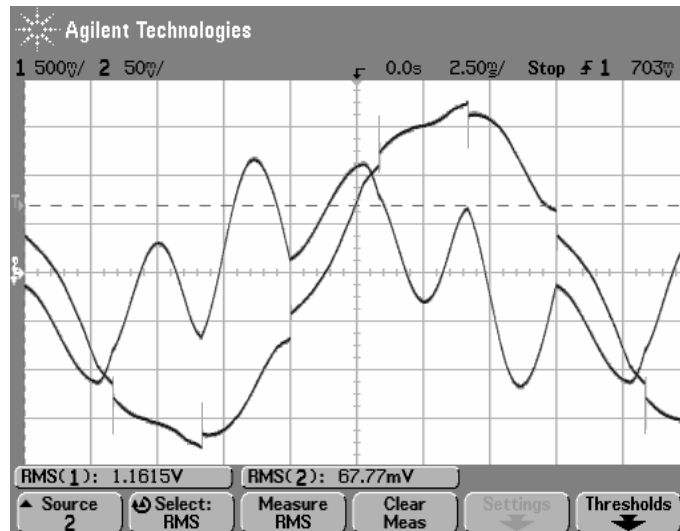
Fig. 5.32 Full-load node P phase voltage and filter capacitor current waveforms for the 5.5 kW rectifier system utilizing IBF (scales: 100V/div, 5A/div, 2.5ms/div).

The full-load AC filter capacitor current and voltage waveforms are shown in Fig. 5.33. The estimated filter efficiency including the three-phase rectifier bridge at full-load is 98.9%.
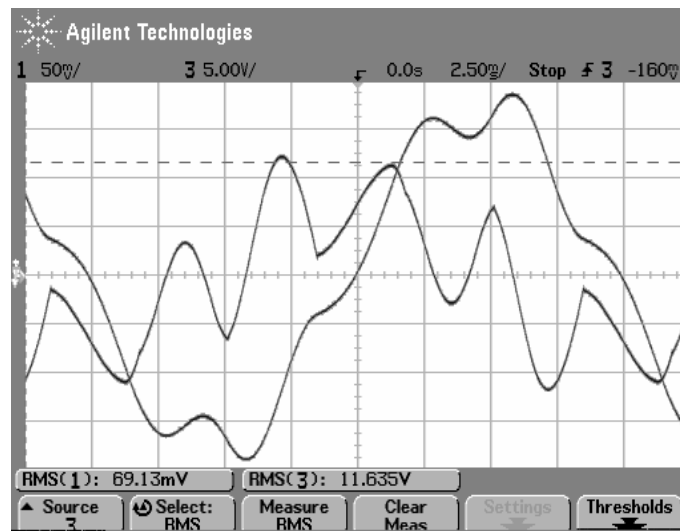
Fig. 5.33 Full-load filter capacitor current and voltage experimental waveform for 5.5kW rectifier system utilizing IBF (scales: 100V/div, 5A/div, 2.5ms/div).

To examine the improved broadband filter full-load performance experimental results accuracy, the modified filter parameters utilized in the lab are implemented in the full model simulation circuit of the IBF. Table 5.4 shows the performance results comparison for the improved broadband filter. As the table indicates the simulation and experimental performance results match with a good accuracy. The difference between the results is attributed to the unmodeled (or approximately modeled) behavior such as the source voltage harmonics, parasitic elements (ESR, ESL, etc. of the elements), tolerance range of the reactors (which are not exactly as we designed and also have nonlinear magnetic characteristics), and the accuracy limits of the measurement equipments utilized. The line current THD_I experimental values for the three-phase lines are presented in the shown range.

Table 5.4 Experimental system and simulation system power quality performance comparison for the 5.5 kW rectifier system

	THD_I (%)	Line PF	ΔV_o (%)	α
Experimental	5.5 -6.4	0.940	4.7	0.59
Simulation	8.6	0.966	3.8	0.58

5.4.2 No-Load Experimental Results of The Improved Broadband Filter Based Rectifier System

In this section, the no-load operating condition experimental results are presented. The load resistors are not connected to the system and the loading switch is kept open during the test. The no-load line current and supply voltage waveforms are shown in Fig. 5.34. The no-load line current harmonic spectrum is shown in Fig. 5.35(a). The power quality analyzer waveforms for the no-load line current and supply voltage are shown in Fig. 5.35(b). In contrast to the tuned filter method which has 22% THD_I, the IBF line current THD_I value has a low value of 7.0% at no-load

170

and the filter blocks the utility current harmonics. However, the IBF no-load current rms value is nearly twice the TF no-load current rms value.
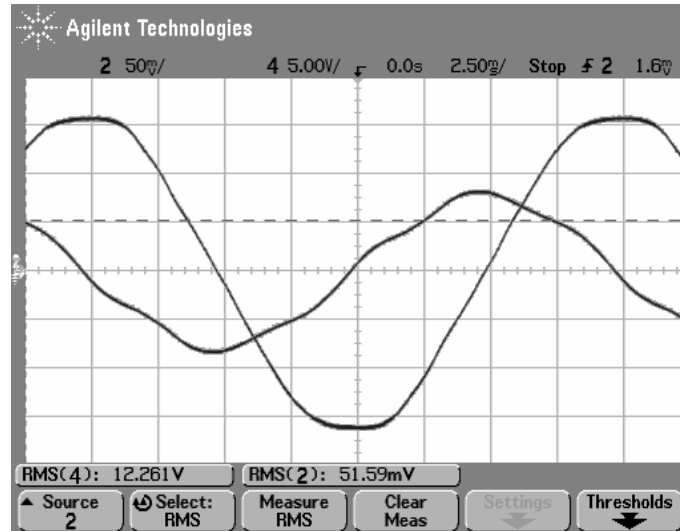
Fig. 5.34 No-load line current and phase voltage waveforms (scales: 100V/div, 5A/div, 2.5ms/div).
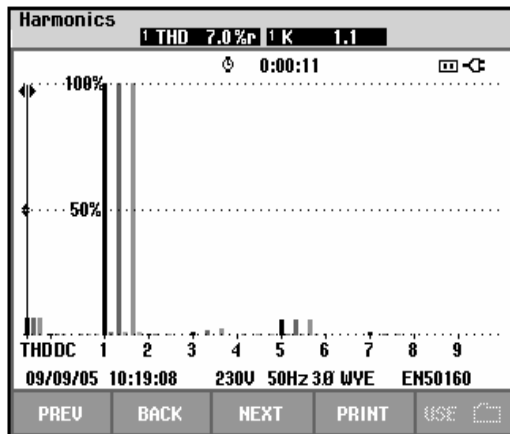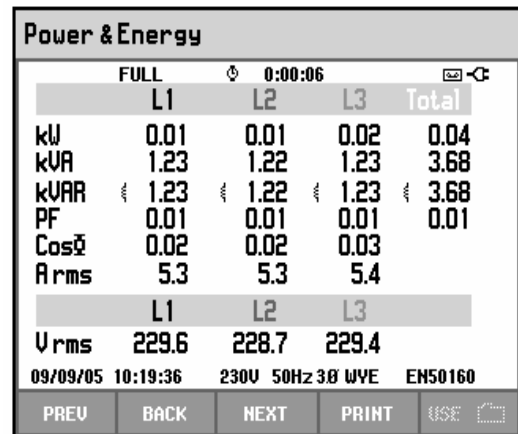
(a)   (b)

Fig. 5.35 (a): No-load line current harmonic spectrum (b): no-load line voltage and current waveform and power factor data for the 5.5 kW rectifier system utilizing IBF.

The no-load filter capacitor current and voltage waveforms are shown in Fig. 5.36. The no-load node P phase voltage and the filter capacitor current waveforms are shown in Fig. 5.37. It seen that the node P voltage variation from no-load to full-load for the IBF is confined to 3.7% (utilizing the rms measured values by the oscilloscope). This value estimated utilizing the digital multi-meter is 4.7% (Table 5.4). In both cases the IBF output voltage is stable.
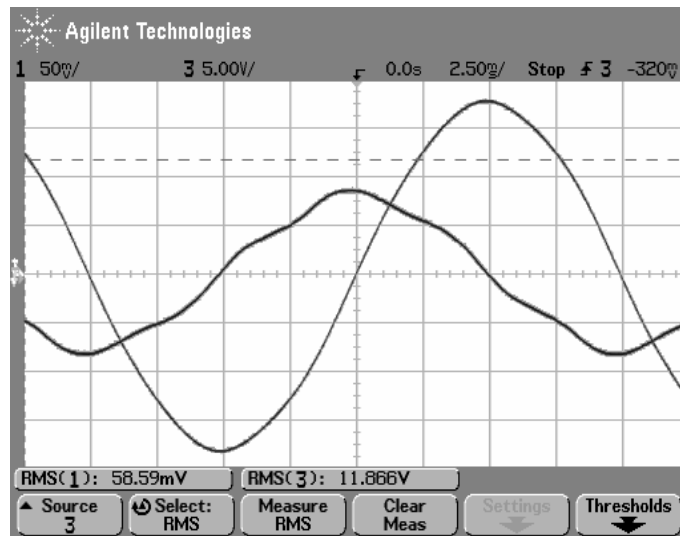
Fig. 5.36 No -load filter capacitor current and voltage experimental waveform for 5.5kW rectifier utilizing IBF (scales: 100V/div, 5A/div, 2.5ms/div).
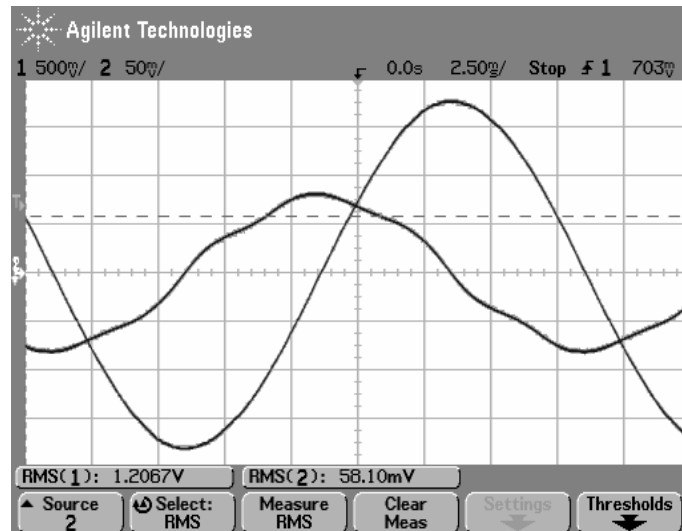
Fig. 5.37 Node P phase voltage and filter capacitor current waveforms (a): at full-load, (b): at no-load for the 5.5 kW rectifier system utilizing IBF (scales: 100V/div, 5A/div, 2.5ms/div).

The IBF circuit built and tested in the laboratory is shown in Fig. 5.38. The picture shows the filter capacitors C_f at the front and the utilized three-phase reactors L_i, L_f and L_o respectively from left to right (behind). Fig. 5.39 shows the three-phase rectifier bridge and the DC link capacitors. The precharge resistors connected to the manual switch are shown at the right (front). The complete laboratory system utilizing IBF for 5.5kW is shown in Fig. 5.40.
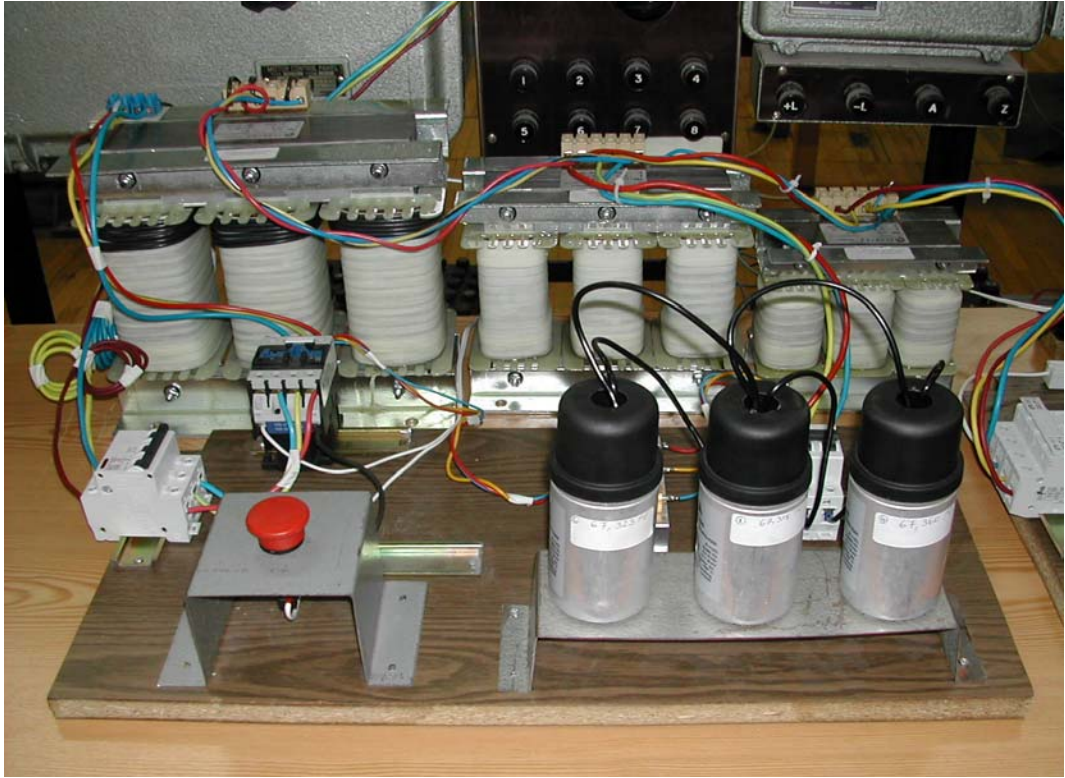
Fig. 5.38 Photograph of the laboratory IBF system.
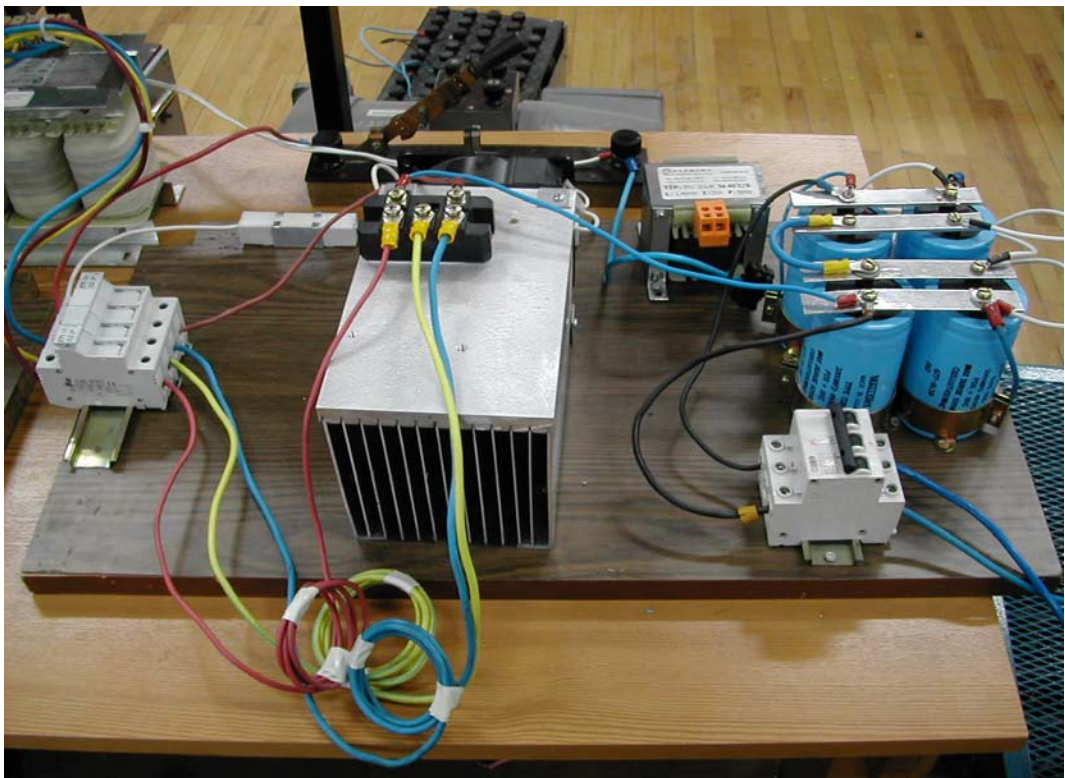
Fig. 5.39 Photograph of the laboratory three-phase rectifier system.

174

Fig. 5.40 Photograph of the overall laboratory test system involving 5.5 kW IBF.

5.5 Improved Broadband Filter Experimental Performance Characteristics

In this section the IBF experimental performance characteristics are obtained. Data from no-load to full-load operating conditions (at 0%, 25%, 50%, 75% and 100% loading) has been collected and the results are shown in the performance characteristic curves in this section. The improved broadband filter line current THD_I, line power factor and energy efficiency (including the rectifier bridge) performance characteristics, from no-load to full-load, are shown in Fig. 5.41 to Fig. 5.42.

The improved broadband filter line current THD_I values are shown in Fig. 5.41. The three-phase line current THD_I values are within the range shown at any operating point condition. The line power factor and the IBF efficiency (including the rectifier bridge) performance curves are shown in Fig. 5.42. In Fig. 5.43 the zoom-in view

shows only the IBF efficiency (including the rectifier bridge) performance involving 25% to 100% load variation curve. As the curves indicate, over a wide range the IBF based system provides high overall performance.   In particular, the input current THD has satisfactory performance in the full operating range. Therefore, the IBF based drive can comply with modern power quality standards.
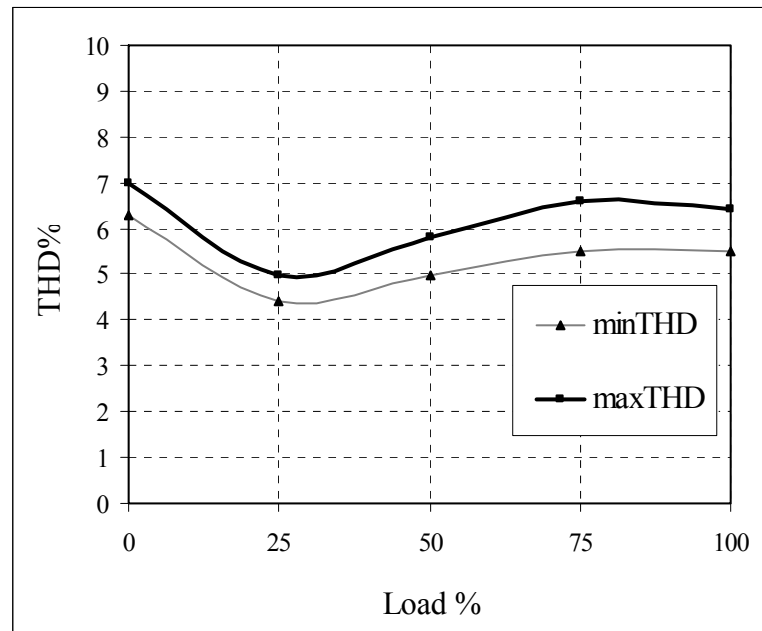
Fig. 5.41 The load current dependency of the IBF line current THD_I.
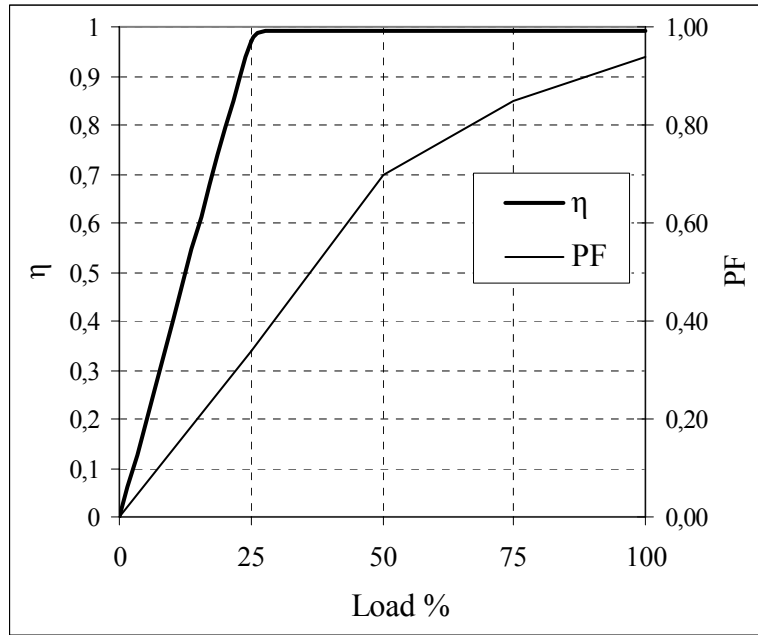
Fig. 5.42 The load current dependency of the IBF input power factor and efficiency (including the rectifier bridge).
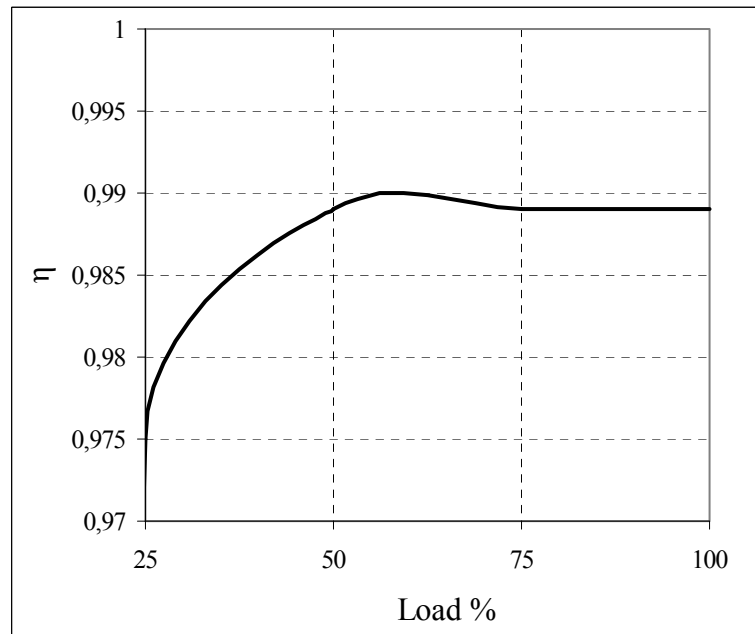
Fig. 5.43 Zoom-in view of the IBF efficiency curve.

5.6 Filter Performance Comparisons

In this section, the experimental results of the improved broadband filter are compared with conventional passive filters (tuned filter, AC line reactors). The comparison involves the rectifier and input current total harmonic distortion, input power factor, output DC voltage value, energy efficiency.

The experimental results obtained are summarized in Table 5.5 and they validate the analytical results and the computer simulation studies carried out in the previous chapters. The full-load DC bus voltage values in the experiments are slightly larger than the simulation results due to the fact that the line voltage at the laboratory is larger than the nominal 380V by as much as 15V. Efficiency measurements are approximate due to the accuracy limits of the Fluke 434 power quality analyzer under distorted waveforms and also due to the line voltage fluctuation at the laboratory. Overall Table 5.5 indicates that the IBF line THD_I is superior to the other filter configurations and has a power factor value near unity (although slightly leading due to the large capacitor). Furthermore, no harmonic resonance, or tuning frequency sensitivity has been observed.

Table 5.5 Experimental full-load performance of various filters for the 5.5 kW rectifier system[*]

Filter Type	3% line reactor	6% line reactor	Tuned Filter	IBF
Full-load rectifier THD_I(%)	39	30	35	42
Full-load input THD_I(%)	39	30	14.4	5.5
Input power factor	0.90 (lag.)	0.92 (lag.)	0.99 (lag.)	0.94 (lead.)
Full load DC Voltage (V) rms	530	513	524	544
Efficiency(%)	98.64	98.74	98.6	98.9

* Supply THD_V = 1.8 - 2.5%.

Table 5.6 provides additional performance data on the tested filters. The data involves the voltage regulation at node P (ΔV_o %) for the TF and IBF along with the line current no-load to full-load ratio. Voltage regulation at the rectifier terminals (ΔV_{rect}%) and at the DC bus ΔV_{dc}(%) is investigated for all filters. Same conclusions as stated in the simulation chapter are valid here. IBF has the poorest voltage regulation compared to other filters. However, the amount of variation is less than observed in the simulation results (1-3% more than the alternative methods).

Table 5.6 Additional performance of various filters for the 5.5 kW rectifier system

Filter Type	3% line reactor	6% line reactor	Tuned Filter	IBF
ΔV_o(%)	-------	--------	2.1	4.7
ΔV_{rect}(%)	1.8	3.2	3.3	5.0
ΔV_{dc}(%)	8.3	10	9.2	9.3
$I_{no-load}/I_{full-load}$	0.0	0.0	0.24	0.59

5.7 Summary

In this chapter the experimental performance characteristics of various filter structures for a 5.5 kW power rated rectifier system have been investigated. Performance evaluation of the built and tested filter prototypes was presented and a comparison provided. The steady-state performance characteristics at various operating points with distorted utility grid operating conditions were considered.

The main power quality parameters (line current THD_I, power factor, and filter output voltage regulation) and energy efficiency attributes have been investigated. The superior overall performance of IBF has been demonstrated. The next chapter summarizes the research results of this work.

CHAPTER 6

CONCLUSIONS

This thesis is concerned with passive harmonic filtering methods for ASD applications. Passive filtering systems are utilized to comply with modern power quality standards involving the current harmonic limits of three-phase rectifier systems utilized in AC motor drives.

6.1 Conclusions

The first stage of the thesis provided general knowledge of the common passive harmonic filtering methods and their associated circuit topologies that are utilized for ASD harmonic mitigation. This has involved a review of operating principles and design rules for three-phase AC line reactors, the DC link inductance, shunt tuned filters, and the simple lowpass LC broadband filter. Weakness, strength, and performance characteristics of the various passive harmonic filtering methods have been presented.

Of the various passive harmonic filtering methods presented, the lowpass broadband filtering method was shown to be the only method with promising line side power quality characteristics, but at the expense of light-load operating condition overvoltages. Therefore, the improved broadband filter which overcomes this weakness has been considered as the main candidate for modern power quality compliance filter.

In the second stage of the thesis the improved broadband filter topology has been developed to achieve better performance at all operating conditions. This improved broadband filter structure has been gaining wide acceptance and becoming a viable

method for harmonic mitigation in ASD applications. The improved broadband filter topology has been shown, its operating principle explained, and design method has been established. The IBF design rule is established and design procedure detailed.

The third stage of the thesis has involved designing the improved broadband filter for given operating conditions and power quality constraints. The design is conducted for 5.5, 55 and 500 power ratings. The filter employs 4% L_o in all power ratings and the three main filter parameters, L_i, L_f, C_f are first calculated by means of simple formulas via the approximate method. Utilizing the approximate method parameters as initial value, the accurate method further optimizes the three filter parameters with high accuracy leading to optimal parameters in terms of meeting the cost and performance criteria selected. For performance evaluation and comparisons design and implementation of various filter structures discussed has been involved.

The fourth stage of the thesis has involved detailed computer simulations that evaluate the performance of ASDs with various filter structures (with emphasis on IBF) and provides comparisons among the discussed filtering methods. The steady-state performance characteristics at various operating points were in focus. Balanced and unbalanced utility grid with or without voltage harmonic distortion operating conditions were considered. The main power quality parameters (line current THD_I, line power factor, and filter output voltage regulation) and energy efficiency attributes have been investigated.

The final stage involved laboratory work. For verification of the theoretical and computer simulation based studies, laboratory implementation of the investigated systems has been considered. The performance results have been investigated. Table 6.1 shows a qualitative comparison of the various filtering method discussed for ASD systems. The comparison involves with the line power quality indices (THD_I and PF), the harmonic resonance problem excitation probability, size, cost, efficiency and unbalance attributes.

According to the laboratory setup built for the various passive filters, the 3% and 6% AC line reactors utilize fewer components than the T-shape 5th and 7th tuned filter and IBF. Consequently, the line reactors are small in size and cost less. However, they are ineffective for effective harmonic mitigation and they can not reduce the

current THD to small values such as 10%. The T-shaped 5th and 7th tuned filter and IBF utilize more components and hence have higher size and cost compared to the AC line reactor filtering method.

The T-shape 5th and 7th tuned filter is utilizing two single shunt 5th and 7th tuned filters, while the IBF is utilizing one shunt branch. However, the single shunt 5th and 7th tuned filters have lower current ratings than the IBF shunt branch and hence the components are lower in size and cost. Concerning the input and output reactors (L_i and L_o) utilized in both methods, only the improved broadband filter input reactor (14% L_i) is higher in size and cost than the T-shape 5th and 7th tuned filter input reactor (6% L_i). The output reactors (L_o) utilized in both topologies are close in size and cost (4% for IBF and 3% for tuned filter).

As a total, IBF is utilizing fewer components with higher current ratings than the T-shaped 5th and 7th tuned filter. However, it has better performance than all harmonic filters presented. Therefore, both T-shape 5th and 7th tuned filter and IBF can be considered comparable in size and cost, and not in performance.

Table 6.1 Performance comparison for various filters for ASDs

Filter Type	THD$_I$	PF	Harmonic Resonance Risk	Size& Structure Complexity	Cost	η %	Voltage Unbalance attributes
Tuned filter	Low	High	High	Large& Complex	High	Medium	sensitive
IBF	Very Low	High	Not An Issue	Medium Simple	High	Medium	not sensitive
3-6% AC line reactor	High	Low	Not An Issue	Small Simplest	Low	High	sensitive

The most important contribution of this thesis is establishing a simple analytical method for the design of the improved lowpass broadband passive harmonic filter. The design method provides accurate filter parameters that result in effective

harmonic filtering of the rectifier harmonic currents and near unity input power factor.

6.2 Future Work

As the lowpass improved broadband filter has shown a superior performance in current harmonic mitigation for ASD application utilizing the 6-pulse diode full bridge rectifier. The topology can be adapted to different front-end rectifiers. This involves the 6-pulse thyristor full bridge rectifier applications. Other than the 6-pulse applications the topology can be also a promising method for 12-pulse front-end applications. As the current harmonic content of each rectifier structure is unique, the filter design rules and optimal parameter selection becomes an issue. Since the method developed in this thesis treats the rectifier as a harmonic current source, knowledge of the rectifier harmonic current ratio is sufficient for the new design. Thus, a study involving 6 pulse thyristor rectifier, 12 pulse diode/thyristor rectifier systems should be considered and their design rules established based on the method established in this thesis.

In case the utilization of the L_o filter is avoided, again the harmonic current ratio becomes different. Then the design principle leads to different filter parameters. The performance comparison between the standard method involving 4% reactor and no-reactor must be considered not only from the technical point of view, but also from the cost and size optimization point of view. Thus, additional study on the subject is required.

Perhaps, as the active harmonic filters remain costly and problematic, passive filtering solutions will continue finding applications. As a result high performance passive or hybrid filters must be developed to meet the increasingly strict power quality requirements of the modern technology era. Thus, new passive filter topologies involving better performance, smaller size, higher efficiency, reduced noise, and most importantly lower cost have to be developed and research in this area is a necessity of the modern power quality era.

REFERENCES

[1] A. Savolainen, "Driving Towards a Better Future," ABB Review, 4, 2004, pp. 34 – 38.

[2] IEEE Recommended Practices and Requirements for Harmonics Control in Electric Power Systems, IEEE Std. 519, 1992.

[3] R. C. Dugan, M. F. McGranaghan, Electrical Power Systems Quality, 2nd Edition, McGraw-Hill, 2002.

[4] M.M. Swamy, "Passive Harmonic Filter Systems for Variable Frequency Drives," U.S.Patent no: 5,444,609, Aug. 1995.

[5] M.M. Swamy, S.L. Rossiter, M.C. Spencer, M. Richardson, "Case Studies on Mitigating Harmonics in ASD Systems to Meet IEEE519-1992 Standards," in Conf. Rec. IEEE-IAS Annu. Meeting, 1994, vol.1, pp. 685 – 692.

[6] "MTE Corporation, Matrix filter product literature [Online]," http://www.mtecorp.com/matrix.html, last accessed: April, 2005.

[7] L.L. Grigsby, "The Electronic Power Engineering Handbook," CRC Press, 2000, ISBN 0-8493-8578-4.

[8] B. Singh, K. Al-Haddad, A. Chandra, "A Review of Active Filters for Power Quality Improvement," IEEE Trans. on Industrial Electronics, vol. 46, no. 5, October, 1999, pp. 960-971.

[9] H. Akagi, "Active and Hybrid Filters for Power Conditioning," IEEE Industrial Electronics Conf. Proc., vol. 1, 2000, pp. TU26-TU36.

[10] S. Bhattacharya, D. Divan, "Active Filter Solutions for Utility Interface of Industrial Loads," Conf. Proc. 1996, Power Electronics, Drives and Energy Systems for Industrial Growth, vol. 2, Jan. 1996, pp.1078 – 1084.

[11] S. Hansen, P. Nielsen, P. Thogersen, F. Blaabjerg, "Line Side Harmonic Reduction Techniques of PWM Adjustable Speed Drives - A Cost-Benefit Analysis," Proc. of NORPIE Conf., 2000, pp. 271-277.

[12] R. Dwyer, H.V. Nguyen, S.G. Ashomre, "C Filters Wide-Bandwidth Harmonics Attenuation with Low Losses," Power Engineering Society Winter Meeting, 2000, vol.4, pp. 2955-2960.

[13] J.C. Das, "Passive Filters – Potentialities and Limitations," IEEE Trans. on Industry Applications, vol. 40, no.1, Jan. /Feb. 2004, pp.232-241.

[14] Matlab 6.5. A numerical computation software, Mathworks Inc., 2002.

[15] S. M. Peeran, C.W.P. Cascadden, "Application, Design, and Specification of Harmonic Filters for Variable Frequency Drives," in Conf. Rec. IEEE-APEC Annu. Meeting, 1994, pp. 909-916.

[16] N.K. Medora, A. Kusko, "Computer-Aided Design and Analysis of Power Harmonic Filters," IEEE Trans. on Industry Applications, vol. 36, no.2 Mar./Apr. 2000, pp.604-613.

[17] K. Lin, M. Lin, T. Lin, "An Advanced Computer Code for Single-Tuned Harmonic Filter Design," IEEE Trans. on Industry Applications, vol. 34, no. 4, Jul./Aug. 1998, pp. 640-648.

[18] S.M. Islam, M.J. Hamilton, W.B. Lawrance, C.V. Nayar, "Investigation of Harmonics from Variable Speed Drives with Six Pulse Rectifiers under Imperfect Supply Conditions," in Conf. Rec. IEEE-IAS Annu. Meeting, 2000, vol.3, pp. 1625-1631.

[19] Ansoft-Simplorer SV 7.0. A power electronics simulation software, Ansoft Corporation, 2004.

[20] V. Gosbell, S. Perera, V. Smith, "Voltage Unbalance," Integral Energy Power Quality & Reliability Centre, Technical Note no.6, Oct. 2002.

[21] Fluke 434, Three-Phase Power Quality Analyzer Users Manual, Sep. 2004.

[22] Agilent Oscilloscopes and Aligent Mixed-Signal Oscilloscopes User's Guide, Sep. 2002.

[23] "Epcos Incorporation [Online]," http://www.epcos.com, last accessed: September, 2005.

APPENDIX

MATHLAB CODE

MATLAB code for calculating the IBF parameters is presented in the following.

```
%------------------------------------------------------------------------
%IMPROVED BROADBAND HARMONIC FILTER DESIGN FOR
ADJUSTABLE SPEED DRIVES
%PROGRAMMED BY: HAZEM ZUBI
%20/9/2005
%------------------------------------------------------------------------
disp('In this project, an analytical design method of the');
disp('improved broadband passive harmonic filter (IBF) for three-phase');
disp('diode rectifier front-end adjustable speed drives');
disp('is utilized to calculate the optimal filter parameters.');
%GIVEN PARAMETERS AND RATINGS
PR=input('enter the ASD rated power value in kW:');
VLL=input('enter the supply line-to-line rated voltage value in V:');
fe=input('enter the supply frequency value in Hz:');
Ls=input('enter the source equivalent reactance value in µH:');
Rs=input('enter the source equivalent resistance value in milliohm:');
THDmax=input('enter the line current THD limit value (THDmax%):');
DelVmax=input('enter the output voltage regulation limit value (DelVmax%):');
                              disp('PLEASE WAIT');
%------------------------------------------------------------------------
%CALCULATE THE BASE PARAMETERS AND RATED OPERATING POINT
VALUES
Vdc=VLL*(3*sqrt(2))/pi;%RATED DC LOAD VOLTAGE
Idc=1000*PR/Vdc;%RATED DC LOAD CURRENT
Rdc=Vdc/Idc;%RATED DC LOAD RESISTANCE
V1=VLL/sqrt(3);%RATED SUPPLY PHASE VOLTAGE RMS VALUE
Beta1=0.79;% RATED RECTIFIER CURRENT FUNDAMENTAL STIFFNESS
FACTOR
IFLP=Beta1*Idc*sqrt(2);%FULL-LOAD LINE CURRENT FUNDAMENTAL
COMPONENT PEAK VALUE
%--- APPLYING APPROXIMATE DESIGN METHOD FOR INITIAL FILTER
PARAMETERS CALCULATION
fs=275;%SELECTED SERIES RESONANCE FREQUENCY
fp=150;%SELECTED PARALLEL RESONANCE FREQUENCY
Alpha=0.5;%SELECTED ALPHA VALUE (NO-LOAD TO FULL-LOAD LINE
CURRENT RATIO)
```

```
We=2*pi*fe;
Wp=2*pi*fp;
Ws=2*pi*fs;
%STAR CONNECTED INITIAL FILTER CAPACITANCE VALUE (EQUATION
3.32)
Cfi=((1000*PR*Beta1*Alpha)/(0.78*(VLL^2)))*((1/We)-(We/(Wp^2)));
Lfi=1/(Ws^2*Cfi);%INITIAL FILTER REACTANCE VALUE(EQUATION 3.30)
Lii=(1/Cfi)*((1/Wp^2)-(1/Ws^2));%INITIAL          INPUT          REACTANCE
VALUE(EQUATION 3.31)
Cfidelta=Cfi/3;%DELTA CONNECTED FILTER CAPACITANCE VALUE
Betarms=0.84;%RMS STIFFNESS FACTOR
Ir=Betarms*Idc;%RATED RECTIFIER CURRENT RMS VALUE
ZBASE=V1/Ir;%SYSTEM BASE IMPEDANCE
Lfperi=100*Lfi*(2*pi*50)/ZBASE;%INITIAL FILTER REACTANCE VALUE IN
PERCENTAGE
Liperi=100*Lii*(2*pi*50)/ZBASE;%INITIAL  INPUT  REACTANCE  VALUE  IN
PERCENTAGE
%----- APPLYING  ACCURATE  DESIGN  METHOD  FOR  FINAL  FILTER
PARAMETERS ESTIMATION
Loper=4;%OUTPUT REACTOR VALUE IN PERCENTAGE
Lo=(0.01*Loper*ZBASE)/(2*pi*50);
RinLo=0.01*(0.01*Loper*V1/Ir);
%----------- RECTFIFIER CURRENT HARMONIC RATIOS (CHR)
CHR(1)=1.0;%FUNDAMENTAL COMPONENT
CHR(5)=0.34;%5th HARMONIC COMPONENT
CHR(7)=0.095;%7th HARMONIC COMPONENT
CHR(11)=0.07;%11th HARMONIC COMPONENT
CHR(13)=0.035;%13th HARMONIC COMPONENT
%---------- SUPPLY VOLTAGE HARMONIC RATIOS (VHR)
VHR(1)=0.0;%FUNDAMENTAL COMPONENT
VHR(5)=0.0225;%5th HARMONIC COMPONENT
VHR(7)=0.0129;%7th HARMONIC COMPONENT
VHR(11)=0.0116;%11th HARMONIC COMPONENT
VHR(13)=0.0088;%13th HARMONIC COMPONENT
Zs=Rs+(100*pi*Ls*sqrt(-1));%EQUIVALENT SOURCE IMPEDANCE
Zsabs=abs(Zs);
%---------- DEFINING THE PAREMERTS STEP SIZE
Lfpermax=Lfperi;%THE  MAXIMUM  FILTER  REACTOR  VALUE  IN
PERECENTAGE
Lipermax=Liperi;%THE  MAXIMUM  INPUT  REACTOR  VALUE  IN
PERCENTAGE
Cfmin=Cfi;%THE MINIMUM FILTER CAPACITANCE VALUE
Liper=Liperi;%INPUT REACTOR VALUE IN PERCENTAGE
Lfper=Lfperi;%INITIAL FILTER REACTOR VALUE IN PERCENTAGE
delLi=-0.5;%INPUT REACTOR STEP SIZE
delLf=-0.2;%FILTER REACTOR STEP SIZE
delCf=0.002*Cfi;%FILTER CAPACITOR STEP SIZE
  x=0;
  y=0;
  Col=1;
```

```
 Cf=Cfmin;
 while x <80%THE FIRST LOOP FOR Cf VARIATION
 x=x+1;
 Cf=Cf+delCf;
    for i=1:15
   Liper=Liper+delLi;%THE SECOND LOOP FOR Li VARIATION
   Lip(i)=Liper;
   Li(i)=(Liper*0.01*ZBASE)*1/(2*pi*50);
   RinLi(i)=0.01*(0.01*Lip(i)*V1/Ir);%ESTIMATING        ESR        FOR        99%
EFFICIENCY
          for j=1:15 % THE THIRD LOOP FOR Lf VARIATION
   Lfper=Lfper+delLf;
   Lfp(j)=Lfper;
   Lf(j)=(Lfper*0.01*ZBASE)*1/(2*pi*50);
   RinLf(j)=0.01*(0.01*Lfp(j)*V1/Ir);%ESTIMATING        ESR        FOR        99%
EFFICIENCY
     LfH=Lf(j);
     %FUNDAMENTAL    CURRENT    COMPONENT    AND    DOMINANT
CURRENT HARMONICS
     %(5th, 7th, 11th and 13th)ARE CONSIDERED
                 for jk=1:2:13
   FS(jk)=(fe*jk); %THE HARMONIC FREQUENCY
   WS(jk)=2.0*pi*FS(jk);
   %-----------------------------------------------------------------------
   IHS(jk)=IFLP*(CHR(jk));%FULL-LOAD RECTIFIER CURRENT HARMONIC
PEAK VALUES
   %TOTAL LINE IMPEDANCE (ZLi+Zs)
   ZSline(jk)=((RinLi(i)+(Rs*1.0e-3))+((Ls*1.0e-6)+Li(i))*WS(jk)*sqrt(-1));
   %TOTAL FILTER IMPEDANCE (ZLf+ZCf)
   Zfilter(jk)=(RinLf(j)+(Lf(j)*WS(jk))*sqrt(-1))-sqrt(-1)/((WS(jk)*Cf));
   abZSline(jk)=abs(ZSline(jk));
   abZfilter(jk)=abs(Zfilter(jk));
   %-----------------------------------------------------------------------
   VHS(jk)=(V1*sqrt(2))*(VHR(jk)); %SUPPLY VOLTAGE HARMONIC PEAK
VALUES
   %-----------------------------------------------------------------------
   %SUPPLY SIDE CURRENT HARMONICS PEAK VALUES
   ILH2(jk)=(VHS(jk))/(abs(ZSline(jk)+Zfilter(jk)));
   %LOAD SIDE CURRENT HARMONICS PEAK VALUES
   ILH1(jk)=(abs(Zfilter(jk)))*(IHS(jk))/(abs(ZSline(jk)+Zfilter(jk)));
   %TOTAL    LINE    CURRENT    HARMONICS    PEAK    VALUES    AFTER
FILTERING
   ILHT(jk)=ILH1(jk)+ILH2(jk);
                 end %for jk
 %LINE CURRENT THD CALCULATION

THDILINE(j)=100*sqrt((ILHT(5)^2+ILHT(7)^2+ILHT(11)^2+ILHT(13)^2)/(IFLP^
2));
 THD=THDILINE(j);
 %FILTER PARALLEL RESONANCE FREQUENCY (Li, Lf AND Cf)
```

```matlab
Fpp=1/((2*pi)*(sqrt(Cf*(Li(i)+Lf(j)))));
%SHUNT BRANCH SERIES RESONANCE FREQUENCY (Lf AND Cf)
Fss=1/((2*pi)*(sqrt(Cf*Lf(j))));
%-------------------------------------------------------------------------
LL=(Lo+Li(i));%COMMUTATION AND VOLTAGE DROP REACTOR
(EMPERICAL FORMULA)
XLo=(100*pi*(Lo+LL))*sqrt(-1);
ZRLo=(XLo+(Rdc/1.823));%TOTAL LOAD IMPEDANCE INVOLVING Lo, LL
AND Rac
abZRLo=abs(ZRLo);
%-------------------- CALCULATING LINE POWER FACTOR --------------------
Ztotal=(ZSline(1))+((ZRLo*Zfilter(1))/(ZRLo+Zfilter(1)));%TOTAL     INPUT
FUNDAMENTAL IMPEDANCE
I1rms=V1/Ztotal;%SUPPLY CURRENT FUNDAMENTAL COMPONENT RMS
VALUE
IFL=abs(I1rms);%FULL-LOAD     LINE     CURRENT     FUNDAMENTAL
COMPONENT RMS VALUE
phaserad=phase(I1rms);
PF(j)=cos((phaserad));
cosfi=PF(j);%FULL-LOAD LINE POWER FACTOR
%---------------------- CALCULATING FULL-LOAD NODE P VOLTAGE -----------
%FULL-LOAD SUPPLY CURRENT FUNDAMENTAL COMPONENT RMS
VALUE
I1(j)=I1rms;
%FULL-LOAD SHUNT FILTER CURRENT FUNDAMENTAL COMPONENT
RMS VALUE
If1(j)=I1(j)*((ZRLo)/(ZRLo+Zfilter(1)));
%FULL-LOAD NODE P VOLTAGE FUNDAMENTAL COMPONENT RMS
VALUE
Vp(1)=If1(j)*(Zfilter(1));
Vprms(1)=abs(Vp(1));
Vp1FLT(j)=Vprms(1);
VnFL=Vp1FLT(j);
%--------------------- CALCULATING NO-LOAD NODE P VOLTAGE ---------------
%NO-LOAD NODE P VOLTAGE FUNDAMENTAL COMPONENT RMS
VALUE
Vp1NL(1)=V1*(abs(Zfilter(1)))/(abs(ZSline(1)+Zfilter(1)));
Vp1NLT(j)=Vp1NL(1);
VnNL=Vp1NLT(j);
%NO-LOAD LINE CURRENT FUNDAMENTAL COMPONENT RMS VALUE
IrmsNL(j)=V1/(abs(ZSline(1)+Zfilter(1)));
INL=IrmsNL(j);
Inoload(i,j)=INL;
%--------------------- CACULATING NODE P VOLTAGE REGULATION -----------
Voverload(j)=((Vp1NLT(j)-Vp1FLT(j))/Vp1NLT(j));
Voverloadper=100*Voverload(j);
%------------------- CHECKING CONSTRAINTS AND STORING RESULTS -------
 if(THD<THDmax)&(THD>(THDmax-
0.1))&(Voverloadper<DelVmax)&(Voverloadper>(DelVmax-0.1))
        Col=Col+1;
```

```
        y=y+1;
        xy(y)=y;
        yy=y;
        LimH(y)=1000*Li(i);%INPUT REACTOR Li
        OptR((y+1),Col)=LimH(y);
        LfmH(y)=1000*Lf(j);%FILTER REACTOR Lf
        OptR((y+1),(Col+1))=LfmH(y);
        CfuFdel(y)=(Cf/3.0)*1000000;%FILTER CAPACITOR Cf
        OptR((y+1),(Col+2))= CfuFdel(y);
        THDi(y)=THD;%LINE CURRENT THD
        OptR((y+1),(Col+3))=THDi(y);
        Voper(y)=Voverloadper;%VOLTAGE REGULATION AT NODE P
        OptR((y+1),(Col+4))= Voper(y);
        PF(y)=cosfi;%LINE POWER FACTOR
        OptR((y+1),(Col+5))= PF(y);
        Fparal(y)=Fpp;%FILTER PARALLEL RESONANCE FREQUENCY
        OptR((y+1),(Col+6))= Fparal(y);
        Fseries(y)=1/((2*pi)*(sqrt(Cf*LfH)));%SHUNT      BRANCH      SERIES
RESONANCE FREQUENCY
        Alpha(y)=100*INL/IFL;
                end
                Col=1;
            end
            Lfinal=Lfper;
            Lfper=Lfpermax;%RESET INITIAL CONDITION
    end
    Lifinal=Liper;
    Liper=Lipermax;%RESET INITIAL CONDITION
end
%------------- LISTING THE FINAL FILTER PARAMETERS AND SYSTEM
PERFORMANCE RESULTS
 OptResult{1,1}='Results';
 OptResult{1,2}='Li(mH)';
 OptResult{1,3}='Lf(mH)';
 OptResult{1,4}='Cf(µF)';
 OptResult{1,5}='THD';
 OptResult{1,6}='DelVo';
 OptResult{1,7}='PF';
 OptResult{1,8}='fp';
 no=y+1;
 while y>0
   OptResult{no,1}=y;
   no=no-1;
   y=y-1;
end
 C=2;
 R=6;
 while R>2
 R=yy+1;
 OptResult{R,C}=LimH(yy);
```
191

```
OptResult{R,(C+1)}=LfmH(yy);
OptResult{R,(C+2)}= CfuFdel(yy);
OptResult{R,(C+3)}=THDi(yy);
OptResult{R,(C+4)}= Voper(yy);
OptResult{R,(C+5)}= PF(yy);
OptResult{R,(C+6)}= Fparal(yy);
yy=yy-1;
end
OptResult
```